MEASUREMENT OF EXHAUST EMISSIONS FROM A 185-GE-5B ENGINE AT SIMULATED HIGH-ALTITUDE SUPERSONIC FREE-STREAM FLIGHT CONDITIONS

R. C. German, et al

Arnold Engineering Development Center

Prepared for:

Federal Aviation Administration

July 1973

AEDC-TR-73-103

MEASUREMENT OF EXHAUST EMISSIONS FROM A J85-GE-5B ENGINE AT SIMULATED HIGH-ALTITUDE, SUPERSONIC, FREE-STREAM FLIGHT CONDITIONS

R. C. German, M. D. High, and C. E. Robinson
ARO, Inc.

July 1973

PROPULSION WIND TUNNEL FACILITY
ARNOLD ENGINEERING DEVELOPMENT CENTER
AIR FORCE SYSTEMS COMMAND
ARNOLD AIR FORCE STATION, TENNESSEE

NOTICES

When U. S. Government drawings specifications, or other data are used for any purpose other than a definitely related Government procurement operation, the Government thereby incurs no responsibility nor any obligation whatsoever, and the fact that the Government may have formulated, furnished, or in any way supplied the said drawings, specifications, or other data, is not to be regarded by implication or otherwise, or in any manner licensing the holder or any other person or corporation, or conveying any rights or permission to manufacture, use, or sell any patented invention that may in any way be related thereto.

Qualified users may obtain copies of this report from the Defense Documentation Center.

References to named commercial products in this report are not to be considered in any sense as an endorsement of the product by the United States Air Force or the Government.

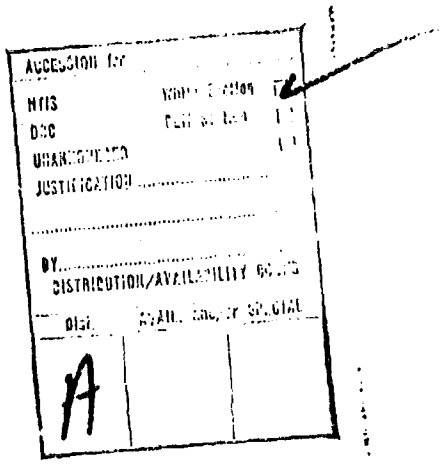

UNCLASSIFIED

Security Classification

DOCUMENT CONTROL DATA - R & D

(Security classification of title, body of abstract and indexing annotation must be entered when the overall report is classified)

1. ORIGINATING ACTIVITY (Corporate author)

Arnold Engineering Development Center
Arnold Air Force Station, Tennessee 37389

2a. REPORT SECURITY CLASSIFICATION

UNCLASSIFIED

2b. GROUP

N/A

3. REPORT TITLE

MEASUREMENT OF EXHAUST EMISSION FROM A J85-GE-5B ENGINE AT SIMULATED HIGH-ALTITUDE, SUPERSONIC, FREE-STREAM FLIGHT CONDITIONS

4. DESCRIPTIVE NOTES (Type of report and inclusive dates)

5. AUTHOR(S) (First name, middle initial, last name)

R. C. German, M. D. High, and C. E. Robinson, ARO, Inc.

6. REPORT DATE	7a. TOTAL NO. OF PAGES	7b. NO. OF REFS
July 1973	138	16

8a. CONTRACT OR GRANT NO.

b. PROJECT NO.

c. Program Element 921K

d.

9a. ORIGINATOR'S REPORT NUMBER(S)

AEDC-TR-73-103

9b. OTHER REPORT NO(S) (Any other numbers that may be assigned this report)

ARO-PWT-TR-73-49
FAA-RD-73-92

10. DISTRIBUTION STATEMENT

Approved for public release; distribution unlimited.

11. SUPPLEMENTARY NOTES

Available in DDC

12. SPONSORING MILITARY ACTIVITY

Federal Aviation Administration,
800 Independence Ave., S.W.,
Washington, D.C. 20590

13. ABSTRACT

Exhaust emissions were measured in the plume of a J85-GE-5 turbojet engine as part of an investigation to determine the impact on the climate of a fleet of supersonic aircraft flying in the stratosphere. Measurements were made at three axial stations (0.22, 9.3, and 19.9 nozzle diameters) downstream of the nozzle exit for both military and partial afterburning power at Mach numbers and simulated altitudes of Mach 1.6/55,000 ft and Mach 2.0/65,000 ft. A continuous sampling technique was used to measure carbon dioxide, carbon monoxide, total unburned hydrocarbons, oxides of nitrogen, and particulates. The experimental results were compared with the calculated emission profiles and were in good agreement. The results represent the only available full-scale turbojet engine emission data to date which have been obtained at simulated high altitude with a supersonic external stream.

DD FORM 1 NOV 68 1473

UNCLASSIFIED

Security Classification

14. KEY WORDS	LINK A		LINK B		LINK C	
	ROLE	WT	ROLE	WT	ROLE	WT
air pollution						
exhaust gases						
exhaust emissions						
turbojet engines						
altitude simulation						
supersonic flow						
Mach number						
plume						
sampling						

AFSC
Aeronautical Systems Division

MEASUREMENT OF EXHAUST EMISSIONS FROM A J85-GE-5B ENGINE AT SIMULATED HIGH-ALTITUDE, SUPERSONIC, FREE-STREAM FLIGHT CONDITIONS

R. C. German, M. D. High, and C. E. Robinson
ARO, Inc.

ii

FOREWORD

The test program reported herein was conducted at the Arnold Engineering Development Center (AEDC) under sponsorship of the Department of Transportation (DOT), Office of the Secretary, Washington, D. C., under Interagency Agreement DOT-AS-20024, Program Element 921K. The DOT test program was monitored by Mr. A. K. Forney, Program Manager, Federal Aviation Administration (FAA), 800 Independence Avenue, S. W., Washington, D. C., and technical liasion was provided by Dr. A. J. Broderick and Dr. M. J. Scotto, DOT Transportation Systems Center, 55 Broadway, Cambridge, Massachusetts.

The test hardware, emission instrumentation, support hardware, test planning, test procedure, and data analysis, exclusive of the J85-GE-5 turbojet engine, and supersonic inlet, were provided by AEDC. The turbojet engine was supplied by the Air Force Aero Propulsion Laboratory (AFAPL), Air Force Systems Command (AFSC), Wright-Patterson Air Force Base, Ohio. The supersonic inlet was provided by NASA Lewis Research Center, Cleveland, Ohio.

The results of the test program were obtained by ARO, Inc. (a subsidiary of Sverdrup & Parcel and Associates, Inc.), contract operator of AEDC, AFSC, Arnold Air Force Station, Tennessee. The test was conducted in the 16-Foot Supersonic Wind Tunnel (16S) of the Propulsion Wind Tunnel Facility (PWT) during the period from December 15, 1972, to January 10, 1973, under ARO Project Nos. PA038 and PB038. The manuscript was submitted for publication on April 25, 1973.

Special appreciation is expressed to R. F. Lauer, Jr., project engineer, who was responsible for the installation and test activities and who wrote the sections of the report to do with the engine, inlet, and test facility. The authors also wish to express special appreciation to J. N. Kemp, project instrumentation engineer, whose tireless effort in maintaining and operating the emission analyzer system made the successful measurement of the engine exhaust emissions a reality.

This technical report has been reviewed and is approved.

L. R. KISSLING
Lt Colonel, USAF
Chief Air Force Test Director, PWT
Directorate of Test

FRANK J. PASSARELLO
Colonel, USAF
Director of Test

ABSTRACT

Exhaust emissions were measured in the plume of a J85-GE-5 turbojet engine as part of an investigation to determine the impact on the climate of a fleet of supersonic aircraft flying in the stratosphere. Measurements were made at three axial stations (0.22, 9.3, and 19.9 nozzle diameters) downstream of the nozzle exit for both military and partial afterburning power at Mach numbers and simulated altitudes of Mach 1.6/55,000 ft and Mach 2.0/65,000 ft. A continuous sampling technique was used to measure carbon dioxide, carbon monoxide, total unburned hydrocarbons, oxides of nitrogen, and particulates. The experimental results were compared with the calculated emission profiles and were in good agreement. The results represent the only available full-scale turbojet engine emission data to date which have been obtained at simulated high altitude with a supersonic external stream.

CONTENTS

APPENDIXES

I. ILLUSTRATIONS

Figure

Figure | Page

II. TABLES

NOMENCLATURE

A_{BY}	Inlet bypass area, m^2 (ft^2) (see Fig. 3b)
A_{EJ}	Ejector bypass door area, m^2 (ft^2) (see Fig. 3b)
A/B	Afterburning engine power setting
ALT	Simulated geopotential altitude, m (ft)
A_8	Nozzle exit area at engine station 8, m^2 (ft^2) (see Fig. 4)
CALC	Calculated $CNO_2 = CNO_x - CNO$
CCO	Emission concentration carbon monoxide, ppmv
CCO_2	Emission concentration, carbon dioxide, percent
CID	Chemiluminescence detector
CNO	Emission concentration, nitric oxide, ppmv
CNO_2	Emission concentration, nitrogen dioxide, ppmv
CNO_x	Emission concentration, total oxides of nitrogen, ppmv
CTHC	Emission concentration, total unburned hydrocarbons, ppmv
D_2	Distortion at compressor face, $(p_{t_2\ max} - p_{t_2\ min})/\bar{p}_{t_2}$
DN	Fixed nozzle exit diameter, 0.454 m (1.49 ft)
EICO	Emission index, carbon monoxide, gm/kg fuel
$EICO_2$	Emission index, carbon dioxide, gm/kg fuel
EINO	Emission index, nitric oxide, gm/kg fuel

$EINO_2$	Emission index, nitrogen dioxide, gm/kg fuel
$EINO_x$	Emission index, total oxides of nitrogen, gm/kg fuel
EITHC	Emission index, total unburned hydrocarbons, gm/kg fuel
FID	Flame ionization detector
(f/a)P	Primary engine fuel-air ratio
(f/a)T	Total engine fuel-air ratio (Primary + A/B)
HORIZ	Horizontal plume survey (see Fig. 7)
LDIAG	Left diagonal plume survey (see Fig. 7)
M	Molecular weight of emitted species
M_∞	Free-stream Mach number
MEAS	Measured concentration
MIL	Military engine power setting
m	Particle mass
NDIV	Nondispersive infrared
NDUV	Nondispersive ultraviolet
n	Particle number density, particles/unit volume
$\dot{n}$	Particle number flow, particles/unit time
PTJ	Impact pressure in exhaust plume, N/cm^2 (psia)
PJ	Static pressure in exhaust plume, N/cm^2 (psia)
PLS	Power lever setting
p	Static pressure, N/cm^2 (psfa)
p_2	Compressor inlet static pressure, N/cm^2 (psfa)
p_{t_∞}	Free-stream total pressure, N/cm^2 (psfa)

p_{t_2}	Compressor inlet total pressure, N/cm² (psfa)
$\bar{p}_{t_2}$	Average compressor inlet total pressure, N/cm² (psfa)
p_{t_3}	Burner inlet total pressure, N/cm² (psfa)
$\bar{p}_{t_2}/p_{t_\infty}$	Inlet total pressure recovery
RDIAG	Right diagonal plume survey (see Fig. 7)
R_N	Radius of fixed nozzle exit, 0.277 m (0.746 ft)
R_P	Radial location of sample probe, m (ft)
RPM	Engine rotor speed, rev/min
R_T	Radial location of thermocouple on sample probe, m (ft) (see Fig. 5)
SCF	Standard cubic feet
T_{t_∞}	Free-stream total temperature, °K (°R)
T_{t_2}	Compressor inlet total temperature, °K (°R)
T_{t_3}	Burner inlet total temperature, °K (°R)
T_{t_5}	Turbine discharge total temperature, °K (°R)
TTJ	Total temperature in exhaust plume, °K (°R)
u	Exhaust velocity, m/sec (ft/sec)
V_3	Burner inlet velocity, m/sec (ft/sec)
VERT	Vertical plume survey (see Fig. 7)
W_a	Compressor inlet airflow, kg/sec (lb/sec)
WAK2	Compressor inlet airflow corrected to standard sea-level temperature and pressure, $W_a\sqrt{\theta_2}/\delta_2$, kg/sec (lb/sec)
WFP	Primary engine fuel flow, kg/hr (lb/hr)
WFT	Total engine fuel flow, kg/hr (lb/hr), (primary + A/B)

XP	Axial probe position, m (ft) (see Fig. 1)
XR	Plume survey axis (see Fig. 7)
XS	Inlet spike position, m (ft) (see Fig. 3b)
δ_2	$P_{t_2}/10.13$ N/cm^2 = (p_{t_2}/2116 psfa)
θ_2	$T_{t_2}/288°K$ = ($T_{t_2}/519°R$)

SUBSCRIPTS

EJEC	Ejector nozzle
f	Fuel
g	Exhaust gas property
NOZ	Nozzle
NAC	Nacelle
p	p^{th} species

SECTION I
INTRODUCTION

The unknown environmental impact of a fleet of supersonic aircraft operating in the stratosphere has resulted in a Department of Transportation (DOT) investigation named the Climatic Impact Assessment Program (CIAP). The results from this program will be used to assess the climatic impact of exhaust emissions from turbine-powered aircraft operating in the stratosphere as projected to the year 1990 (Ref. 1). The CIAP will provide a data base for six monographs:

1. "The Natural Stratosphere of 1974"
2. "The Engine Emissions on the Stratosphere of 1990"
3. "The Perturbed Stratosphere of 1990"
4. "The Perturbed Troposphere of 1990 and 2020"
5. "The Biological Effects of the Tropospheric Changes"
6. "The Social and Cost Measures of the Biological Changes"

The exhaust emission data presented in this report will provide valuable information for the second monograph and should add greatly to the state of the art of aircraft turbine engine emissions. The data presented are the only known emission data which have been obtained at simulated high altitude, using a full-scale, turbojet engine.

The test was conducted in the Propulsion Wind Tunnel (PWT), Supersonic (16S) for DOT using a General Electric J85-GE-5 turbojet engine (Ref. 2) mounted in an isolated nacelle with a NASA/Lewis Research Center, mixed compression, axisymmetric, supersonic inlet (Ref. 3). The objective of the PWT test was to determine the influence of the mixing of the engine exhaust gases with the external supersonic free-stream flow on the exhaust emissions of a full-scale turbojet aircraft engine.

A special rotating sampling probe was designed by PWT engineers to withstand the 2000°K (3600°R) engine exhaust as well as to maintain the gas sample at 422 ± 5.6°K (760 ± 10°R) while it was pumped through a 3.5 to 42.6 m (110 to 140 ft) length of gas transfer line to the gas analyzer. The gas analysis system used was originally designed (Ref. 4) and used by the Engine Test Facility (ETF) to measure the exhaust emissions at the nozzle exit of General Electric J93-GE-3 afterburning turbojet engine (Ref. 5). A continuous sampling technique was used to obtain measurements of carbon monoxide (CO), carbon dioxide (CO_2), nitric oxide (NO), nitrogen dioxide (NO_2), other oxides of nitrogen (NO_x), and the total hydrocarbons (THC). The particulate emissions were also

measured using gravimetric filters and electrostatic grids. All measurements were made in general accordance with SAE ARP 1256 (Ref. 6). A continuous sample of the flow approaching the inlet was also maintained to monitor the concentrations of CO_2 and THC recirculated in the wind tunnel.

A method of calculating the exhaust plume characteristics and the emission concentration profiles is presented, and comparisons with the experimental data are shown.

SECTION II
APPARATUS

2.1 TEST FACILITY

Tunnel 16S is a closed-circuit, continuous-flow wind tunnel that can be operated over a nominal Mach number range from 1.50 to 4.75. For this test, engine exhaust products were removed from the tunnel atmosphere by a 183-m (6-ft) diameter open, sharpslip, scavenging scoop located 10.62 m (34.9 ft) downstream of the engine nozzle exit as shown in the installation sketch (Fig. 1, Appendix I) and in the photograph (Fig. 2).

2.2 TEST ARTICLE

2.2.1 Inlet/Engine Model

The inlet used in this investigation was as axisymmetric mixed-compression inlet (Fig. 3) on loan from the NASA Lewis Research Center, and its performance and description has been well documented in Refs. 3, 7, and 8. External compression was accomplished with a 12.5-deg half-angle conical, remotely translatable centerbody. Inlet boundary-layer removal was accomplished by suction through porous sections on the centerbody and cowl surfaces with the bleed flow being discharged overboard. The aft porous section of the cowl bleed was sealed closed, and only the forward cowl bleed was used. There were provisions for engine cooling by the remotely operable ejector bypass valves which discharged into the engine nacelle. Inlet/engine airflow matching was accomplished with overboard bypass doors. A control system was designed and fabricated that permitted the inlet shock position to be maintained during engine transients by appropriately controlling the position of the overboard bypass doors.

The engine, a General Electric J85-GE-5, S/N E230336, (the same engine used during the sea-level tests of Ref. 9) is a single-rotor, afterburner-equipped turbojet. The engine compressor is an eight-stage fixed-stator unit with interstage bleed valves which extract air from Stages 3, 4, and 5; the bleed air was discharged overboard. Variable inlet guide vanes operated in conjunction with the interstage bleed valves. An ejector nozzle shroud which had an exit diameter of 0.455 m (17.9 in.) was fitted to the primary exhaust nozzle as shown in Fig. 4.

The distances to the three axial positions of the emission sampling probe (Fig. 1) were measured from the plane of the nozzle shroud exit, but the primary nozzle exhaust plane was about 0.14 m (5.5 in.) upstream of the shroud plane at military power levels and about 0.157 m (6.2 in.) upstream at the augmented power conditions. A more detailed engine description may be found in Ref. 2.

The engine nacelle and model support system were designed by Boeing Company for a previous test requirement. All fire-fighting equipment, fuel, externally supplied air, electrical control cables, pressure and electrical signals, etc., were supplied through the support strut (see Figs. 1 and 2). The inlet was mounted to the engine nacelle using a PWT-designed adapter which provided a cylindrical flow path for the primary engine air from the inlet and additional passages for the inlet ejector/engine nacelle cooling airflow (see Fig. 3b). A free-stream gas sample probe was provided in the support system, immediately above the inlet (Fig. 1), so that the tunnel atmospheric concentrations of CO_2 and THC could be periodically sampled during the test, thereby ensuring that the scavenging scoop was capturing all of the engine exhaust products and that the tunnel atmosphere was not being contaminated.

2.2.2 Exhaust Emission Sampling Probe

A sketch of the PWT-designed exhaust emission sampling probe is given in Fig. 5. The rotary probe arm could be positioned from the vertical plane of the support strut to ±180 deg. The probe support strut could be rotated approximately ±30 deg from the vertical, except in axial position one, where travel was limited to between +19 and +34 deg (looking upstream) to prevent interference with the engine nacelle. By appropriately positioning the main probe support strut and the rotary probe arm, exhaust gas emissions in a 2.3-m (7-ft) diameter circle and over an arc length of 3.96 m (13 ft) could be sampled in a plane perpendicular to the free-stream airflow at probe axial position two (mid position) (Fig. 2) and probe axial position three (aft position) (Fig. 6a). At axial probe position one (nozzle exit position) (Fig. 6b), the area was reduced, but the complete exhaust stream could still be sampled. The radials which were surveyed at each probe position are shown in Fig. 7.

The sample line was constructed from 304 stainless steel tubing 1.27 cm (0.50 in.) OD by 0.089 cm (0.035 in.) wall thickness and was maintained at this ID except at three locations where it was required to enlarge the ID to 1.27 cm (0.50 in.) for short distances through bends in the probe support structure. Bends in the sample line were kept to a minimum with the smallest bend radius being 1.5-in. radii in the motor drive assembly. A special flow splitter was designed to divide the flow between the gaseous emission and the particulate emission instrumentation with a minimum of disturbance.

2.2.3 Sample Conditioning System

A unique sample probe design was required in that not only was the probe to be cooled to withstand the 2000°K (3600°R) engine exhaust, but the gas sample must be quenched very rapidly and must be maintained at 422 ± 5.6°K (760 ± 10°R) as it is pumped along the long transfer lines to the analyzer to prevent condensation of the various

gaseous constituents (particularly the unburned hydrocarbons). The exhaust gas transfer line from the sample probe to the analyzer had lengths of 35.0, 39.6, and 42.6 m (115, 130, and 140 ft), respectively, for probe positions 1, 2, and 3. The entire length of the transfer line from probe tip to the analyzer was concentrically water-jacketed to maintain the gas temperature constant with the exception of two short sections (approximately 0.305 m) (1 ft) where a 1.27-cm (0.5-in.) inside diameter Teflon® line was used and wrapped with external heater tape. A schematic of the sample conditioning system is shown in Fig. 8.

Within the analyzer, the sample temperature was maintained at 422 ± 5.6°K (760 ± 10°R) up to the hydrocarbon analyzer which was located nearest the analyzer inlet. The exhaust sample was then maintained at 339 ± 2.8°K (610 ± 5°R) throughout the remainder of the analyzer. Bellows pumps, located at the analyzer inlet, were used to pump the gas sample from the probe inlet at a pressure of 2.07 to 3.45 N/cm^2 (3.0 to 5.0 psia) to the analyzer inlet at the 10.32 N/cm^2 (15 psia) required by the instrumentation. A back pressure regulator located on the downstream end of the sample line in the analyzer console was used to control the line pressure from the bellows pumps. The sample line and each of the emission instruments utilized a common overboard vent through which the emission sample was discharged.

2.3 INSTRUMENTATION

Steady-state data obtained during this investigation were digitized and scanned, and raw data inputs were recorded on magnetic tape by the PWT Raytheon 520® digital computer. The raw data were reduced, selected parameters were printed in the Control Room on a line printer operating in conjunction with the computer, and computed parameters were written on magnetic tape.

2.3.1 Inlet

The 32 centerbody (spike) surface static pressures and 20 internal cowl surface static pressures on the inlets were measured by the PWT pressure system and were monitored in the Control Room for inlet operation. Compressor-face total-pressure recovery, distortion, and primary engine airflow were computed from six, ten-tube, total-pressure rakes with static taps at the cowl and afterbody walls of each rake. This instrumentation array (Fig. 9) was located in the subsonic diffuser of the inlet, upstream of the engine compressor face (Fig. 3b). Additionally, the centerbody bleed, cowl bleed, ejector bypass, and overboard bypass flows were metered using appropriate pressure instrumentation.

Two model-mounted strain-gage transducers were used for inlet operation. The one sensing the total pressure in the subsonic diffuser was used for monitoring inlet stability, and the other transducer sensed a cowl surface static pressure downstream of the normal shock in the subsonic diffuser for inlet overboard bypass control.

The overboard bypass doors could be operated either manually or in a closed-loop mode with the feedback being the signal from the cowl surface pressure transducer. This system controlled the position of the inlet normal shock by maintaining a pre-set surface static pressure. This was accomplished by opening the bypass doors when the pressure began to rise and conversely, to close the doors when the pressure began to decrease.

Spike axial position, each of the six overboard bypass door positions, and the ejector bypass door positions were monitored and recored by the PWT data systems.

2.3.2 Engine

The engine had the minimum amount of instrumentation required for safe engine/facility operation. Measured were: power lever angle; nozzle and interstage-bleed-valve/inlet-guide-vane positions; engine rotor speed; vibrations from the forward, main, and turbine frames; primary and total fuel flows; temperature, and pressures which include oil temperatures and pressures, compressor discharge static pressure, turbine discharge temperature, engine skin, and nacelle environment temperatures.

2.3.3 Gas Sample Probe

Both the main probe support strut and the rotary probe arm were instrumented so that the angular position of each was displayed in the Control Room and recorded on the data. The total temperature (TTJ) of the gas sample was measured by an iridium-iridium/rhodium thermocouple located 5.09 cm (2 in.) from the sample orifice on the rotary probe arm (see Fig. 5). There was sufficient instrumentation along the sample conditioning line so that the gas sample temperature could be maintained at the required 422°K (760°R), and instrumentation was also available to sense the probe structural temperature so that sufficient cooling water flow was maintained.

The impact pressure in the exhaust stream, PTJ, was measured with the sample probe and was recorded by a transducer located just below the lower probe strut assembly. The flow of the gas sample was stopped by valves located in the sample line at the bellows pump inlet when an exhaust impact pressure survey was being taken.

2.3.4 Gaseous Emission

The gaseous emissions contained in the engine exhaust were measured with seven instruments designed to identify and measure the concentration of six gas constituents. A photograph of the instrument console is shown in Fig. 10. The constituents measured were total unburned hydrocarbons (THC), nitrogen oxide (NO), nitrogen dioxide (NO_2), oxides of nitrogen (NO_x), carbon monoxide (CO), and carbon dioxide (CO_2). The instruments used employ various techniques to measure the consituents of interest, and each is briefly described below. Each instrument is identified in Table I (Appendix II). A more detailed description of the operating principles of the instruments can be found in Ref. 4.

2.3.4.1 Hydrocarbon Measurement

Unburned hydrocarbons were measured with the Beckman Model 402 Hydrocarbon Analyzer. This instrument is classified as a flame ioniza ion detector (FID) and utilizes a hydrogen-rich flame through which the sample gas is passed. The unburned hydrocarbons in the sample gas are burned and an increase in ionized particles results. The ions are collected on a plate inserted in the area just above the hydrogen flame. An electrical current proportional to the hydrocarbon concentration is induced on the collector plates by the ionized hydrocarbons. The magnitude of the current is amplified and measured for concentration calculation. The current magnitude is also displayed on a meter located on the analyzer console for test monitoring. A schematic of the hydrocarbon instrument is presented in Fig. 11a.

2.3.4.2 Oxides of Carbon Measurement

The instruments used to measure concentrations of carbon monoxide and carbon dioxide are classified as Nondispersive Infrared (NDIR) detectors. This type of analyzer uses an infrared source, sample and reference cells, a detector, and an electronic signal processor. Figure 11b is a schematic of a typical infrared detector. An infrared light is shown to a detector through two cells containing gas. The gas in the reference cell (nitrogen) is nonabsorptive in the infrared band while the sample gas passing through the other cell absorbs energy proportional to the values of CCO or CCO_2. Because of the energy absorption in the sample, the gas within the two detector chambers is unevenly heated, and a pressure difference results. This pressure difference is proportional to the concentration of the compound of interest in the sample cell.

Three nondispersive infrared detectors were used to measure CCO and CCO_2. Two of the instruments, Beckman 315B and 315BL, measured CCO. The difference in the two instruments lies in the length of the cells. The longer cell length is used to measure lower values of CCO. The CCO_2 was measured with a Beckman 315B. The long cell instrument was not necessary for CCO_2 measurement because the value of CCO_2 in a turbojet exhaust is always very high.

2.3.4.3 Oxides of Nitrogen

A chemiluminescence analyzer was used to determine the values of nitrogen oxide (CNO) and the oxides of nitrogen (CNO_x). This analyzer utilizes the principle that ozone (O_3) when combined with certain compounds produces a luminous emission. The emitted light is proportional to the number of reacting molecules which can be related to constituent concentration if pressure, temperature, and flow rate are maintained constant through the analyzer, and an excess of O_3 exists.

Both CNO and CNO_x were measured using a Thermo-Electron Corporation (TECO) 10A chemiluminescence instrument. The instruments differed only in that for the CNO_x measurement the instrument had a CNO_2 to CNO converter which broke CNO_2 down to CNO. A schematic of the TECO 10A analyzer is shown in Fig. 11c.

2.3.4.4 Nitrogen Dioxide (NO_2)

A nondispersive ultraviolet (NDUV) analyzer (Beckman 255 BL) was used to measure the value of CNO_2. This type of analyzer is similar to the nondispersive infrared analyzer described earlier with the exception that an ultraviolet light source replaces the infrared source, and the light beam energy is measured directly using a photo cell detection device rather than sensing pressure changes as described in the infrared system. The ratios of the received energy from the two beams is proportional to the value of CNO_2 in the sample gas. A schematic of the NDUV analyzer is presented in Fig. 11d. All emission instruments operated well except the NDUV. The physical method of measuring the signal was sensitive to many things. The limitations of this instrument is discussed in Appendix III.

2.3.5 Particulate Emission

Two methods of determining particulate concentration in the turbojet emission were used. The two methods are described below.

2.3.5.1 Gravimetric Filters

Five-micron absolute filters which had been autoclaved and weighed prior to use were employed in conjunction with a gas flow totalizer (wet test meter) to determine the weight of particulates per standard cubic foot of emission gas (Fig. 10). The total particulate accumulation was determined by substracting the weight of the exposed filter from its weight prior to use and by dividing this delta weight by the total gas flow passing through the filter.

2.3.5.2 Electrostatic Capture Grid

An electrostatic precipitator is used to charge the particles contained in the sample stream. These charged particles are drawn onto a grid of opposite charge and are captured. Particle size and distribution can be determined from the grid with the aid of an electron-microscope. Data were obtained by manual analysis which was performed by the DOT.

2.3.6 Gas Constitutent Measurement Variances

Table II presents the instrument accuracies based on information provided by the instrument manufacturer with the exception of the CNO, CNO_x, and CNO_2 instruments which were taken from Ref. 10. The nominal accuracies quoted are from ±1.0 to ±5.0 percent of full-scale reading depending upon the range of interest, which is within the accuracies specified by the SAE Committee E-31 (Ref. 6) for measurements excluding sampling technique inaccuracies.

All measurements of the gas concentrations will have inaccuracies introduced by the sampling technique. Some of the inaccuracies to be considered are interference in the

instrument caused by water present in the sampling gas, instrument sensitivity to constituents other than the constituent being measured by a given instrument and, in the case of nitrogen dioxide (NO_2) and carbon dioxide (CO_2), conversion in the sample line from the dioxide state to the monoxide state. Table III lists the results of NO_2 and CO_2 conversion checks conducted for this investigation. The gas was introduced at the sample probe, and measurements were taken at two gas sample line temperatures (150 and 300°F). Sample line temperature had a pronounced effect on the amount of conversion from NO_2 to NO; however, the effect of temperature was less pronounced on the conversion from CO_2 to CO. The conversion investigation conducted also revealed an effect of time on the percent of conversion. As time increased, the percent conversion for both NO_2 and CO_2 decreased. Insufficient data were taken, however, to make a definitive statement other than to observe that the phenomenon exist

Water interference and cross constituent interference checks (effect of one constituent on an instrument designed to measure another) were conducted, and no interference on any of the instruments was observed.

At the conclusion of the test, a commercial calibration gas cross-reference service was also used at the request of DOT to verify overall operation of the emission measurement system. This service provides gases having the same concentration of predetermined constituents to each of its users. The certified values of the concentrations are not made available to the user until after the results have been submitted to DOT. The concentrations were measured with the instrumentation system and calibration gases used during the test, and a report of the results was made to DOT. The results of the cross-reference service check show very good agreement in Table IV with the supplier as well as the majority of the users of this service (Refs. 11 and 12).

SECTION III
PROCEDURES

Prior to the test, a fuel sample was taken from the single batch of JP-5 fuel that was used during the test and was analyzed by the AEDC chemical laboratory to determine the hydrogen-carbon ratio and the trace element content. A report of this analysis is given in Table V. Military JP-5 fuel was used throughout the test program and is quite similar to commercial Jet A-1.

Engine inlet pressure and temperature settings during the test program were determined from the geopotential altitude values of the U. S. 1962 standard Atmosphere Tables.

Flow visualization of the engine exhaust was accomplished at tunnel stations 13.7 and 24.4 by the use of a shadowgraph for selected test conditions.

3.1 TEST OPERATION

During the tunnel starting sequence, the inlet was manually controlled with the spike extended and the overboard and ejector bypass doors open. After supersonic flow was established in the wind tunnel, which occurred at low tunnel total pressure, the tunnel pressure was gradually increased to the desired level, and the spike was gradually retracted to keep the inlet from operating too supercritically. When the tunnel was at the desired test conditions (Mach 2.00/65,000 ft, T_{t_∞} = 390°K (702°R) or Mach 160/55,000 ft, T_{t_∞} = 328°K (590°R)), the scavenging scoop suction was set, and the inlet spike was translated to the desired position. The ejector bypass door was then closed to set the inlet normal shock at the desired position. At the point, the inlet was placed in an automatic control mode so that the overboard bypass doors modulated automatically to maintain the inlet diffuser pressure, and hence, the normal shock position. At both the conditions, engine ignition was possible from the windmill condition with the JP-5 fuel required for the test. All testing was accomplished with the model at 0-deg angle of attack.

After the engine was brought to the desired power level (military or partial afterburning power), the exhaust gas sample probe was positioned into the exhaust gas stream, and data were taken at discrete locations in horizontal, vertical, and/or diagonal planes through the exhaust plume. It was normally possible to obtain data in a given plane of interest (10 to 15 data points) in one-half to one hour. This could be accomplished in one continuous time period for the military power settings; however, in afterburning power, it was not possible to maintain the engine setting for more than about 15 min without exceeding the engine skin temperature limits. Therefore, during afterburning, the engine was reduced in power after each four or five points for cooling. It normally required three periods at afterburning power to obtain one complete plume survey.

Care was taken to set the total fuel flow at the same level during each test period at a given power setting to ensure compatibility in the data when making various comparisons. Regular samples of the free-stream flow entering the inlet were taken to check the possible contamination of the tunnel air with the exhaust constituents which were not captured by the capture scoop. Measurements of the levels of CCO_2 and CTHC were used as indications of contamination.

3.2 GAS ANALYZER

The emission sample transport line was temperature conditioned to 422°K (760 ± 10°R) approximately four hours prior to testing and was maintained at that temperature throughout the test period. Calibration of the seven instruments for measuring the gas constituents was accomplished immediately prior to the start of the test period and at approximately two-hour intervals during the test period using calibration gases consisting of a mixture of known concentrations of each constituent of interest (CTHC, CCO, CCO_2, CNO, and CNO_2) in nitrogen. The calibration gas concentrations used in data reduction are presented in Table II. These certified calibration gases were provided by Scott Research

Laboratory, Plumsteadville, Pennsylvania. Instrument zero levels were set using a "zero" calibration gas which consisted of "bone-dry" (99.998 percent purity) nitrogen. A calibration curve on each instrument, provided by the manufacturer, which established a millivolt/concentration relationship for each instrument range was programmed into the on-line digital computer. A single point calibration on each instrument range was obtained with a calibration gas and was applied to the millivolt/concentration relationship.

The procedure followed during the test after the instruments were calibrated was to set the gas sample pressure at approximately 10.32 N/cm^2 (15 psia) using the bellows pumps (Fig. 8) and to check that the gas temperatures were maintained at 422°K (760°R) for the hydrocarbon instrument and at 339°K (610°R) for the remaining instruments. Once engine conditions and probe position were established, the analyzer instruments were observed until steady-state was established, at which point data were obtained through the on-line digital computer. At selected test conditions, sample bottles were also filled with exhaust gas for future analysis by the University of California at Los Angeles, California.

The free-stream gaseous emissions, CTHC and CCO_2, which were monitored regularly at the engine inlet station were found not to exist in significant concentrations during the test, except during long periods of afterburning power when a noticeable increase (10 to 20 ppmv) was noted in CTHC. The normal tunnel operating level produced approximately 10 ppmv. This influence on the data was minimized by limiting the engine power setting when in afterburning to 15 min. The free-stream levels of CTHC are noted on the results where it exceeded 20 ppmv.

3.3 PARTICULATE SAMPLING

The gravimetric filters used for determining particulate concentration were autoclaved, weighed, and placed in sealed pewter dishes by the AEDC Chemical Laboratory. After one of the prepared filters was placed in the filter holder, the gas flow totalizer was set to zero, and the gas sample flow was then established through the filter. Each filter remained in the filter holder until an entire probe survey (horizontal or vertical) was completed. After a probe survey, which required from one-half to one hour, the gas flow was terminated, the gas flow totalizer was read and recorded, and the filter was removed from the holder, replaced in the pewter dish, and sealed. The filters were then returned to the Chemical Laboratory for weighing to determine the mass of the particulates captured.

The electrostatic grids were prepared by the DOT and were sealed in test tubes. To obtain an electrostatic grid sample, the grid was removed from the test tube and was inserted into the retainer on the electrostatic precipitator. A potential of 40 v was maintained on the precipitator for a period of 60 sec while engine exhaust was passed through the unit. After the 60 sec, the grid was removed and sealed in the test tube once again. The exposed grids were returned to the DOT for analysis. A minimum of seven electrostatic grid samples were taken for either the horizontal or vertical probe survey at each engine power setting, Mach number/altitude condition, and axial probe location.

SECTION IV
RESULTS AND DISCUSSION

Exhaust emission data were obtained at three axial stations downstream of the nozzle exit of a J85-GE-5 turbojet engine [XP/DN = 0.22 (nozzle exit station), 9.3 (mid station), and 19.9 (aft station)] at two simulated flight conditions (Mach 1.6/55,000 ft and Mach 2.0/65,000 ft) for two engine power settings (military and partial afterburning). A theoretical calculation and measured total temperature profiles of the exhaust plume for Mach 2.0/65,000 ft are shown in Fig. 12. A discussion of the more significant results obtained is given in the following sections.

4.1 INLET/ENGINE CONDITIONS

The engine was operated at military power (92-deg power lever angle) and at partial afterburning power (107.5-deg power lever angle) which were held constant (constant fuel flow) throughout the test for each of the two free-stream test conditions. The inlet was operated at a fixed operating point for each free-stream Mach number. The nominal free-stream and engine/inlet operating conditions are listed in Table VI. Any slight variations in the inlet or engine operating conditions were essentially eliminated by the presentation of the data in the form of an emission index which normalizes the data. The steady-state distortion at the compressor face produced by the inlet is shown in Fig. 13 for the two Mach/altitude conditions.

4.2 GASEOUS EMISSIONS

The primary objective of the test was to determine the influence of an external supersonic free stream on the emission characteristics in the exhaust plume of a turbojet engine which was capable of operating at conditions similar to those of supersonic transports. One of the first steps taken to investigate the exhaust emissions was to calculate the expansion of the exhaust plume into an external supersonic flow field using known engine exhaust performance parameters. The plume boundaries and profiles shown in Fig. 12 were calculated using the procedure discussed in Appendix IV.

4.2.1 Comparison of Axial Probe Position

The variation of the emission characteristics for values of CCO, CCO_2, CNO_x, CNO, and $(CNO_2)_{CALC}$ shown in Fig. 14 for Mach 1.6/55,000 ft, follow the trends of the temperature in Fig. 14a. It is noted that a rather uniform distribution of these parameters exists at the nozzle exit station, but the concentrations and temperature decrease toward the outer edge of the plume for the mid and aft stations. This is the result of the mixing region that exists in the downstream plume. The concentrations of THC are not uniform at the nozzle exit for the military power setting (Fig. 14b) because of continued burning which occurs at a radial position equal to the location of the afterburner flame holders. Complete burning takes place on the nozzle centerline. The CTHC profile changes as the flow moves downstream in the plume.

Measured and calculated values of CNO_2 (calculated $CNO_2 = CNO_x - CNO$) are shown in Fig. 14d. Although the measured values of CNO_2 are in error for most of the data presented, they have been shown to give other investigators a feeling for the problems which occur in attempting this measurement using continuous sampling techniques with existing instrumentation. The performance of the CNO_2 instrument is discussed further in Appendix III. Corrections can be applied to some of the measured CNO_2 data by accounting for a zero drift initially and a contamination of the measuring cells beyond the centerline point for values of $-R_P/R_N$ (sampling moved from + to - values of R_P/R_N).

The calculated emission indices which are presented in Figs. 14e through g show similar trends to the concentrations results, however, the values of EI did not drop off to their free-stream values at the same value of R_P/R_N as did the concentration parameters. This is believed to be the result of the small magnitude of the parameters at military power, and because of the variations in CTHC. The emission index number which is discussed in Section 4.2.7 is a mass-flow integration of the concentration profiles (see Appendix V) and gives a more accurate number than can be obtained from a weighted average of the profile plots of the emission index.

4.2.2 Effect of Mach Number and Altitude

Although the results from only two Mach number and altitude test conditions are available for comparison, a comparison of the Mach 2.0/65,000 ft data in Fig. 15 with the Mach 1.6/55,000 ft data in Fig. 14 for military engine power shows some changes in the temperature and pressure profiles as a result of additional plume expansion at higher altitudes. In general, the oxides of nitrogen were higher for the Mach 2.0/65,000 ft conditions, but the CCO levels are nearly the same at the exit plane for the two conditions. The Mach 1.6/55,000 ft mid position CCO level was considerably higher than the Mach 2.0/65,000 ft level. This level was also higher than that obtained at the exit plane, and the reason for this is yet unexplained. There seemed to be little difference in the measured hydrocarbons for the two conditions. Plots of the emission indices show no appreciable change.

The same general comments made for a comparison of the data for a military power apply to the afterburning power data shown in Figs. 16 and 17.

4.2.3 Effect of Engine Power

A comparison of the military and afterburning power for either Mach 1.6 or 2.0 shows that the temperature on the nozzle centerline is slightly higher at the mid station (Fig. 16a). This can be accounted for by continued burning that occurs in the plume, as evidenced by the large reduction in THC on the centerline at the mid station. The additional plume expansion at Mach 2.0/65,000 ft also results in more of the hydrocarbons being burned as shown in Fig. 17b. The other concentrations follow very closely the variation in total temperature.

4.2.4 Effect of Radial Probe Position

A question of the validity of a single radial survey through the plume arose early in the test program. Because of this more than one radial across the plume at a given probe station was surveyed to obtain an accurate indication of the emission profiles. Figure 18 shows a three-dimensional comparison of the horizontal and vertical surveys at each probe station for Mach 1.6/55,000 ft. This shows a vivid variation in the profiles at the probe stations. To obtain a more accurate comparison of the variation of the concentrations at more than one plane at a given station, selected comparisons are made at each probe station. Figures 19 and 20 show these variations at Mach 1.6/55,000 ft for military and afterburning powers, respectively, at the exit station. Mach 2.0/65,000 ft data are also added to Fig. 20 for comparison. These show little if any variation in the emission characteristics at the nozzle exit, with the exception of the measured CNO_2 (Fig. 20d) whose results are in question.

At the mid probe station (Fig. 21), a change in the profiles is noted. It is believed that the decreased concentration at $+R_P/R_N$ for the vertical survey (which is in the top quadrant) is the nacelle strut effect. This is further verified by the pressure data in Fig. 21a. At the aft station, (Fig. 22) complete mixing has occurred to remove any noticable variation in the emission characteristics for the planes investigated.

4.2.5 Comparison with Sea-Level-Static Tests

A direct comparison of the wind tunnel exhaust emissions results reported here and the static results reported in Ref. 10 is difficult since the emission data reported in that reference were the first obtained at AEDC and used a different probe and instrumentation system. The data are presented here primarily to point out that emission data does exist for the General Electric J85-5 turbojet engine at both sea-level-static and high altitude flight conditions. Considerable experience was gained by the investigators of Ref. 10 as well as by the investigators of the emission measurements for the J93 turbojet engine (Ref. 5) which greatly aided in preparing for the test program reported herein.

The free-stream conditions and an estimate of the burner inlet conditions for the J85 turbojet engine used during the exhaust emission tests are given in Table VII. The pressure and temperature were calculated from data obtained for the J85 during earlier tests at AEDC. Also shown are the exit plane values of the emission indices for each free-stream condition at a military power setting. In general, with the exception of the carbon monoxide (CCO), the wind tunnel data are all lower than the sea-level data, at least in terms of concentration on a parts per million basis. Neither of the parameters shown will correlate all of the data; however, the parameter $\sqrt{p_i}\ T_i^3$ does give a fair correlation for the two wind tunnel data points (excluding CCO and CCO_2). It is worth noting that the emission index for CCO does follow the general trend of decreasing with increasing pT/v as shown in Ref. 13. This would indicate a lower combustion efficiency for the wind tunnel operating conditions. On the other hand, the unburned hydrocarbons emitted per 1000 pounds of fuel burned is considerably higher at the sea-level operating condition, indicating a less efficient combustion process.

Comparisons of the exit plane profiles for the gaseous emissions are shown in Fig. 23. The CCO_2 levels measured during the wind tunnel tests agree very well with those calculated from Eq. (V-7) (Appendix V) and the measured f/a, CCO, and unburned hydrocarbon concentrations. However, the measured value of CCO_2 at sea-level appears to be approximately 0.5 percent by volume higher than that calculated using the same procedure. The sea-level calculation was adjusted allowing for the small difference in the H/C ratio between JP-4 and JP-5 type fuels. The f/a ratio given in Ref. 9 for the military power setting was used in the calculation. Since the data do not correlate well, not a great deal of effort was expended in trying to reconcile differences or to search for more appropriate correlations.

4.2.6 Comparison of Experimental Data and Theoretical Predictions

The theoretical values of the properties in the plume were computed using the method described in Appendix IV. The analysis and theoretical calculations were performed and presented primarily to show consistency of the measured species and plume properties. As will be shown, the overall agreement between theory and experiment was good, and the experimental data can be seen to be very consistent at least in the trends which were measured. Several deficiencies exist in the theory which could be corrected, but such modifications were not within the scope of this project. As pointed out in Appendix IV, the turbulent mixing calculations made for the exhaust plume assume that the exit plane profiles (the plane from which the mixing layer calculations were started) are uniform. It is obvious from the data presented that this was not quite the case at military power and was never the case when operating the engine at a partial afterburning power setting. In making comparisons of the plume properties at the exit plane, an inviscid core flow is combined with the mixing region. The inviscid core flow was computed by a Method of Characteristics solution (Ref. 14) which has a uniform total temperature across the exhaust (i.e. ideal gas assumed at appropriate value of the specific heat ratio). Although theoretical calculations were made for the four conditions at which emission data were obtained, only the Mach 2.0/65,000 ft, military and partial afterburning conditions are shown. The agreement (or lack of agreement) is the same for the Mach 1.6/55,000 ft conditions. Figure 24 shows the comparison between theory and experiment for the three axial locations of the probe with the free-stream conditions of Mach 2.0/65,000 ft and military engine power setting. The engine parameters corresponding to this power setting are shown in Table VI. Shown in Fig. 24 are the variations of impact pressure, total temperature, and concentrations of carbon dioxide (CO_2), carbon monoxide (CO), and the oxides of nitrogen (NO and NO_x) with both exhaust plume radius and axial position. Figure 24a shows the comparison of the measured and predicted impact pressure. This parameter was presented to illustrate that a complex shock wave pattern may exist in the wind tunnel. The impact pressure (pitot pressure) is sensitive to Mach number through the pressure recovery and, hence is sensitive to expansions or recompressions in the flow. As a result, the agreement between experiment and theory is not good at the two down-stream probe positions. An estimate of the shock wave pattern which may exist is shown in Fig. 25, Unfortunately the shadowgraph coverage of a region approximately 3 ft square on the tunnel centerline, was not adequate to observe the shock waves as

pictured, with the exception of the Mach number 1.6 cowl lip-inlet spike reflection. This reflection passes just aft of the engine exit plane and was observed in the shadowgraphs obtained. The obvious question is whether the presence of reflected shock waves affect the concentration of pollutants in the exhaust plume. The good agreement shown in Fig. 24 shows no discernible effects of the shock wave structure. A comparison of the experimental with the theoretical results in Fig. 24 shows total temperature profiles in good agreement. The outer radius of the plume, where the temperature approaches free stream, was somewhat larger than that predicted by the theory. However, the radius of the plume implied by the point where the concentrations approach the free-stream levels agree very well with the theoretical prediction of the plume radius. The CCO reaches a peak at a higher value at the plume centerline for the probe in the mid position than at the exit plane. The frozen chemistry assumption does not appear to hold for the CCO in the inviscid portion of the plume. The CCO_2, CNO, and CNO_x agree very well with the theoretical predictions and exhibit classical fully mixed plume profiles. There does not appear to be any afterburning in the exhaust plume because of the low levels of unburned hydrocarbons that were measured. No comparison of the hydrocarbons is made since the levels measured are near the lower limit where the flame ionization technique can be considered reliable and are also near the free-stream level of the wind tunnel. The static temperature and flow velocity are shown in Figs. 24g and h. Both the static temperature and flow velocity are computed from the experimentally measured values of the impact pressure and the total temperature measured by the method described in Appendix V for computing the emission indices. The results show that agreement of the profiles at the exit plane is not very good, but as the plume mixing continues the theoretical calculations are in better agreement. There are two sources of possible error in obtaining the static temperature and flow velocity: one is in the inaccuracies in the theoretical analysis, and the second is the inaccuracies involved in computing properties in front of the shock wave from the measured impact pressure and total temperature. The centerline decay of the concentrations and the total temperature are shown in Fig. 26 compared with the theoretical predictions. Again, except for two data points, the plume properties agree quite well with the turbulent mixing calculations. Note that the plume becomes fully mixed at approximately 3.05 m (10 ft) downstream of the exit plane.

A comparison of the theoretical and experimental results is made in Figs. 27 and 28 for the Mach 2.0/65,000 ft conditions and the partial afterburning engine setting conditions given in Table VI. Because of the continual combustion taking place outside the engine in the inviscid portion of the plume, there was very poor agreement between the theory and the experiment so that only a comparison of the impact pressure, total temperature, and CCO_2 are shown. In order to make accurate theoretical predictions of the plume behavior, it becomes necessary to take into account the effect of combustion on the conditions at the internal boundary of the mixing region. It is interesting to note that the plume appears to become fully mixed in approximately the same axial distance for afterburning as the military case. Once the plume is mixed, it behaves similar to the military case for the downstream positions. If the profiles at the mid and aft probe positions and the plume radius are normalized with the centerline values of the properties, they agree with the corresponding normalized theoretical profiles. The effect of afterburning

on the concentration levels and total temperature are shown clearly in Fig. 28 by comparison of the experimental and theoretical centerline decay of the flow properties.

An additional check on the validity and consistency of the afterburning data can be made by comparing either the fuel-air ratio implied from the measured CO_2, CO, and unburned hydrocarbons used in Eq. (V-7) of Appendix V, with that implied by the measured total temperature; or by comparing the CO_2 levels computed from Eq. (V-7) using the fuel-air ratio implied from the total temperature and the measured values of CO and unburned hydrocarbons. Figure 29 shows the CO_2 levels computed with those measured at the exit plane for the Mach 2.0 afterburning case. The fuel-air ratio necessary, at 100-percent combustion, to produce the measured total temperatures across the exhaust is obtained from combustion temperature versus fuel-air ratio curves for a hydrocarbon fuel with the same heating value as JP-5. The fuel-air ratios along with the measured CO and unburned hydrocarbons are substituted into Eq. (V-7). It is seen that the agreement is good both in level and shape, which implies that the measurements of total temperature, CO, and unburned hydrocarbon levels are consistent with one another. One additional comment might be made concerning the unburned hydrocarbon levels at the exit plane for the afterburning condition. Figure 17b shows a local fuel-air ratio of approximately 0.0078 at the centerline of the engine. If one computes the temperature rise that results from the combustion at that fuel-air ratio and adds that to the centerline value of the exit plane temperature (from Fig. 27, TTJ = 2040°F) a value of 2600°R is obtained. It can be seen from the middle position profile in Fig. 27 that a value of approximately 2570°R was measured, indicating that combustion was nearly complete at the centerline before the exhaust plume became fully mixed.

Finally, it should be noted that all of the experimental data that have been compared with the theoretical predictions were obtained with the probe being swept in the horizontal plane. Also these data are shown as distance from the tunnel centerline to which the probe was referenced. It can be seen that peak values of the plume properties are displaced from the tunnel centerline. It was found that the engine installation was slightly yawed ($\approx$ 0.3 deg) in the tunnel causing the plume to be off the tunnel centerline. The theoretical profiles were shifted so that the theoretical centerline values were matched with the peak values of the experimental data. The fact that the exhaust was slightly yawed can further be seen in the CO_2 of Fig. 24 by observing that levels to the left side of the tunnel centerline are slightly higher than the theory, thereby exhibiting the behavior observed when a jet is placed in a cross flow. The experimental data obtained at Mach 1.6 does not show as much skewness since the tunnel dynamic pressure was considerably higher and prevented the exhaust from penetrating the tunnel flow as much, thereby reducing the cross-flow component to almost zero.

4.2.7 Emission Indices

Since the plume profiles were not completely uniform, the emission indices were calculated using an integrated mass technique. The gas properties were calculated from the measured impact pressure and total temperature. The mass flux of the species being emitted was then divided by an integration of the experimental point-by-point values of CO_2, CO, and CTHC which respresented the fuel flow. The method and procedure

is described in Appendix V. This procedure is complicated by the relatively few experimental points taken across the plume which makes numerical integration difficult; however, it was felt that an integration of the emitted species provided a more realistic evaluation of the emission index. An analysis of the calculated emission index as a function of the axial distance from the exit plane provides information on the influence of external stream mixing on emission characteristics. If the emission index of a species is nearly constant as a function of axial position, then there has been a conservation of species and either no significant reactions have taken place during the plume mixing or no afterburning occurred outside the engine. Table VIII shows the values of the emission indices obtained at each axial location for each gaseous emission measured. (Values for the military case from Ref. 9 are shown for comparison.) Several observations can be made concerning the values shown starting with the first column and proceding across the table. The $EICO_2$ is, as expected, nearly constant since the CCO_2 level depends primarily on the fuel-air ratio and combustion efficiency. Very good agreement is seen at military power for Mach 1.6 and 2.0.

The EITHC at the exit plane is very low for military power although the Mach 2 conditions are almost a factor of two higher. The results show that the EITHC also increases with axial distance. This can be attributed to the entrainment of hydrocarbons from the tunnel flow, which for the military power setting had tunnel levels (6 to 10 ppmv) that were a significant fraction of those measured at the exit plane. An estimate of the increase in EITHC at the mid and aft probe stations for the Mach 2.0, military condition was made by using the tunnel levels of the THC measured at the engine inlet and the theoretical entrainment rates for the turbulent mixing calculations. The calculated EITHC values, considering those CHTC entrained (shown in parenthesis), show that the increase is not unexpected. The difference in the value calculated and that found by integrating the profile at the aft position is probably due to the fact that the theoretical plume rate is smaller than that used in the integration of the experimental data. This would give less entrainment, and hence, a lower value for EITHC. The level of the CTHC in the tunnel was not significant enough to affect the EITHC computed for the afterburning power setting. During afterburning power, the EITHC increased from the exit to the mid plane probe station. One possible explanation for this increase can be given even though combustion takes place. It appears that the engine may have emitted significant level of unburned hydrocarbons around the periphery of the nozzle that were not detected at the exit plane because the radial probe travel was limited. Evidence of this can be seen from Figs. 16b and 17b which show isolated points of high levels of unburned hydrocarbons out near the edge of the jet. These were mixed with the colder external stream and were not consumed during combustion. The unburned hydrocarbons were then mixed and subsequently measured at the next two axial locations. The most reliable EITHC for these particular conditions would probably be that measured at the aft position since the amount entrained from the tunnel flow was very much lower than the levels in the plume.

The EICO values are fairly consistent for a given power setting showing an increase with afterburning. At the present, no good reason can be given for the apparent increase in the CO levels at the mid position for the military conditions since no instrumentation errors occured during these measurements.

The emission indices of the oxides of nitrogen are almost the same for each axial location and show the correct trends between the different tunnel and engine conditions. The $EINO_x$ for each condition shown exhibits the best behavior as far as being constant for each axial location and, as discussed in Section 4.2.5, correlating with the parameters shown. Since trouble was experienced with the NO_2 instrument, the $EINO_2$ values are obtained for the CNO_2 levels computed from the measured CNO and CNO_x. This results in a well-behaved trend which follows the EINO and $EINO_x$.

It is felt that the emission indices given in Table VIII as computed from Eq. (V-5) Appendix V, are very reliable since any errors involved in numerical integration and in computing the gas properties tend to cancel out when the two integrals in Eq. (V-5) are divided. A check on the numerical integration was made by comparing the integrated fuel flows at the exit plane with those measured by a flowmeter during the engine operation. The best agreement was a calculated fuel flow within 2.7 percent of the measured value at the Mach 2.0 military condition, and the worst was a 20-percent difference at the Mach 1.6 military condition with the calculated values always being higher. These errors are traceable to not being able to properly define the edge of the plume where all of the flow properties return to their free-stream values.

4.3 PARTICULATE EMISSIONS

The results of the particulate emission measurements using the electrostatic grid (Section 2.3.5) will be the subject of a later report by DOT. Although the analysis of the electrostatic grid with an electron-microscope are not available for inclusion in this report, DOT has reported verbally that initial analysis of the grids indicates a very low particle distribution. This agrees also with the gravimetric filter results. A very low ratio of particle weight to mass flow through the filter (g/SCF) resulted during the test with the highest weight-mass flow occurring at the nozzle exit station during afterburning. The results of the gravimetric filter analysis are shown in Table IX. An attempt was made to plot the results as a function of axial probe position, engine power, and test condition in Fig. 30. Although there is a general trend toward a decrease in the weight-to-mass flow ratio with axial position downstream of the nozzle exit, the results are inconclusive because of certain uncontrolled variables such as the amount of time the probe was at a given sampling point for each test condition. The requirement to cool the turbojet engine every 15 min during afterburning and the probability of generating a different particle distribution when a return to the power setting was made on a given survey also introduce a variable in the analysis.

During an investigation of the particulate emissions at static sea level for this same engine (Ref. 10), it was reported that no visible smoke was produced. Posttest inspection of the sample line also revealed no major accumulation of carbon deposits.

SECTION V
SUMMARY OF RESULTS

The exhaust emissions were measured at three axial stations in the exhaust plume of a J85-GE-5 turbojet engine while operating at two simulated high altitude test conditions with a supersonic external stream. Two Mach numbers and two engine power settings were investigated for each axial sample probe position. A continuous sampling technique was used to measure the emission constituents. The experimental data were compared with theoretical predictions of the emission characteristics. The major results of the test program are summarized below:

1. The consitituents of the exhaust including concentrations of carbon dioxide, carbon monoxide, total unburned hydrocarbons, oxides of nitrogen, and particulates were measured successfully at three axial stations (0.22, 9.3, and 19.9 nozzle diameters) downstream of the nozzle exit for both military and partial afterburning engine power at Mach numbers and simulated altitudes of Mach 1.6/55,000 ft and Mach 2.0/65,000 ft.

2. The mixing with the external free stream did not result in further reaction of the gas constituents, other than the conditions where combustion was occurring in the exhaust plume. A calculation of the emission indices at the three axial stations in the exhaust plume indicate that no significant reaction of the oxides of nitrogen occurred.

3. The effect of the external supersonic stream and resulting mixing on the exhaust emission concentrations was predicted theoretically and was in good agreement with the experimental concentration profiles. This should provide validity to the experimental results.

4. The existence of the reflected shocks in the tunnel had no discernible effect on the emission concentrations.

REFERENCES

1. Grobecker, A. J. "Climatic Impact Assessment Program." Presented at the Second Conference on the Climatic Impact Assessment Program, November 14-17, 1972.

2. General Electric Company. "Model Specification E1023-B, Engine Aircraft, Turbojet J85-GE-5." June 30, 1960.

3. Cubbison, R. W., Meleason, E. T., and Johnson, D. F. "Performance Characteristics from Mach 2.58 to 1.98 of an Axisymmetric Mixed-Compression Inlet System with 60-percent Internal Contraction." NASA TM X-1729, February 1969.

4. Grissom, J. L. "Instrumentation and Measurement for Determination of Emissions from Jet Engines in Altitude Test Cells." AIAA Paper No. 72-1068, Presented at the AIAA/SAE Eighth Joint Propulsion Specialist Conference, November - December 1972.

5. Davidson, D. L. and Domal, A. F. "Emission Measurements of a J93 Turbojet Engine." AEDC-TR-73-00.

6. SAE Committee E-31. "Procedure for the Continuous Sampling and Measurement of Gaseous Emissions from Aircraft Turbine Engines." ARP 1256, July 12, 1971.

7. Cubbison, R. W., Meleason, E. T., and Johnson, D. E. "Effect of Porous Bleed in a High Performance Axisymmetric, Mixed-Compression Inlet at Mach 2.50." NASA TM X-1692, November 1968.

8. Coltrin, R. E. and Choby, D. A. "Steady-State Interactions from Mach 1.98 to 2.58 between a Turbojet Engine and an Axisymmetric Inlet with 60-Percent Internal Area Contraction." NASA TM X-1780, April 1969.

9. Lazalier, G. R. and Gearhart, J. W. "Measurement of Pollutant Emissions From an Afterburning Turbojet Engine at Ground Level, Part II. Gaseous Emissions." AEDC-TR-72-70 (AD747773), August 1972.

10. Siegel, R. D. "Measurement of Aircraft Engine Pollutant Emissions." Journal of the Air Pollution Control Association, Volume 22, No. 11, November 1972.

11. Scott Research Laboratories, Inc. "Nitric Oxide Cross Reference Service, Report No. 3, 1972." February 1973.

12. Scott Research Laboratories, Inc. "Diesel Cross Reference Service, Report No. 3, 1972." February 1973.

13. Briehl, D., Papathakos, L., and Strancar, R. J. "Effect of Operating Conditions on the Exhaust Emissions from a Gas Turbine Combustor." NASA TN D-6661, February 1972.

14. Prozan, R. J. "Solution of Non-Isoenergetic Supersonic Flow by Method of Characteristics." Lockheed Missile and Space Company, Huntsville Research and Engineering Center (LMSC-HREC D162220-I, II, III, and IV), July 1971.

15. Gearhart, J. W. and Benek, J. A. "Measurement of Pollutant Emissions from an Afterburning Turbojet Engine at Ground Level, Part I. Particulate Emissions." AEDC-TR-72-64 (AD744048), June 1972.

16. Patankar, S. V. "Heat and Mass Transfer in Turbulent Boundary Layers." Ph.D. Thesis, Imperial College of Science and Technology, Department of Mechanical Engineering, London, June 1967.

APPENDIXES

I. ILLUSTRATIONS
II. TABLES
III. NITROGEN DIOXIDE INSTRUMENTATION DEFICIENCIES
IV. THEORETICAL CALCULATIONS OF EXHAUST PLUME PROPERTIES
V. INTEGRATED EMISSION INDEX CALCULATION PROCEDURES

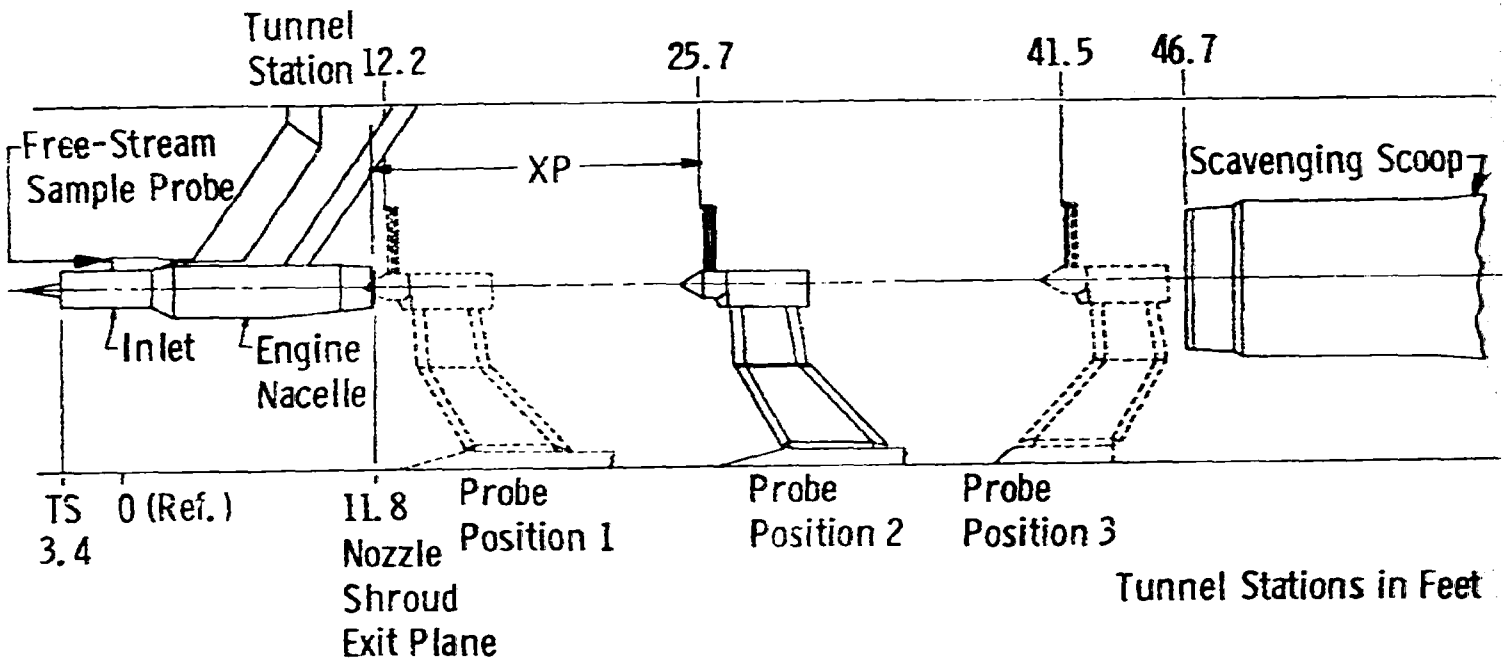

Fig. 1 DOT J85 Engine Exhaust Emissions Test Installation

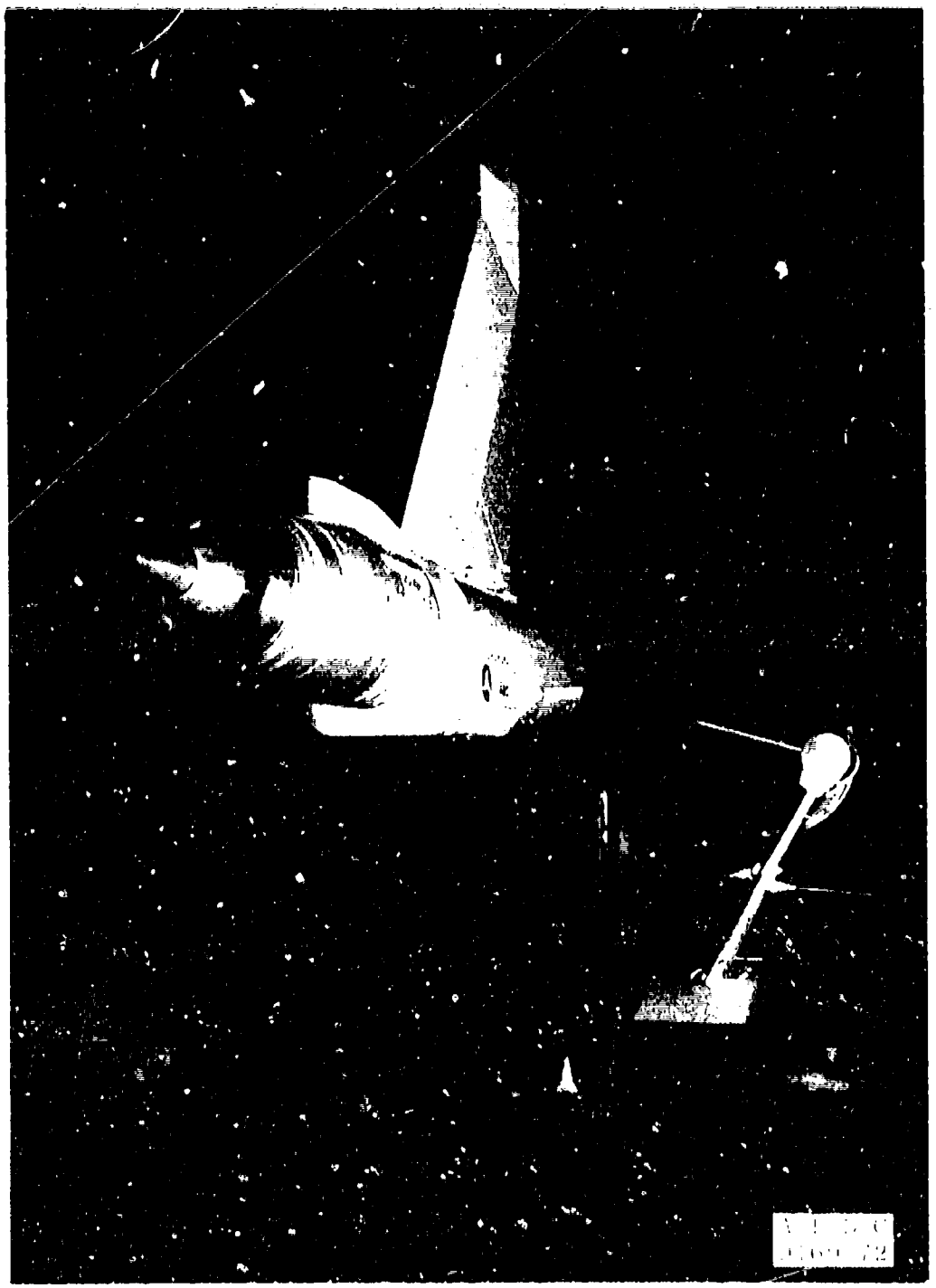

Fig. 2 Installation Photograph with Sample Probe at Position 2 (Mid Position)

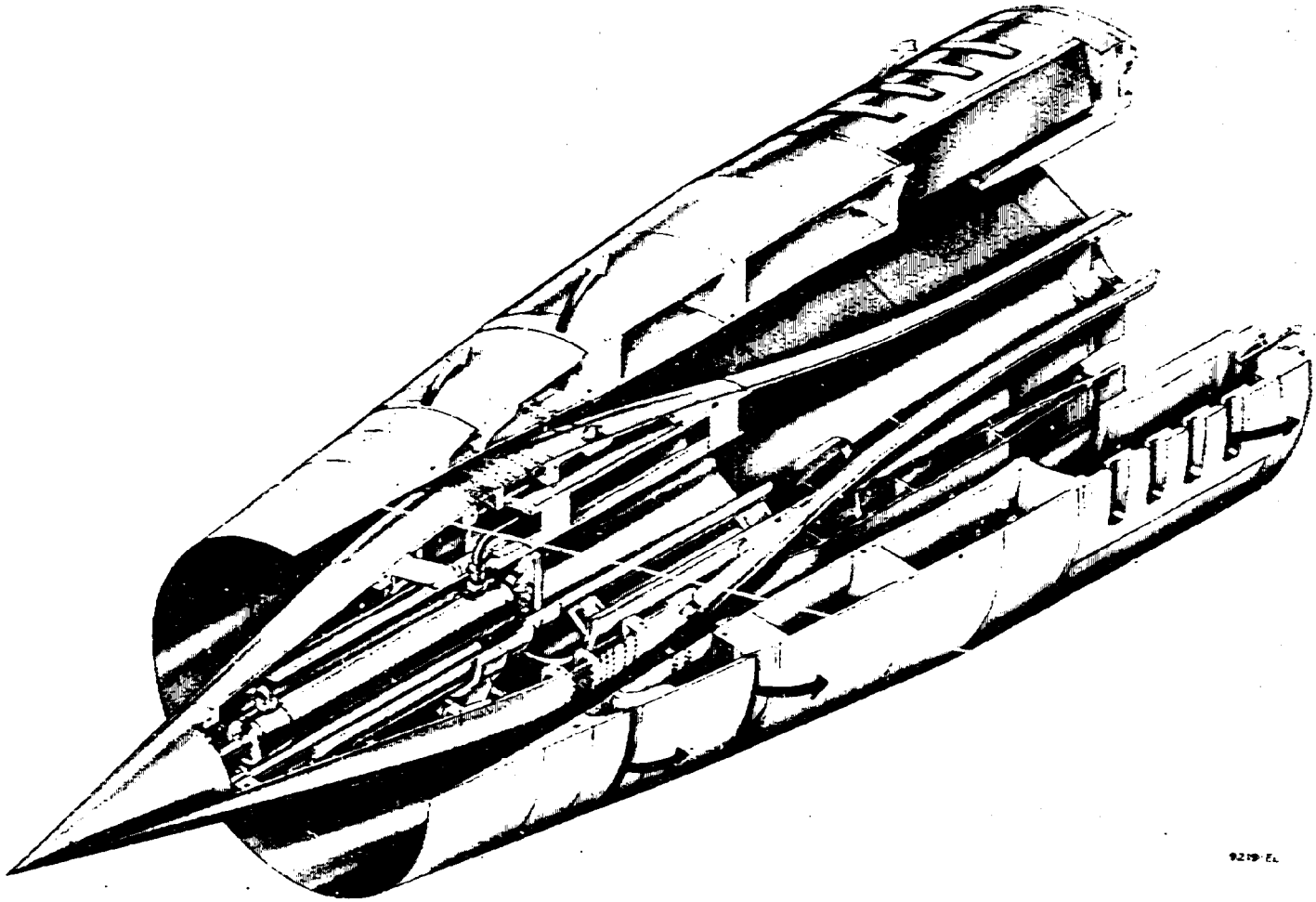

a. Isometric View (Courtesy of NASA Lewis Research Center)

Fig. 3 NASA/Lewis Mixed Compression Inlet

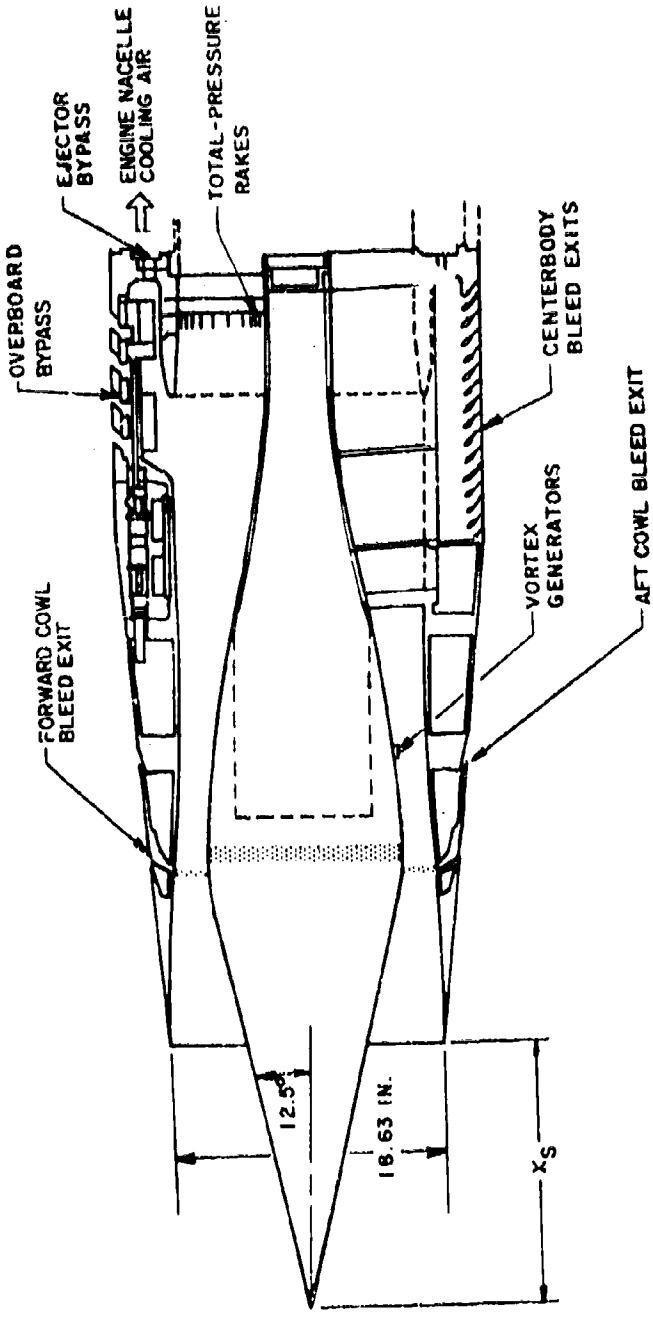

b. Schematic
Fig. 3 Concluded

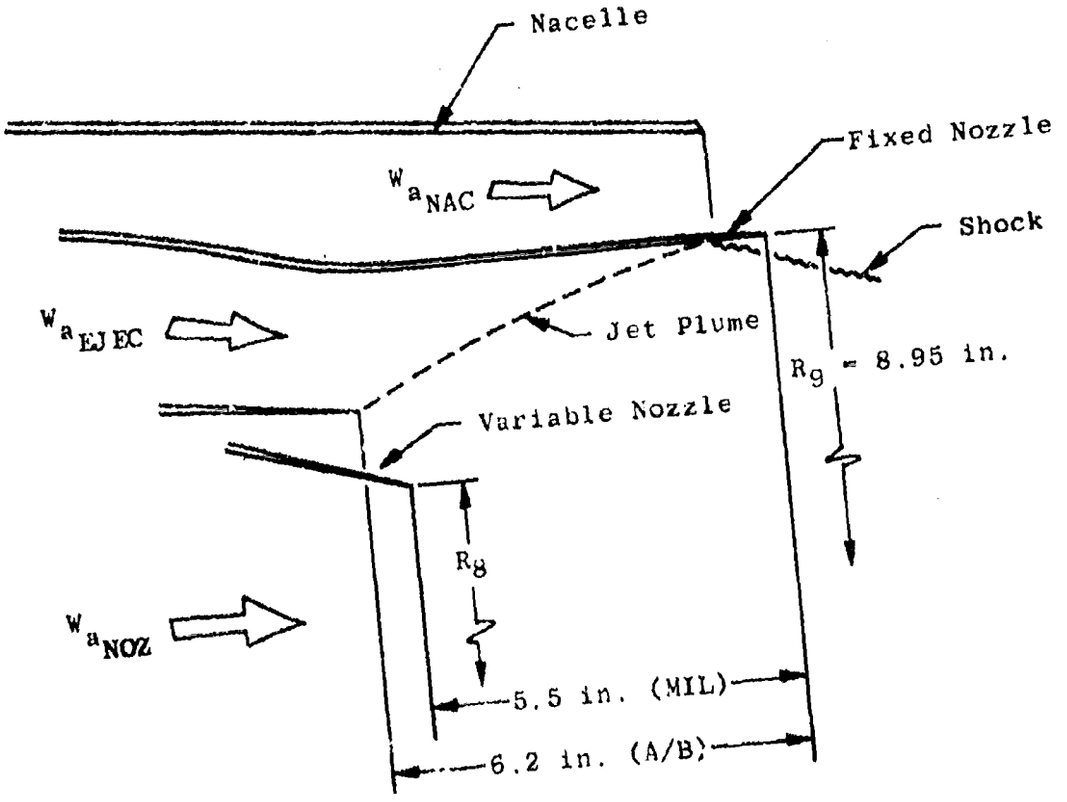

Fig. 4 J85-GE-5 Ejector Nozzle Shroud Schematic

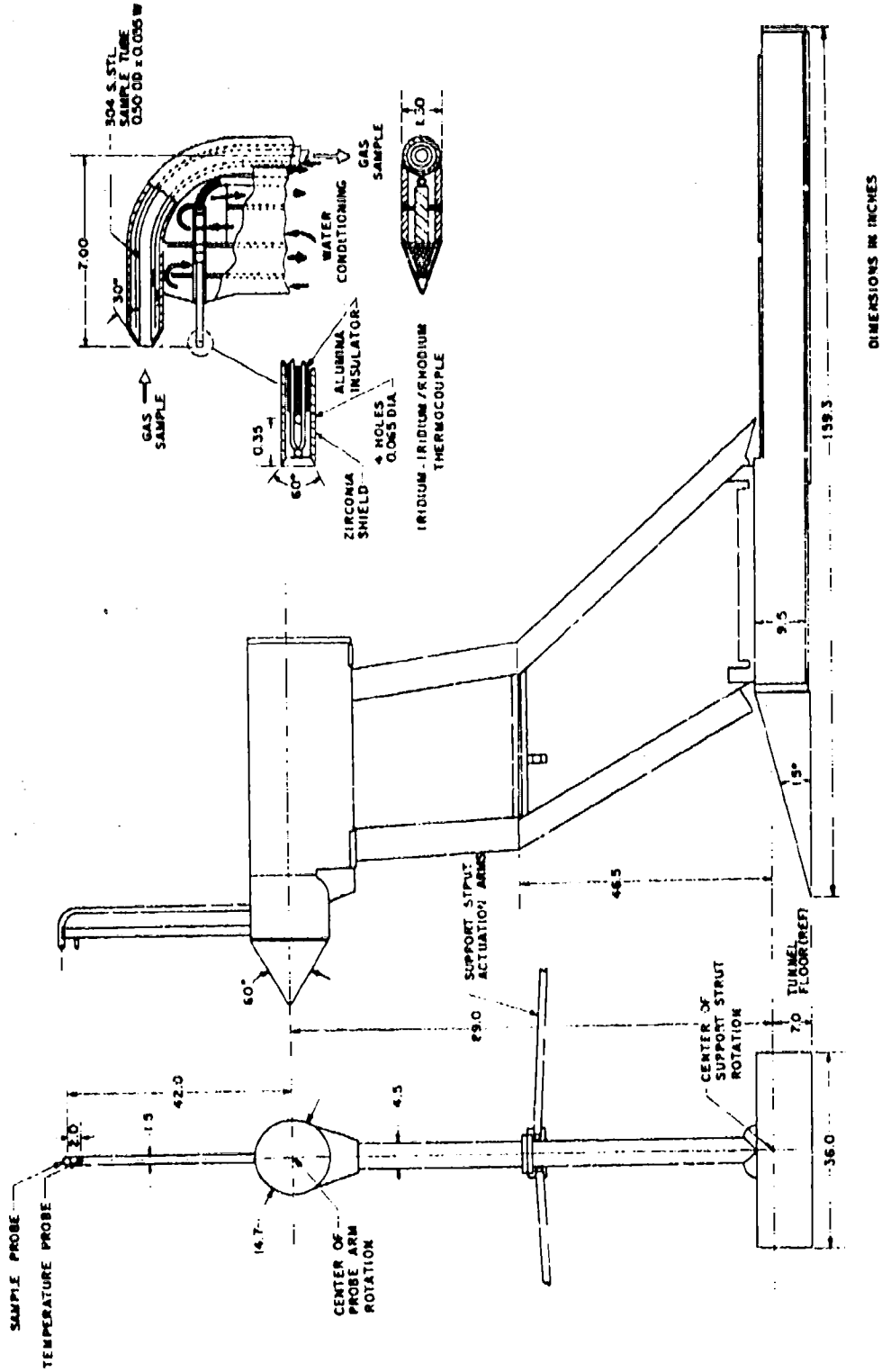

Fig. 5 Exhaust Emission Sample Probe Assembly

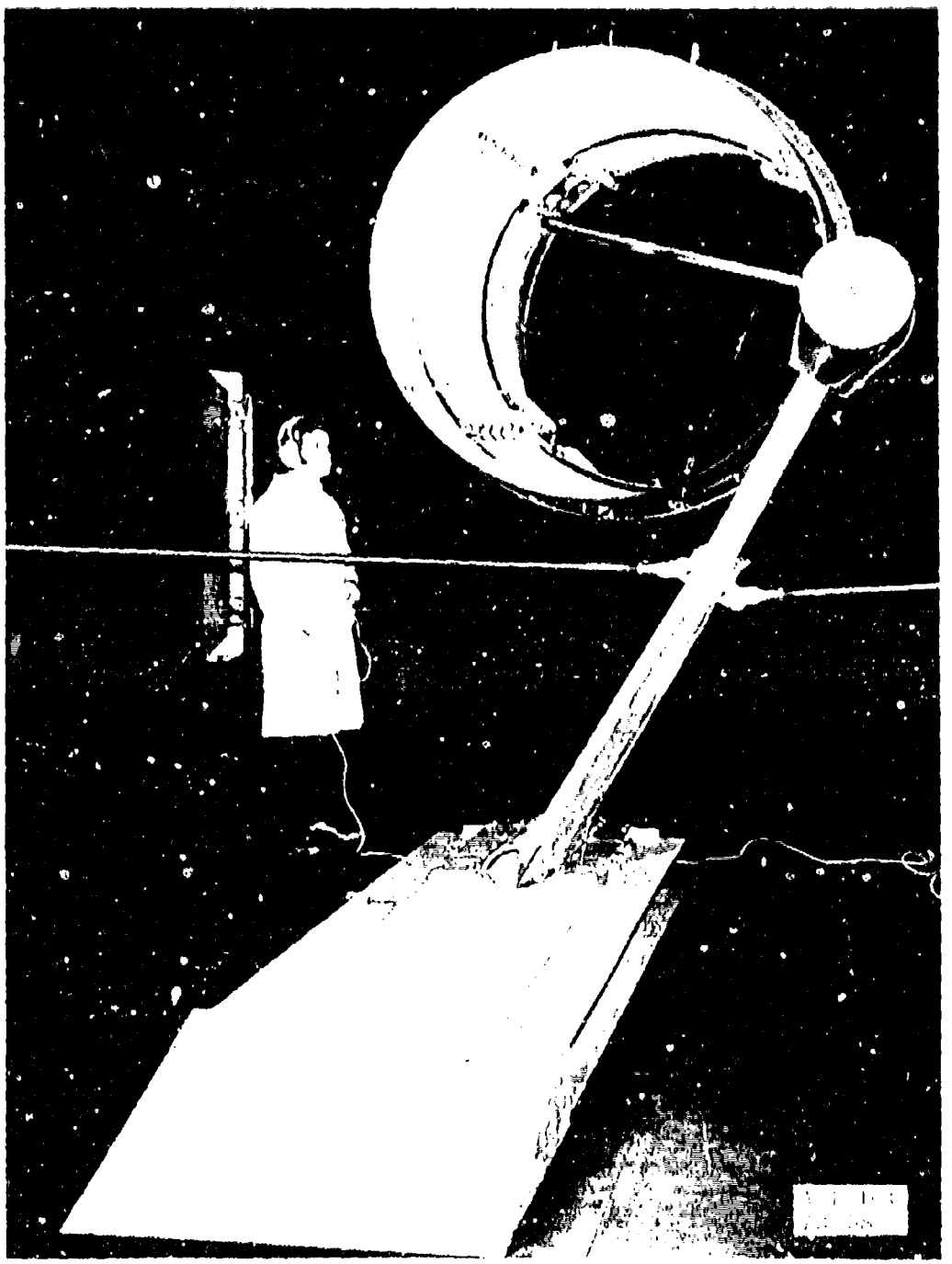

a. Axial Probe Position 3 (XP/DN = 19.9), Aft Station

Fig. 6 Sample Probe Installation

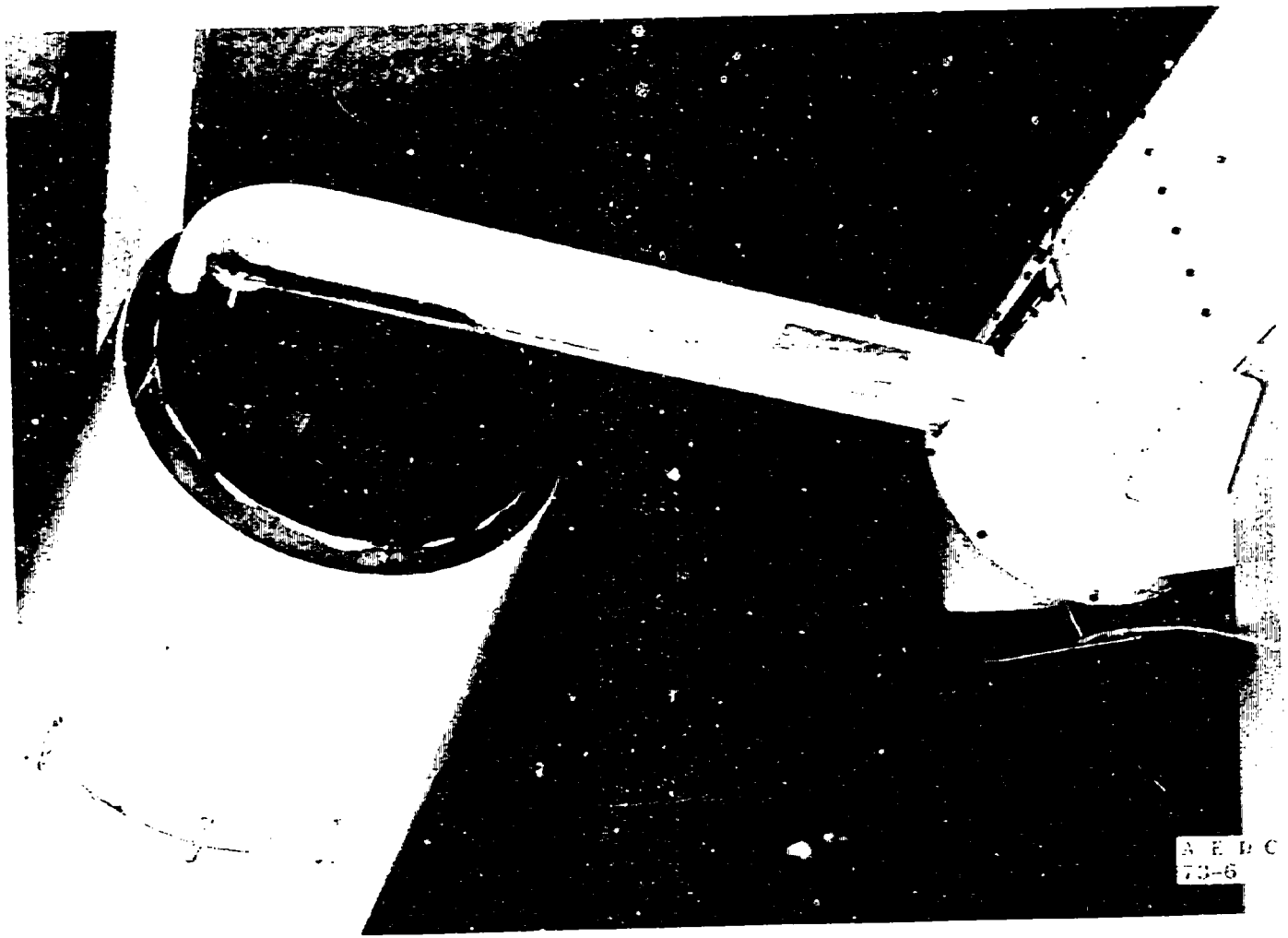

b. Axial Probe Position 1 (XP/DN = 0.22), Exit Station

Fig. 6 Concluded

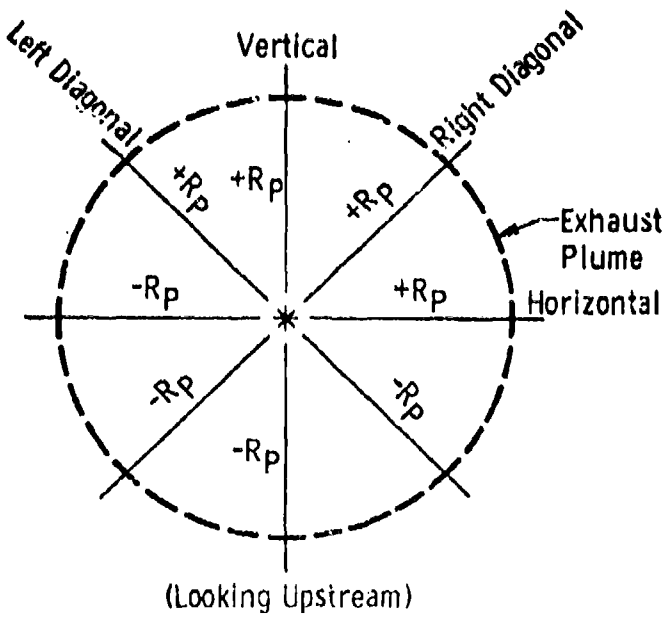

XP/DN	Plane of Survey, XR			
	M_∞ = 1.6/55,000		M_∞ = 2.0/65,000	
	Mil	A/B	Mil	A/B
0.22 (Pos. 1)	Horiz. Vert.	Horiz. Vert.	Horiz.	Horiz. R. Diag.
9.30 (Pos. 2)	Horiz. Vert.	Horiz. Vert.	Horiz. Vert.	Horiz. Vert.
19.90 (Pos. 3)	Horiz. Vert.	Horiz.	Horiz. Vert. L. Diag. R. Diag.	Horiz. Vert. L. Diag. R. Diag.

Fig. 7 Schematic of Exhaust Planes Surveyed at Each Axial Probe Position

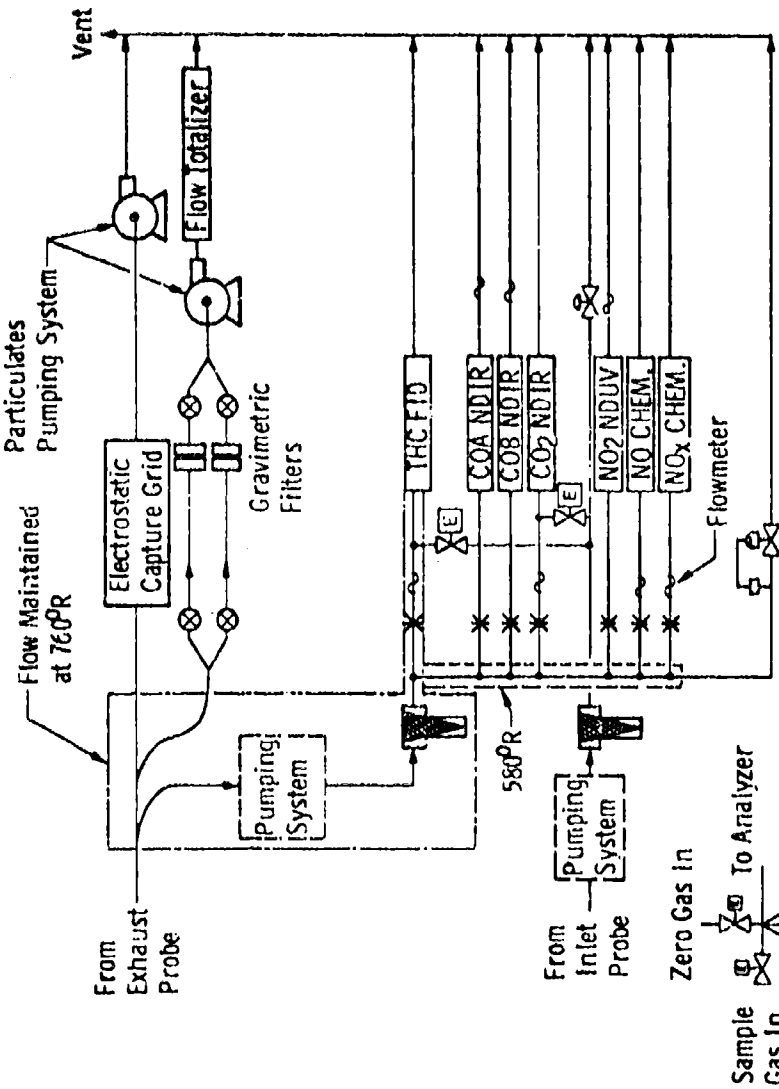

Fig. 6 Schematic of Sample Conditioning and Gas Analysis System

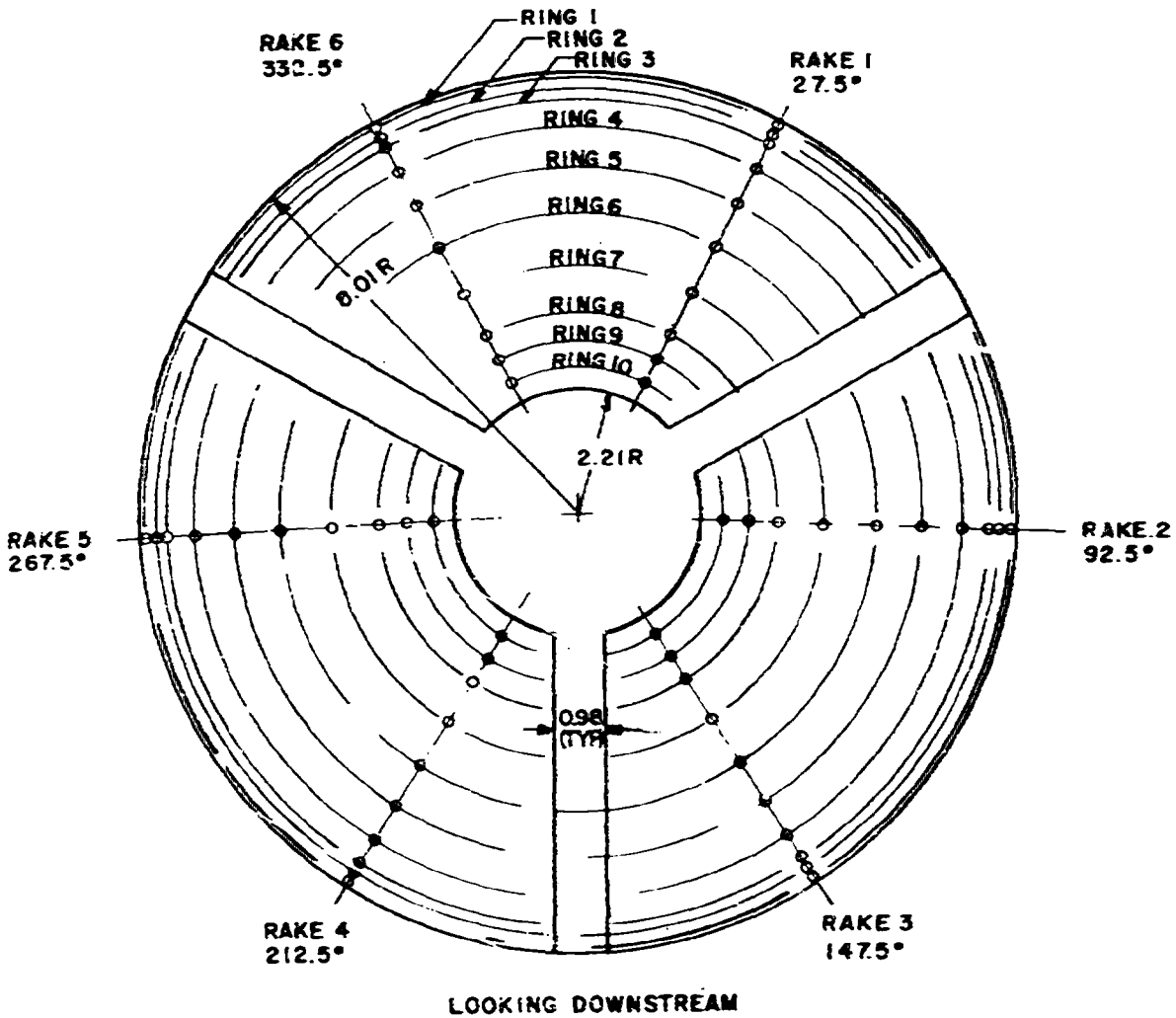

RING	RADIUS m(in)
1	0.201 (7.91)
2	0.196(7.71)
3	0.191 (7.50)
4	0.178(7.00)
5	0.159(6.26)
6	0.139(5.46)
7	0.113(4.46)
8	0.092(3.64)
9	0.080(3.15)
10	0.067(2.62)

Fig. 9 Compressor Face Total Pressure Instrumentation

AEDC-TR-73-103

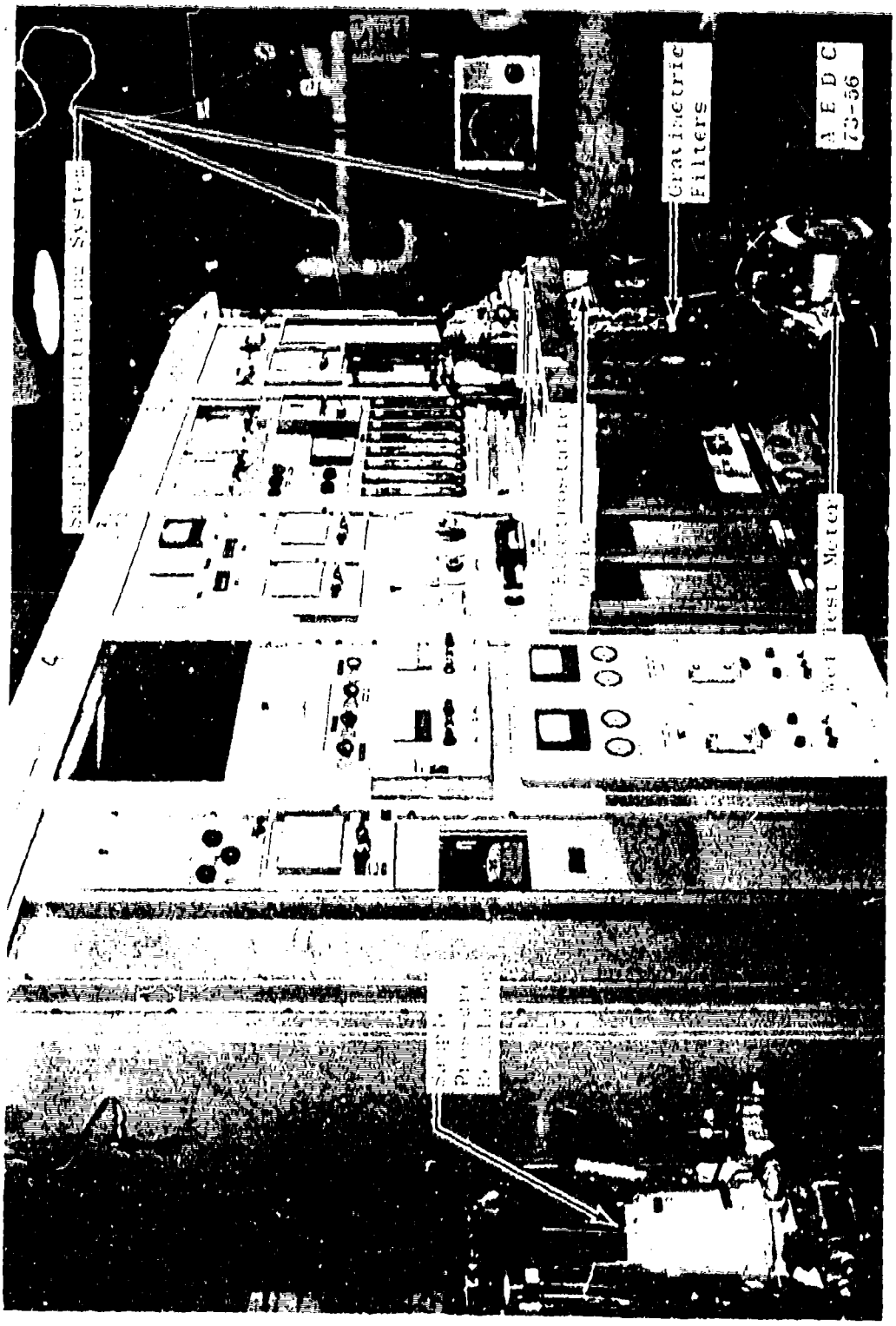

Fig. 10 Exhaust Emission Analyzer Console

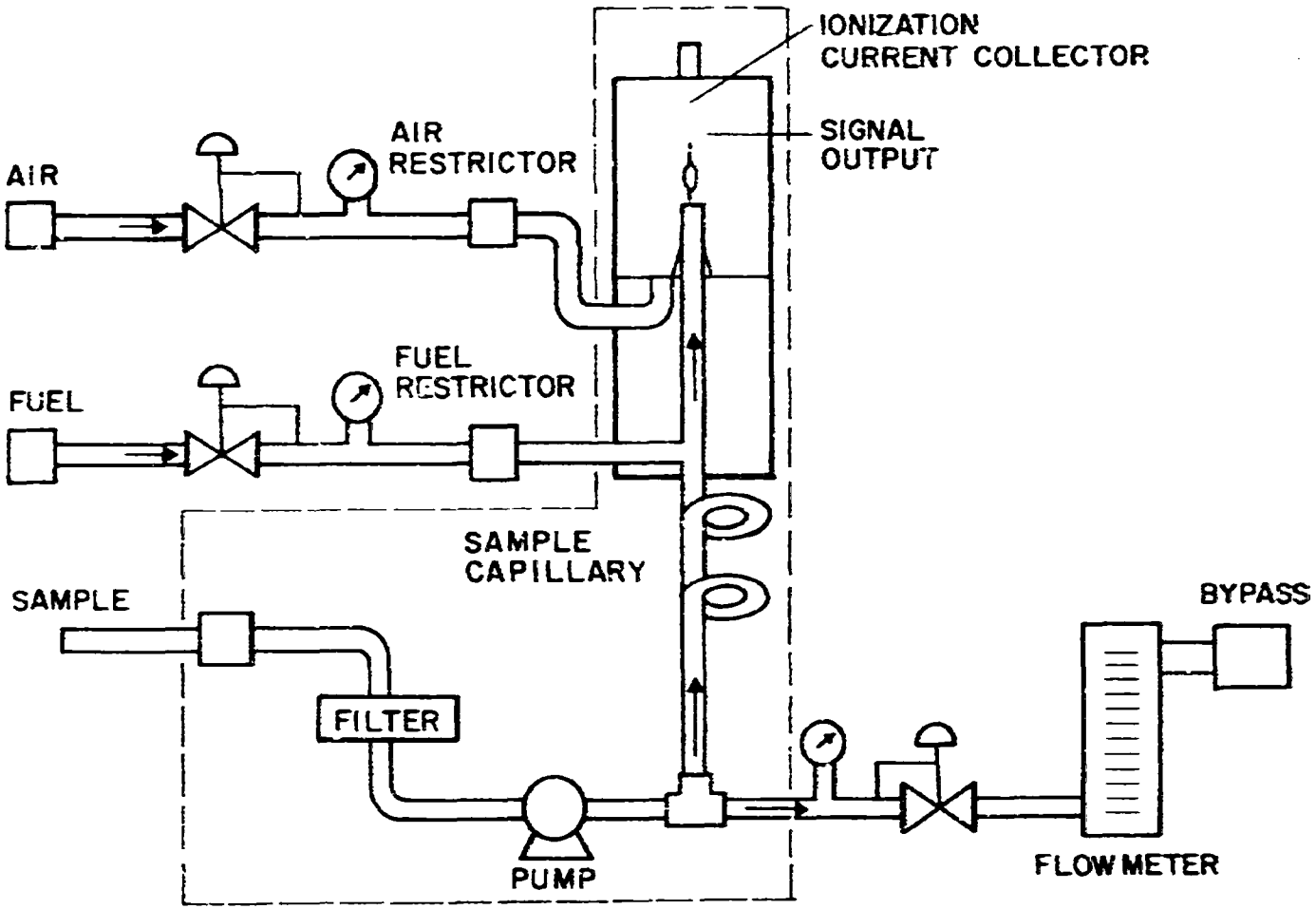

a. Flame Ionization Detector (THC)

Fig. 11 Exhaust Emission Instrumentation Schematics

AEDC-TR-73-103

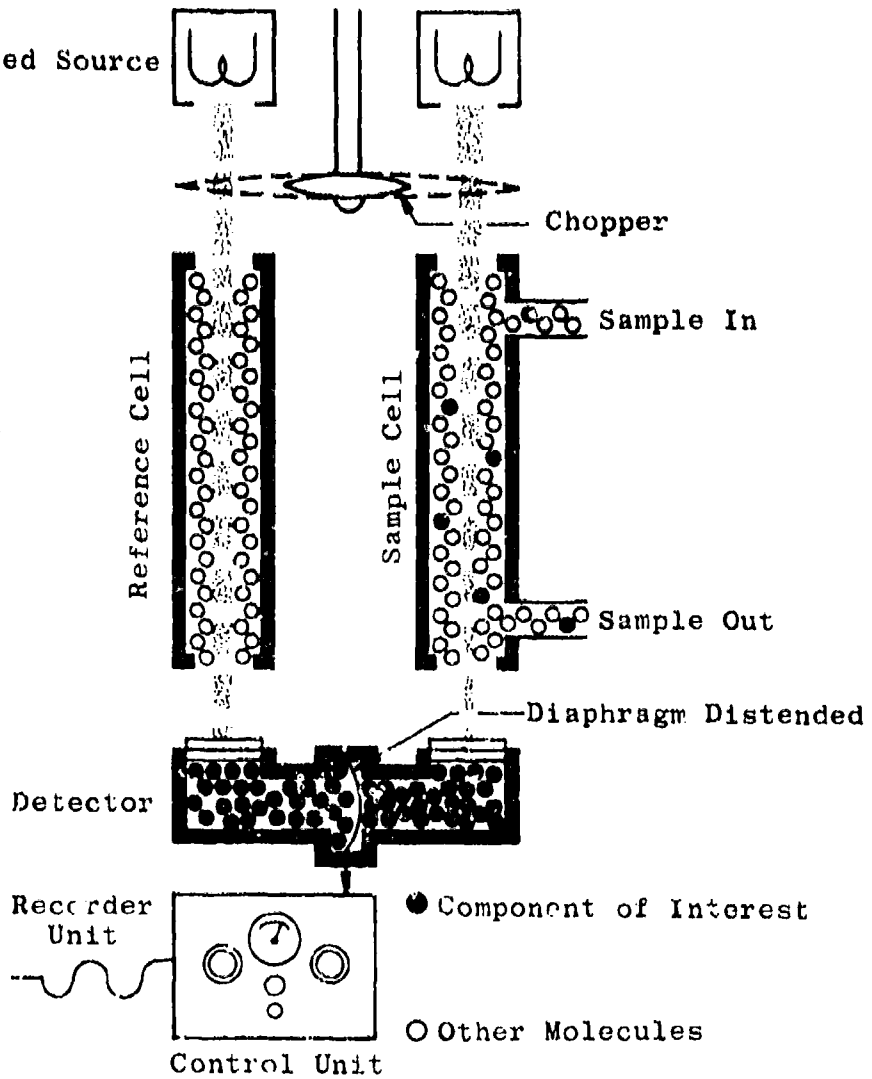

b. Typical NDIR Detector (CO, CO_2)
Fig. 11 Continued

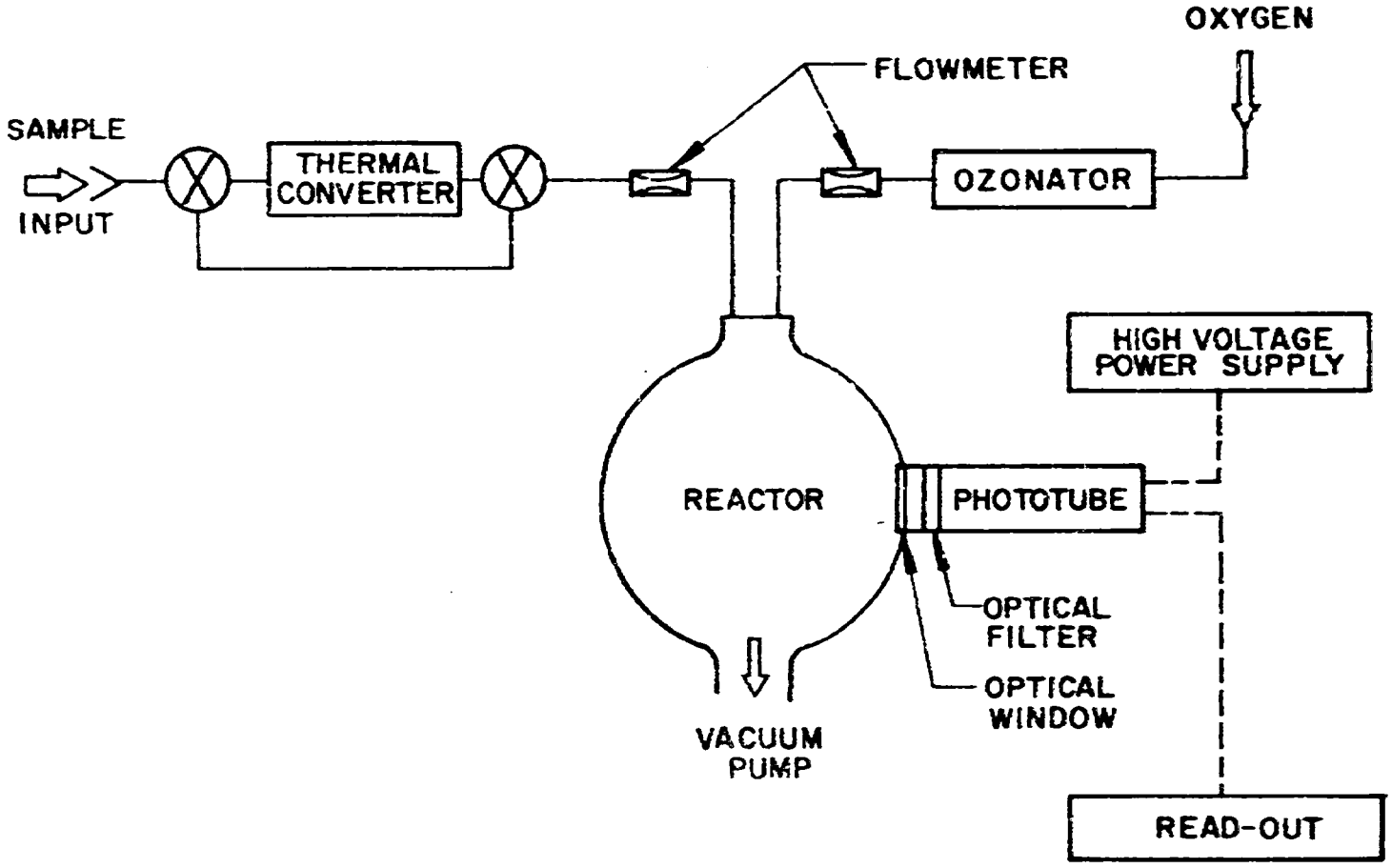

AEDC-TR-73-103

c. Chemiluminescence Detector (NO, NO_x)
Fig. 11 Continued

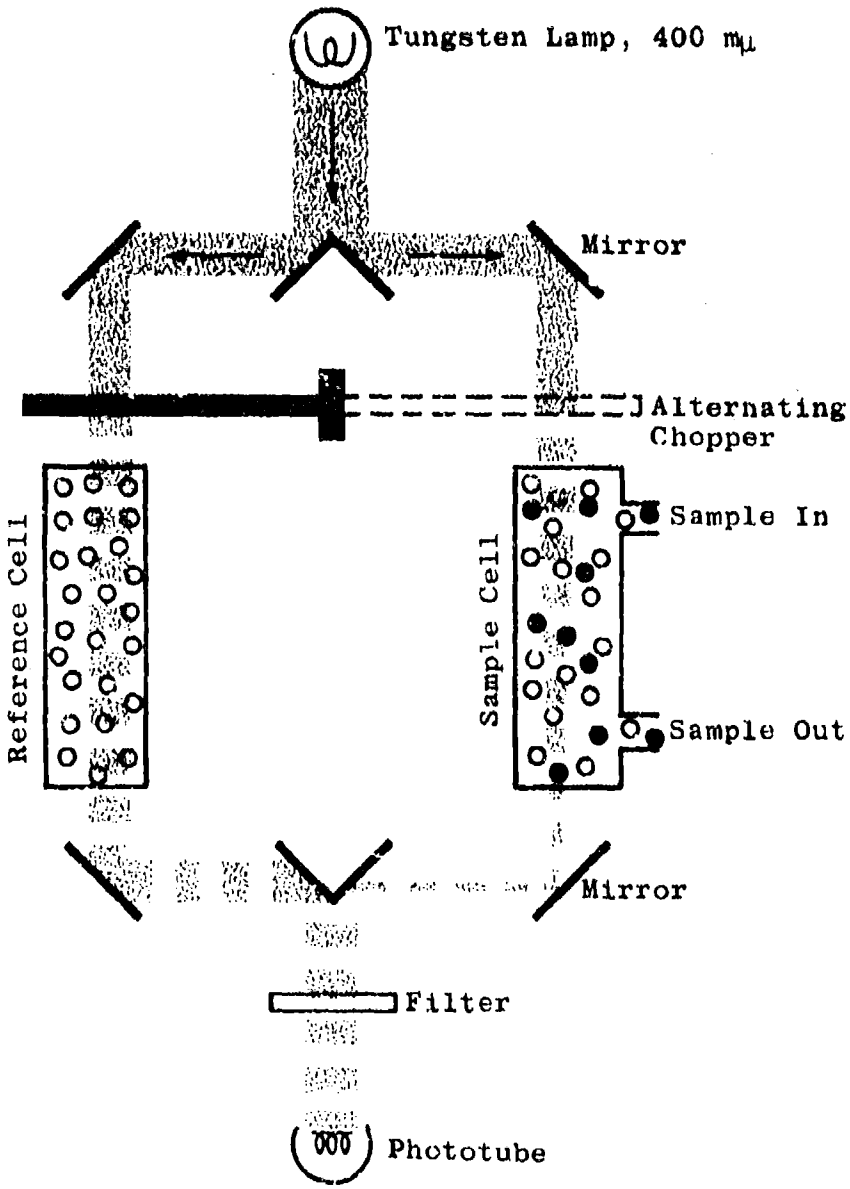

d. NDUV Detector (NO_2)
Fig. 11 Concluded

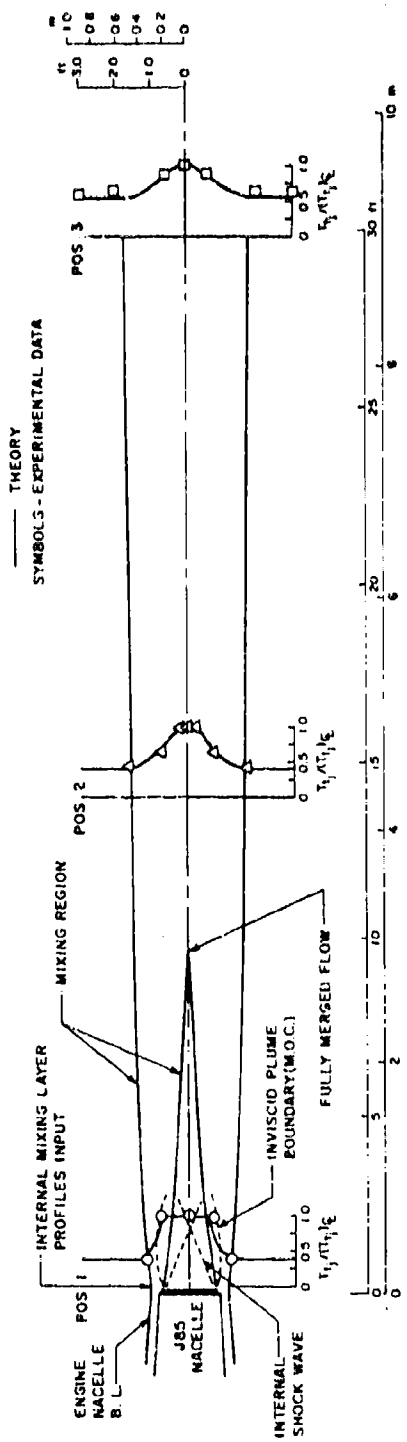

Fig. 12 Theoretical Plume Expansion with Typical Exhaust Temperature Profiles (Mach 2.0/65,000 ft, MIL)

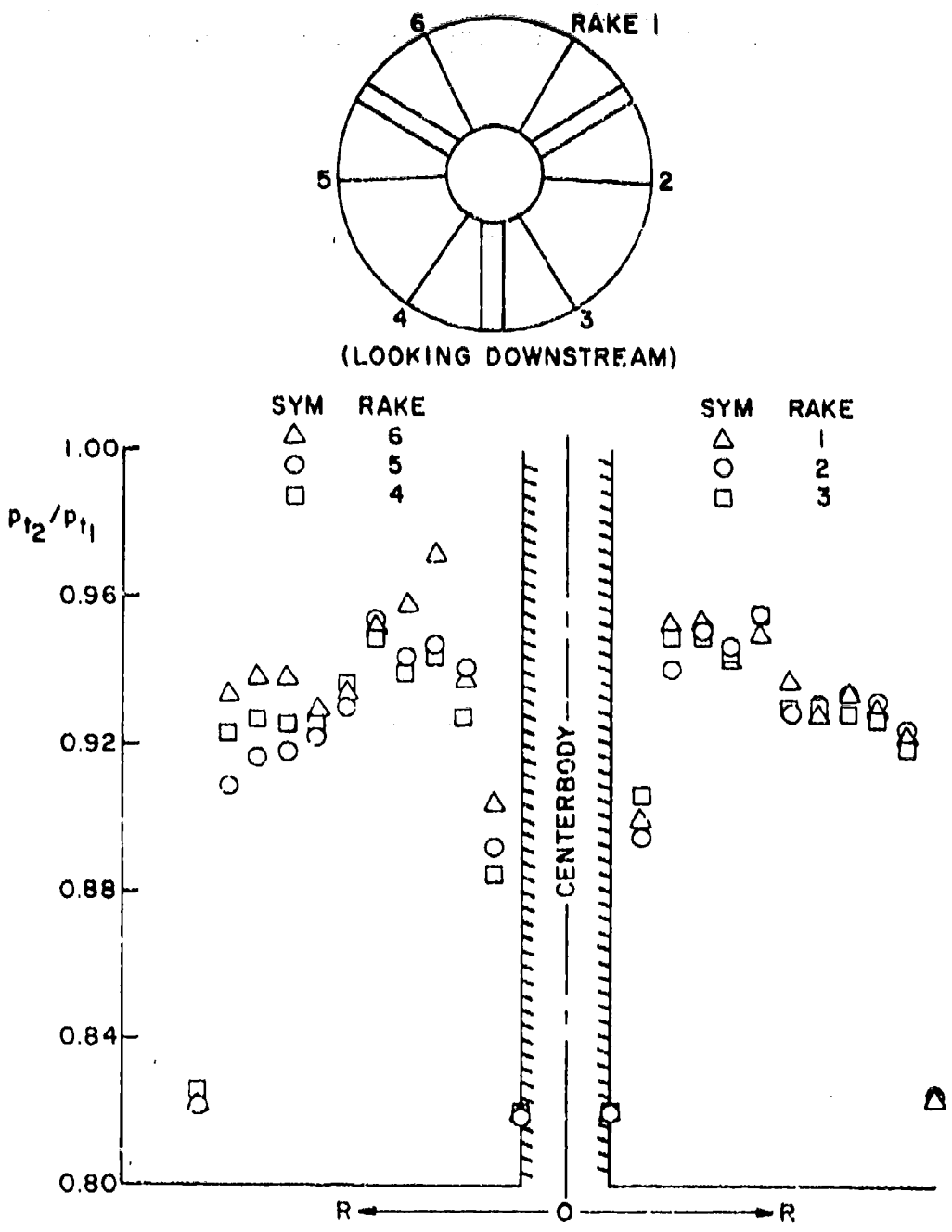

a. M_∞ = 1.6/55,000 ft

Fig. 13 Typical Pressure Profiles at Compressor Inlet

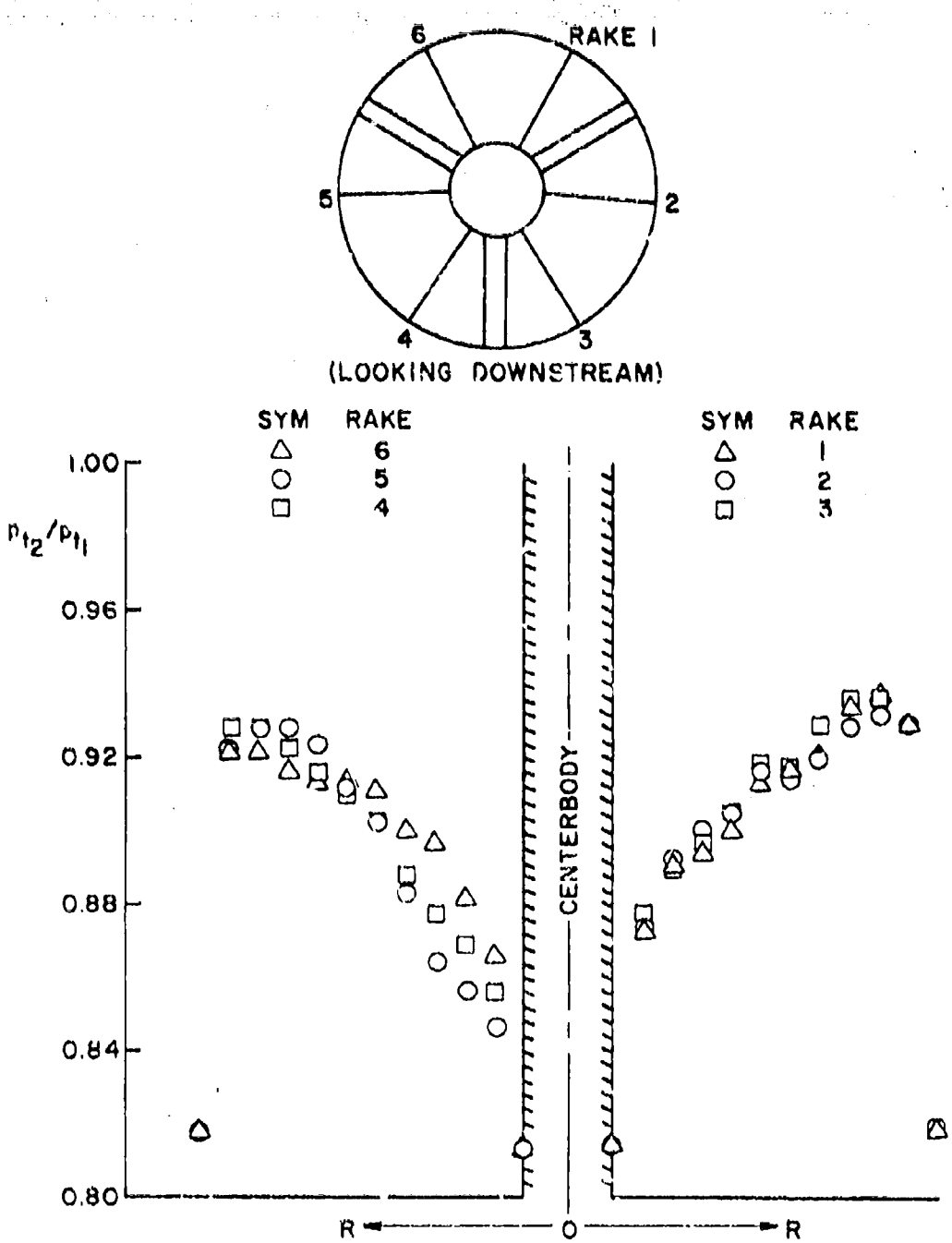

b. $M_\infty = 2.0/65{,}000$ ft
Fig. 13 Continued

SYMBOL	M_∞	ALT	PLS	XP/DN	XR
○	1.6	55K	MIL	0.22	HORIZ
△	1.6	55K	MIL	9.30	HORIZ
□	1.6	55K	MIL	19.90	HORIZ

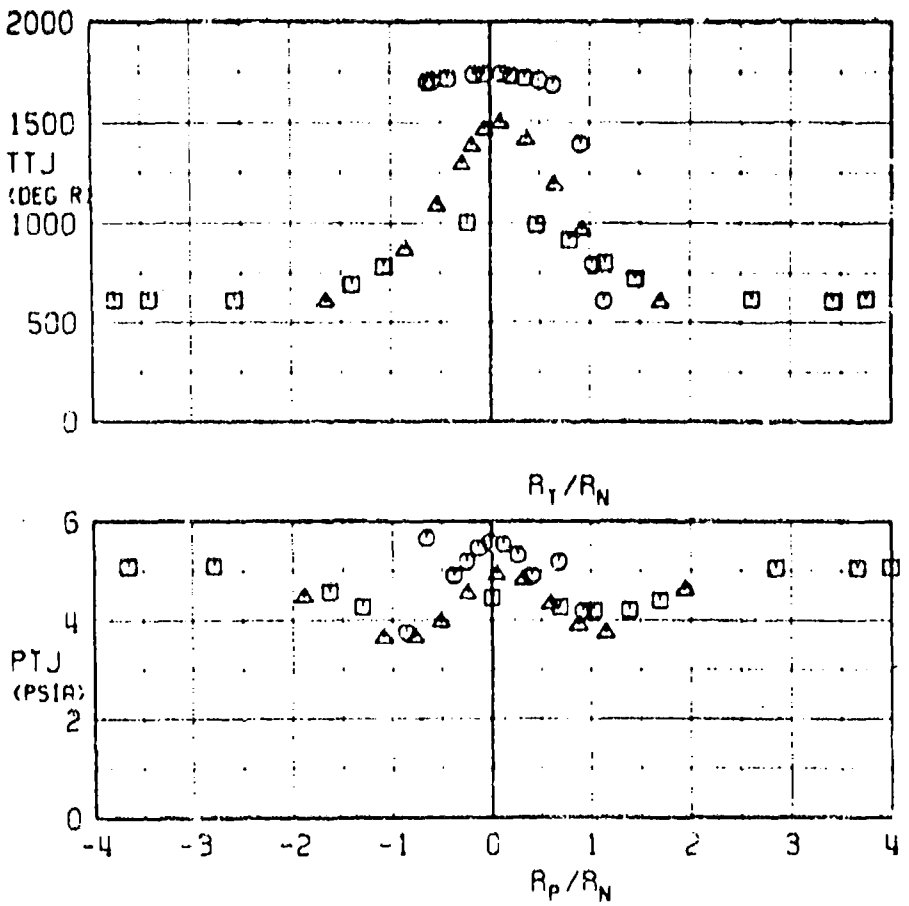

a. TTJ versus R_T/R_N, PTJ versus R_P/R_N

Fig. 14 Variation of Emission Characteristics with Axial Probe Position (Mach 1.6/55,000 ft, MIL)

SYMBOL	M_∞	ALT	PLS	XP/DN	XR
○	1.6	55K	MIL	0.22	HORIZ
△	1.6	55K	MIL	9.30	HORIZ
□	1.6	55K	MIL	19.90	HORIZ

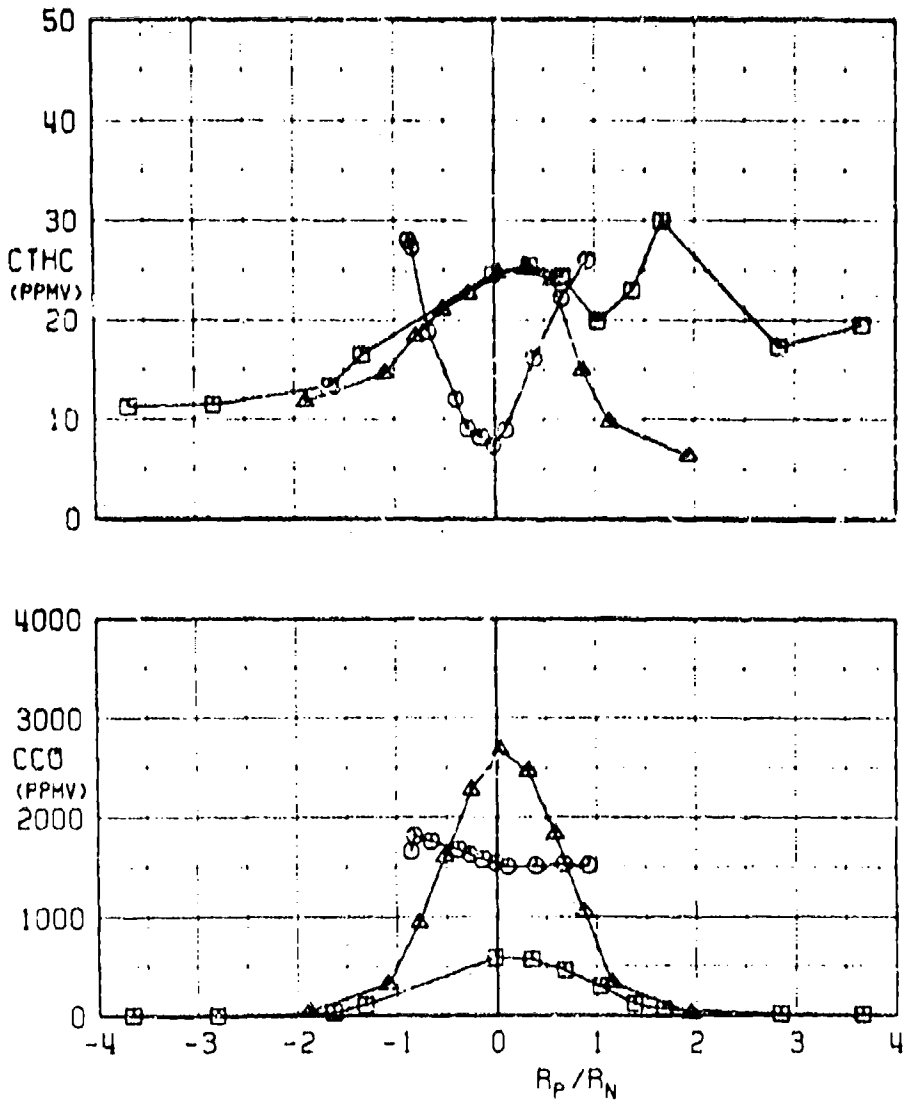

b. CTHC and CCO versus R_P/R_N
Fig. 14 Continued

SYMBOL	M_∞	ALT	PLS	XP/DN	XR
○	1.6	55K	MIL	0.22	HORIZ
△	1.6	55K	MIL	9.30	HORIZ
□	1.6	55K	MIL	19.90	HORIZ

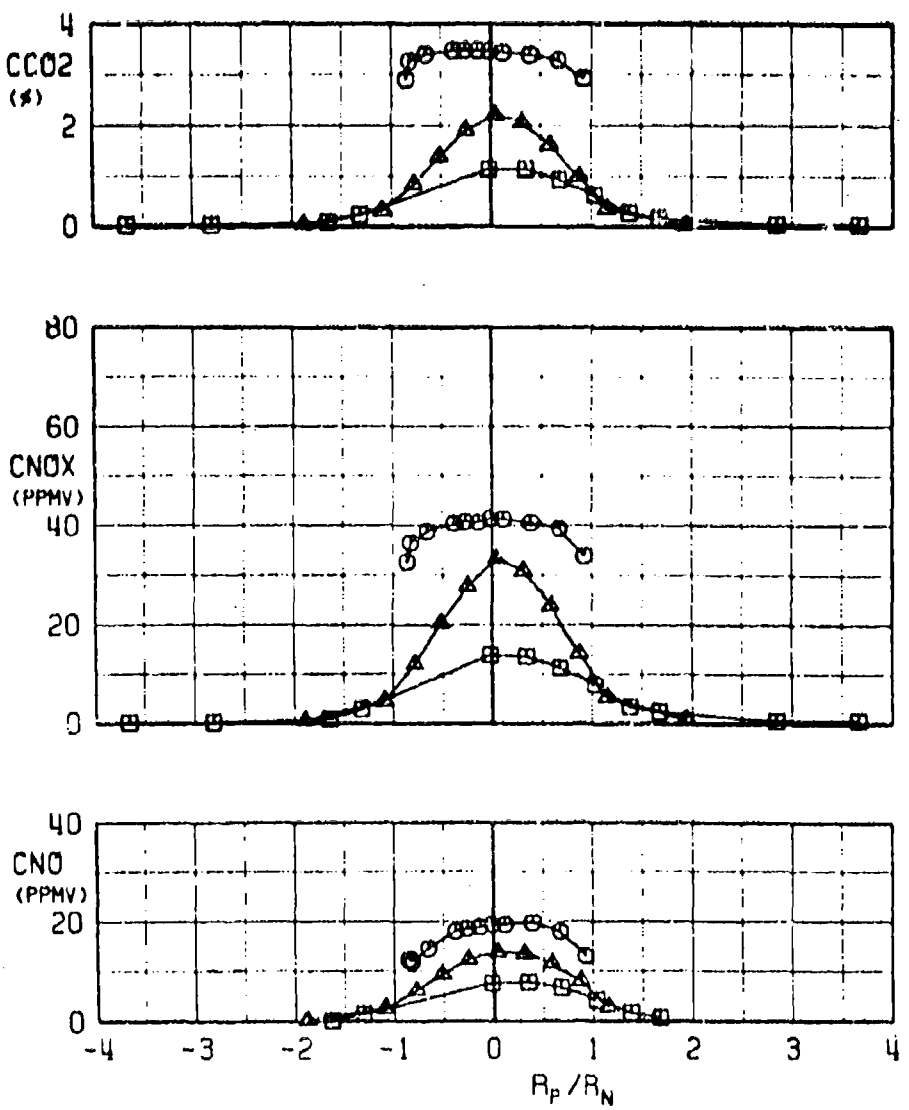

c. CCO_2, CNO_x, and CNO versus R_P/R_N
Fig. 14 Continued

SYMBOL	M_∞	ALT	PLS	XP/DN	XR
○	1.6	55K	MIL	0.22	HORIZ
△	1.6	55K	MIL	9.30	HORIZ
□	1.6	55K	MIL	19.90	HORIZ

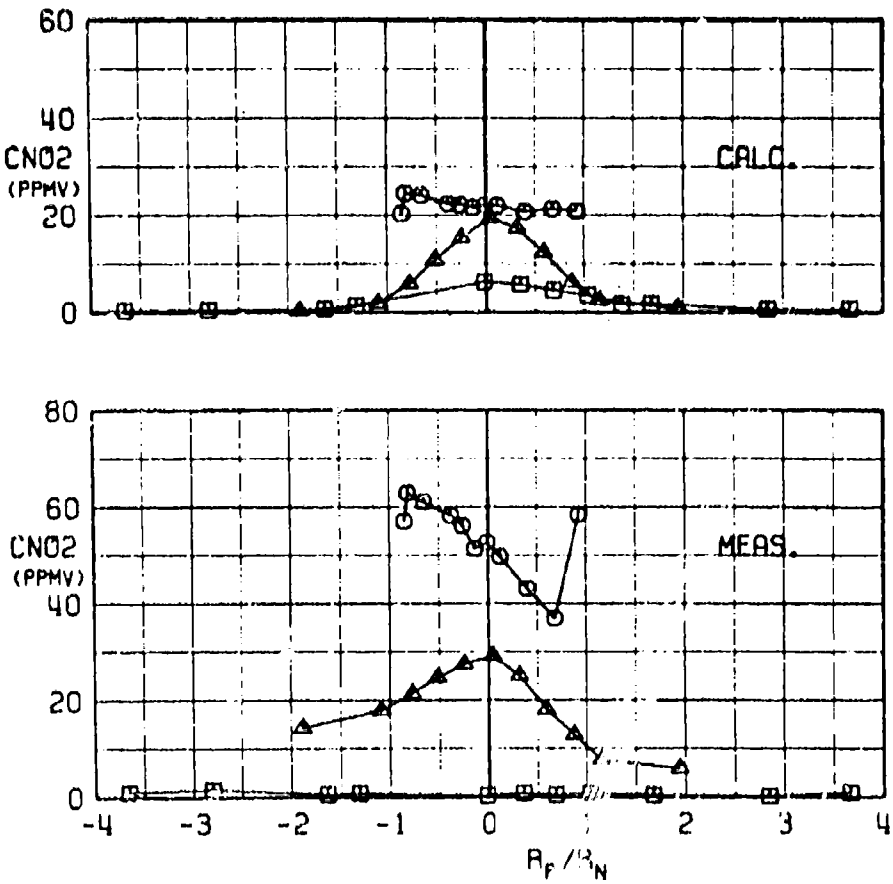

d. Calculated and Measured CNO_2 versus R_P/R_N
Fig. 14 Continued

SYMBOL	M_∞	ALT	PLS	XP/DN	XR
○	1.6	55K	MIL	0.22	HORIZ
△	1.6	55K	MIL	9.30	HORIZ
□	1.6	55K	MIL	19.90	HORIZ

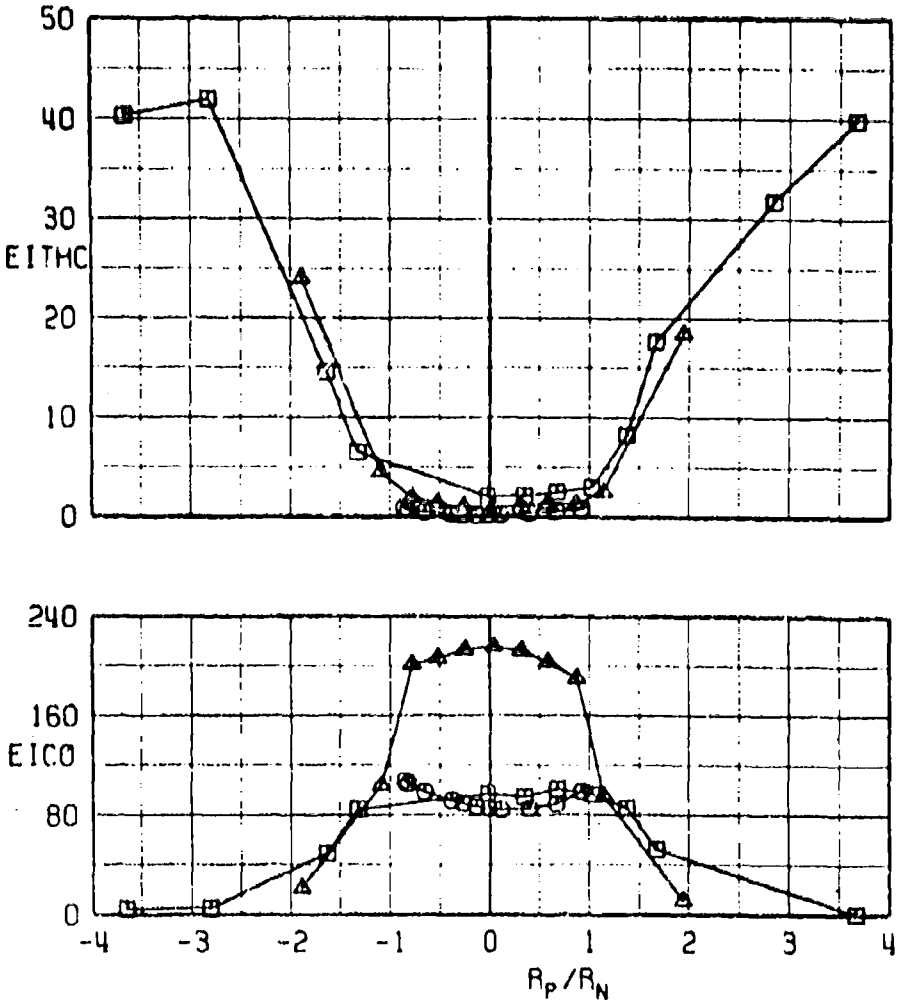

e. EITHC and EICO versus R_P/R_N

Fig. 14 Continued

SYMBOL	M_∞	ALT	PLS	XP/DN	XR
○	1.6	55K	MIL	0.22	HORIZ
△	1.6	55K	MIL	9.30	HORIZ
□	1.6	55K	MIL	19.90	HORIZ

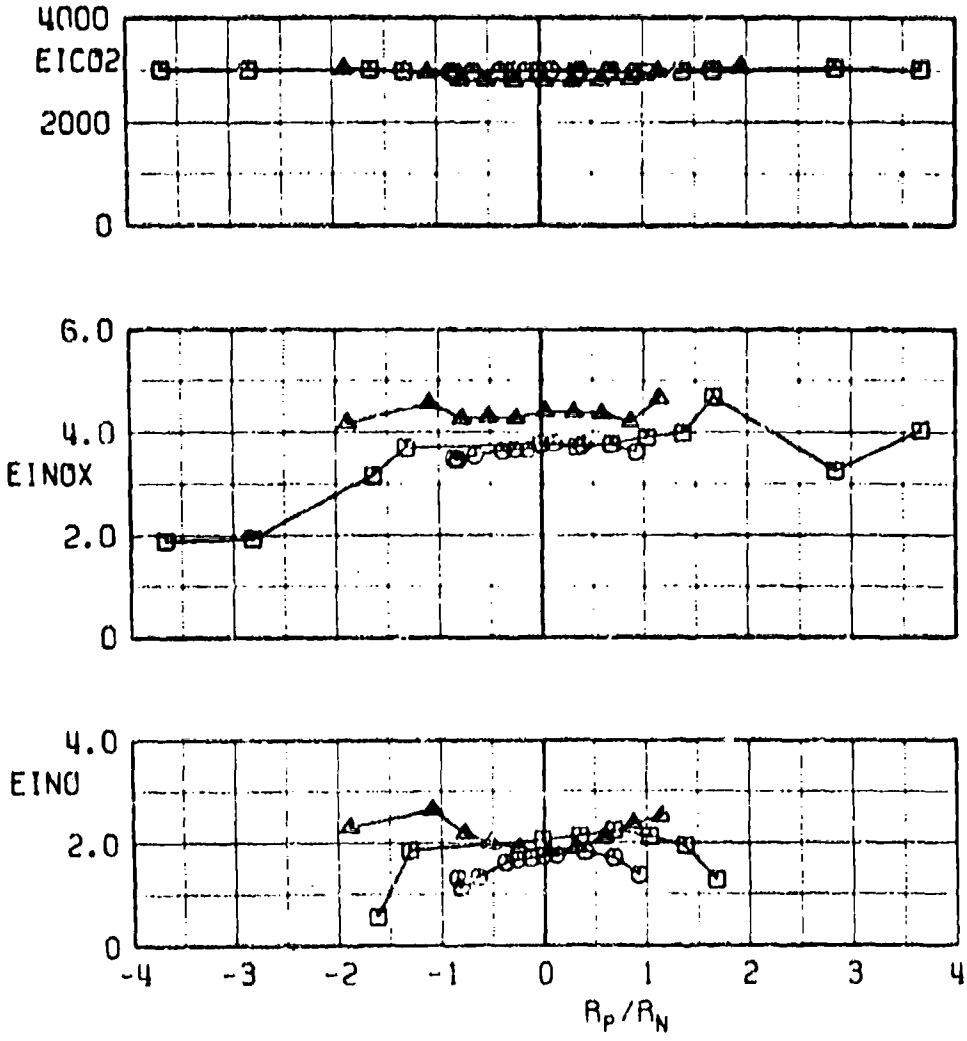

f. $EICO_2$, $EINO_x$, and EINO versus R_P/R_N
Fig. 14 Continued

SYMBOL	M_∞	ALT	PLS	XP/CN	XR
○	1.6	55K	MIL	0.22	HORIZ
△	1.6	55K	MIL	9.30	HORIZ
□	1.6	55K	MIL	19.90	HORIZ

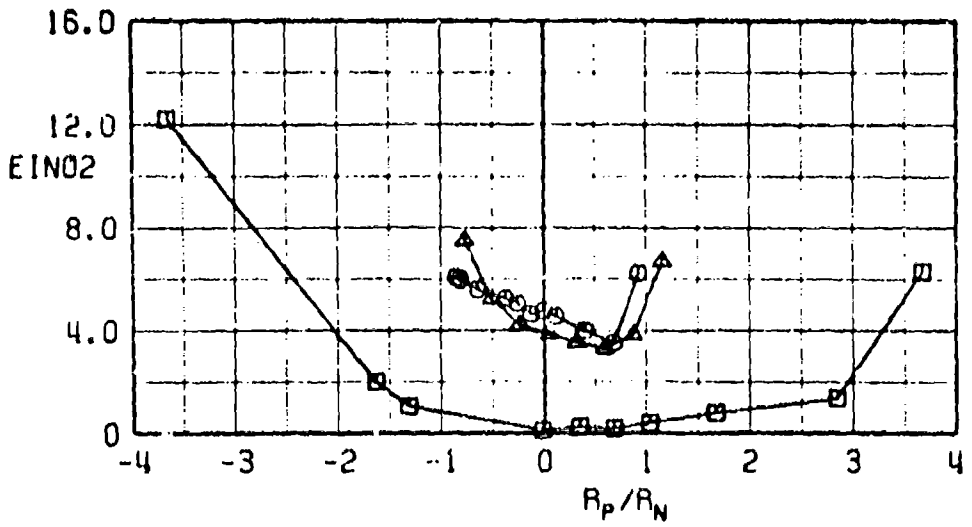

g. $EINO_2$ versus R_P/R_N
Fig. 14 Concluded

SYMBOL	M_∞	ALT	PLS	XP/DN	XA
○	2.0	65K	MIL	0.22	HORIZ
△	2.0	65K	MIL	9.30	HORIZ
□	2.0	65K	MIL	19.90	HORIZ

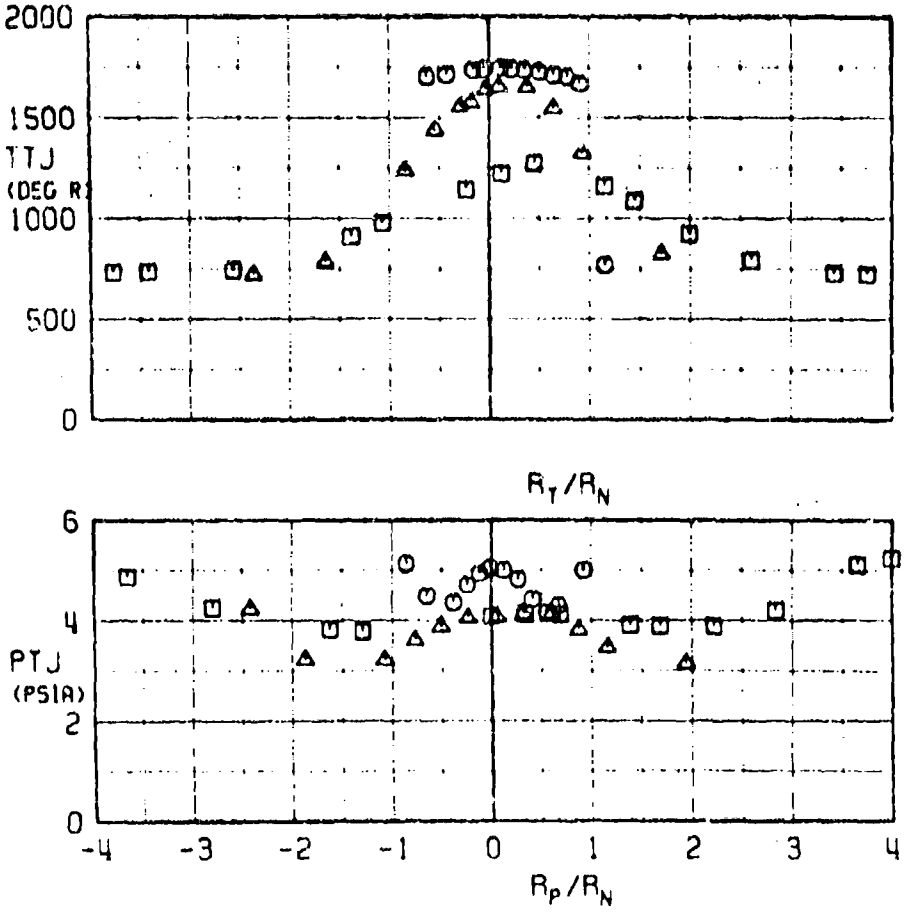

a. TTJ versus R_T/R_N, PTJ versus R_P/R_N

Fig. 15 Variation of Emission Characteristics with Axial Probe Position (Mach 2.0/65,000 ft, MIL)

SYMBOL	M_∞	ALT	PLS	XP/DN	XR
○	2.0	65K	MIL	0.22	HORIZ
△	2.0	65K	MIL	9.30	HORIZ
□	2.0	65K	MIL	19.90	HORIZ

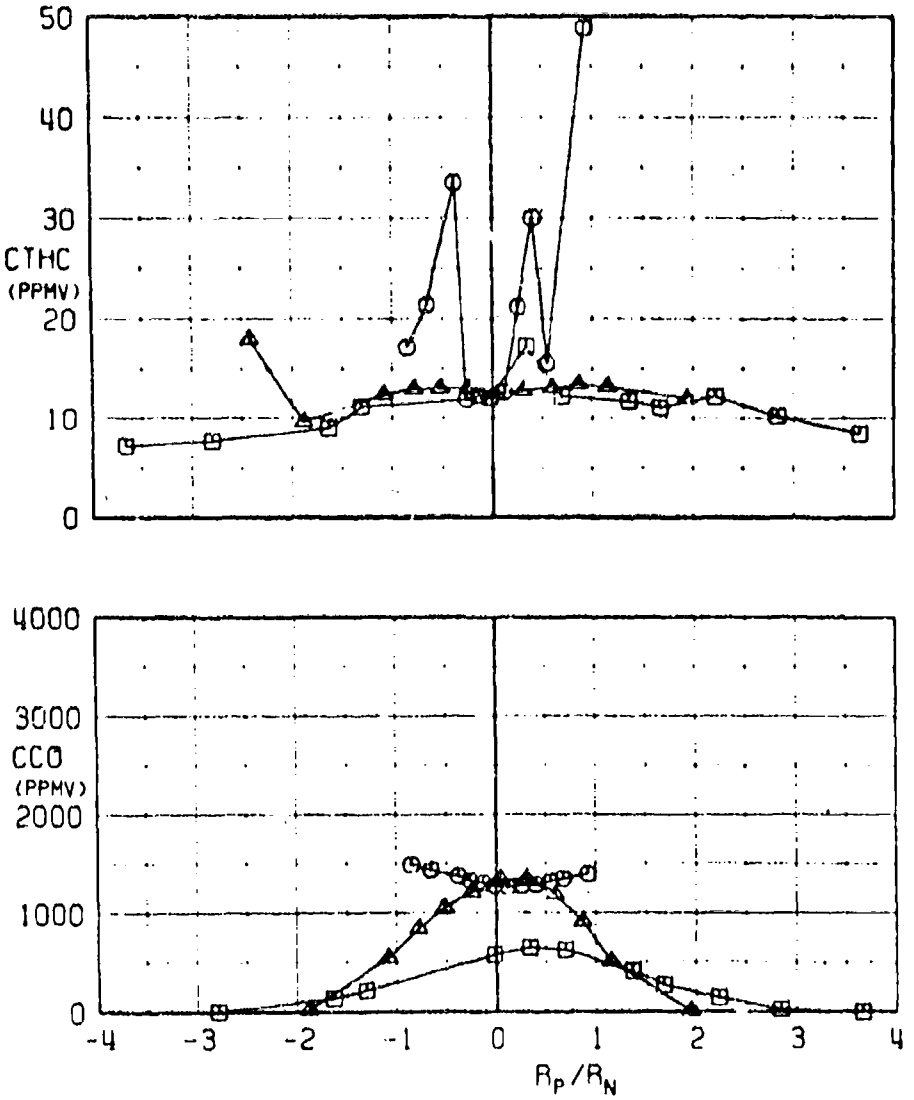

b. CTHC and CCO versus R_P/R_N
Fig. 15 Continued

SYMBOL	M_∞	ALT	PLS	XP/DN	XR
○	2.0	65K	MIL	0.22	HORIZ
△	2.0	65K	MIL	9.30	HORIZ
□	2.0	65K	MIL	19.90	HORIZ

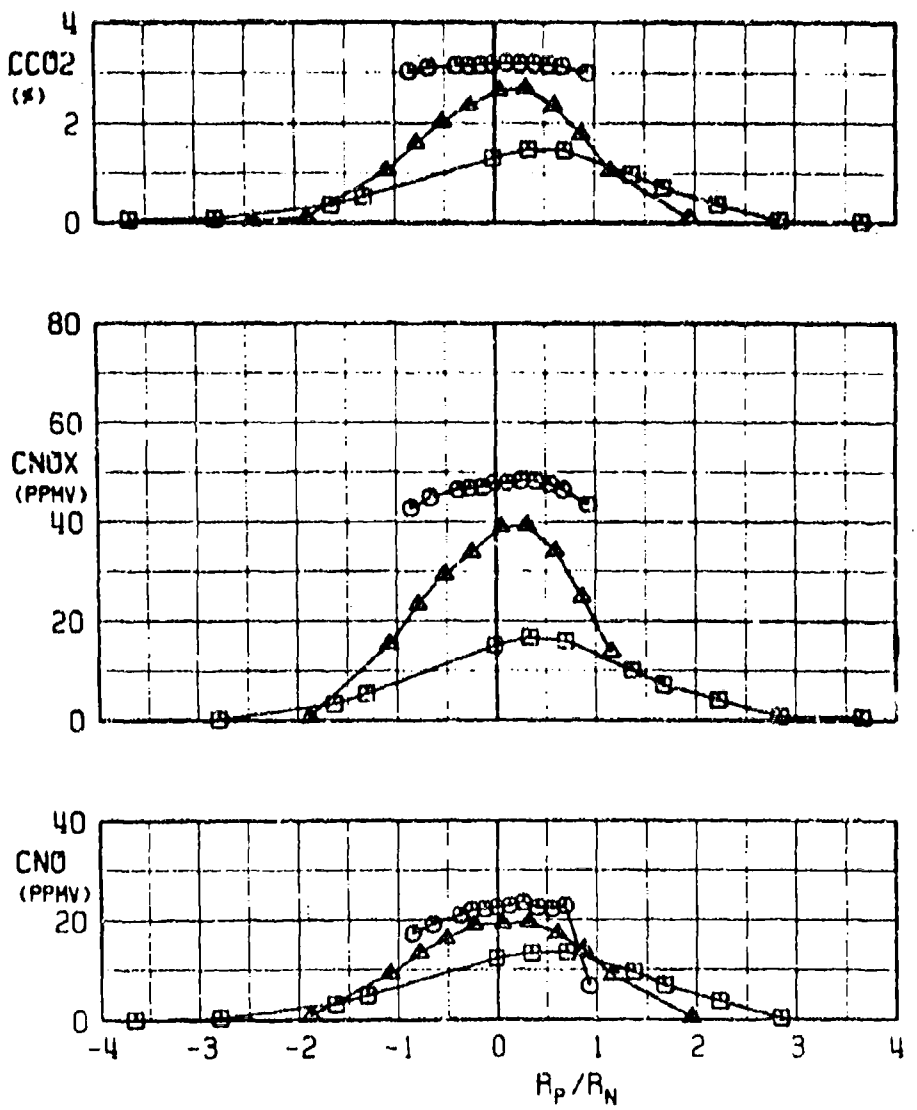

c. CCO_2, CNO_x, and CNO versus R_P/R_N
Fig. 15 Continued

SYMBOL	M_∞	ALT	PLS	XP/DN	XR
○	2.0	65K	MIL	0.22	HORIZ
△	2.0	65K	MIL	9.30	HORIZ
□	2.0	65K	MIL	19.90	HORIZ

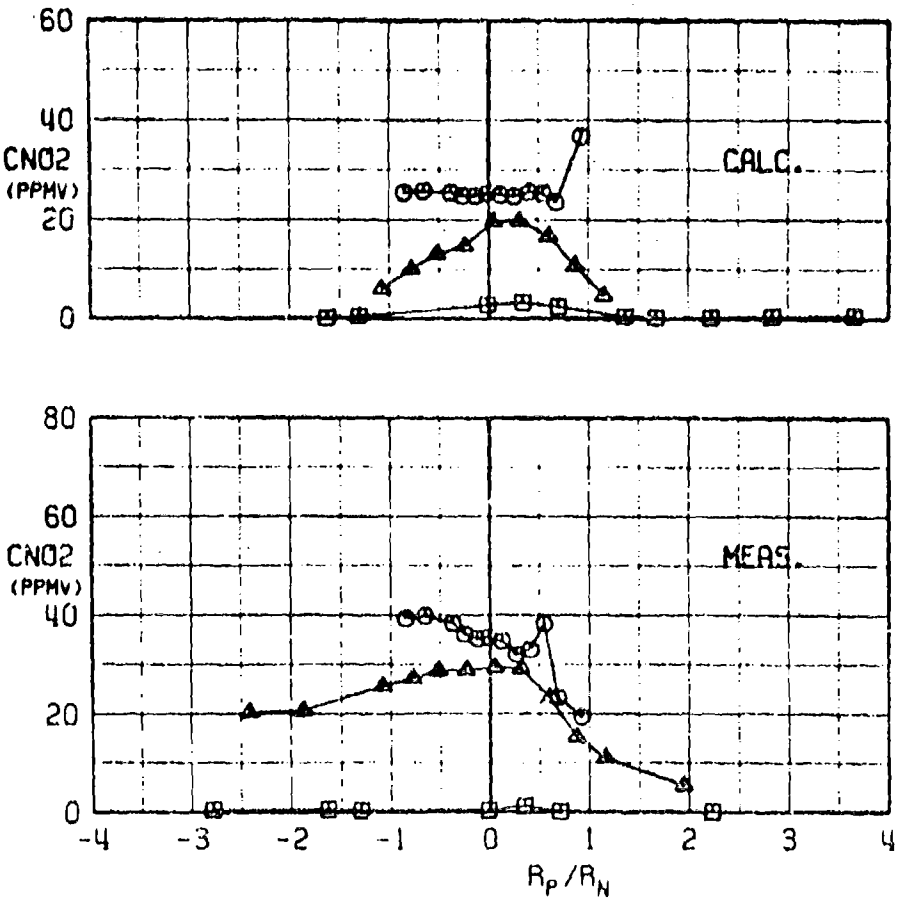

d. Calculated and Measured CNO_2 versus R_P/R_N
Fig. 15 Continued

SYMBOL	M_∞	ALT	PLS	XP/DN	XR
⊡	2.0	65K	MIL	0.22	HORIZ
⧋	2.0	65K	MIL	9.30	HORIZ
⊡	2.0	65K	MIL	19.90	HORIZ

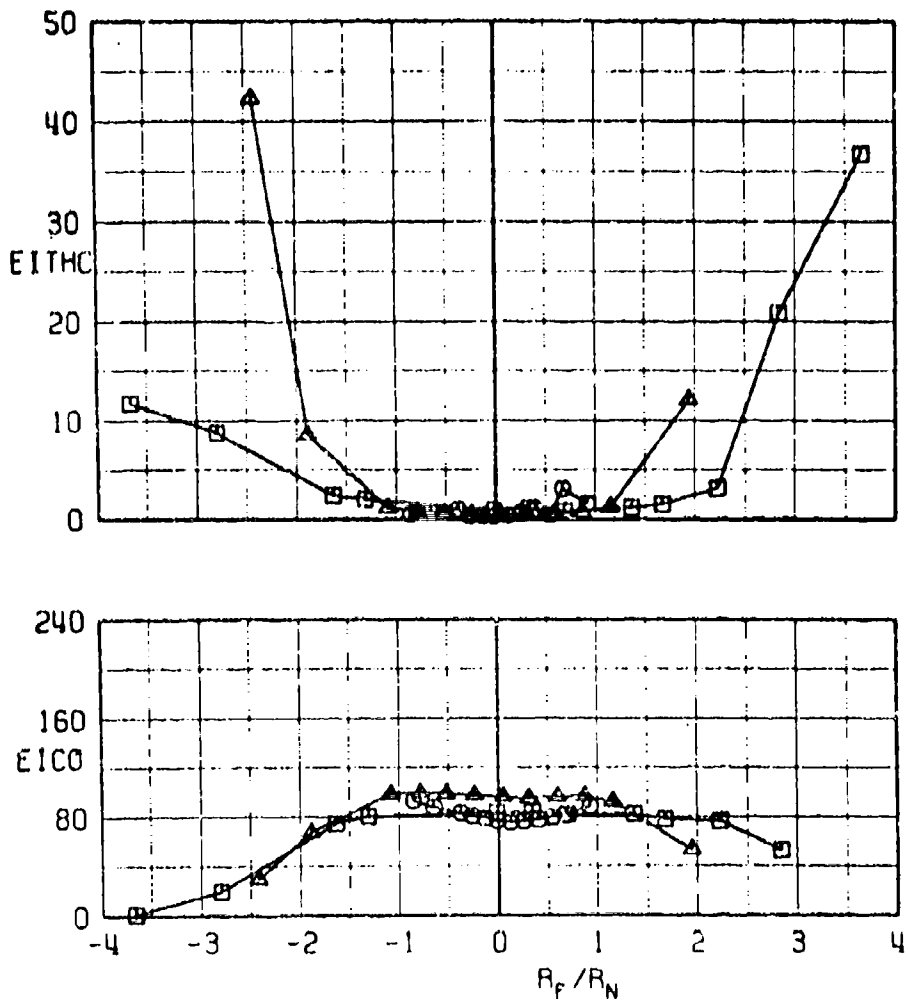

e. EITHC and EICO versus R_P/R_N
Fig. 15 Continued

SYMBOL	M_∞	ALT	PLS	XP/DN	XR
○	2.0	65K	MIL	0.22	HORIZ
△	2.0	65K	MIL	9.30	HORIZ
□	2.0	65K	MIL	19.90	HORIZ

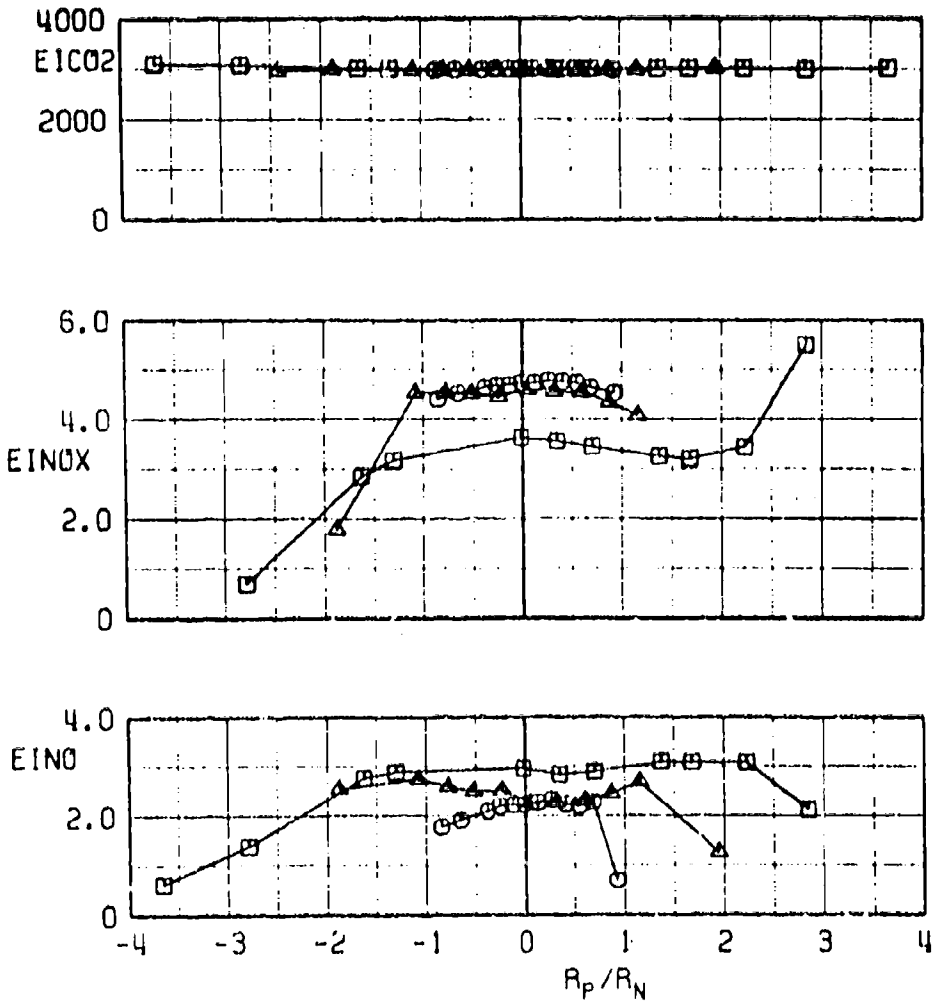

f. $EICO_2$, $EINO_x$ and EINO versus R_P/R_N
Fig. 15 Continued

SYMBOL	M_∞	ALT	PLS	XP/DN	XR
○	2.0	65K	MIL	0.22	HORIZ
△	2.0	65K	MIL	9.30	HORIZ
□	2.0	65K	MIL	19.90	HORIZ

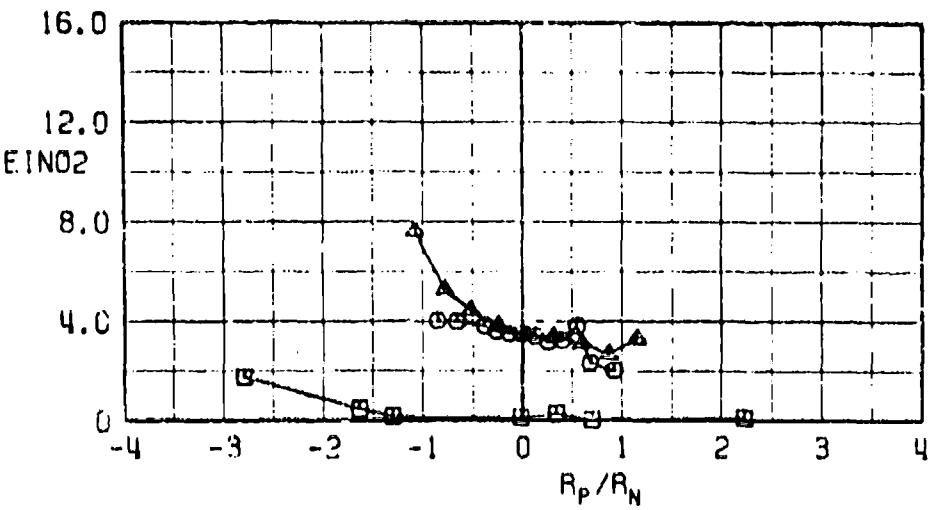

g. $EINO_2$ versus R_P/R_N
Fig. 15 Concluded

SYMBOL	M_∞	ALT	PLS	XP/DN	XR
○	1.6	55K	A/B	0.22	HORIZ
△	1.6	55K	A/B	9.30	HORIZ
□	1.6	55K	A/B	19.90	HORIZ

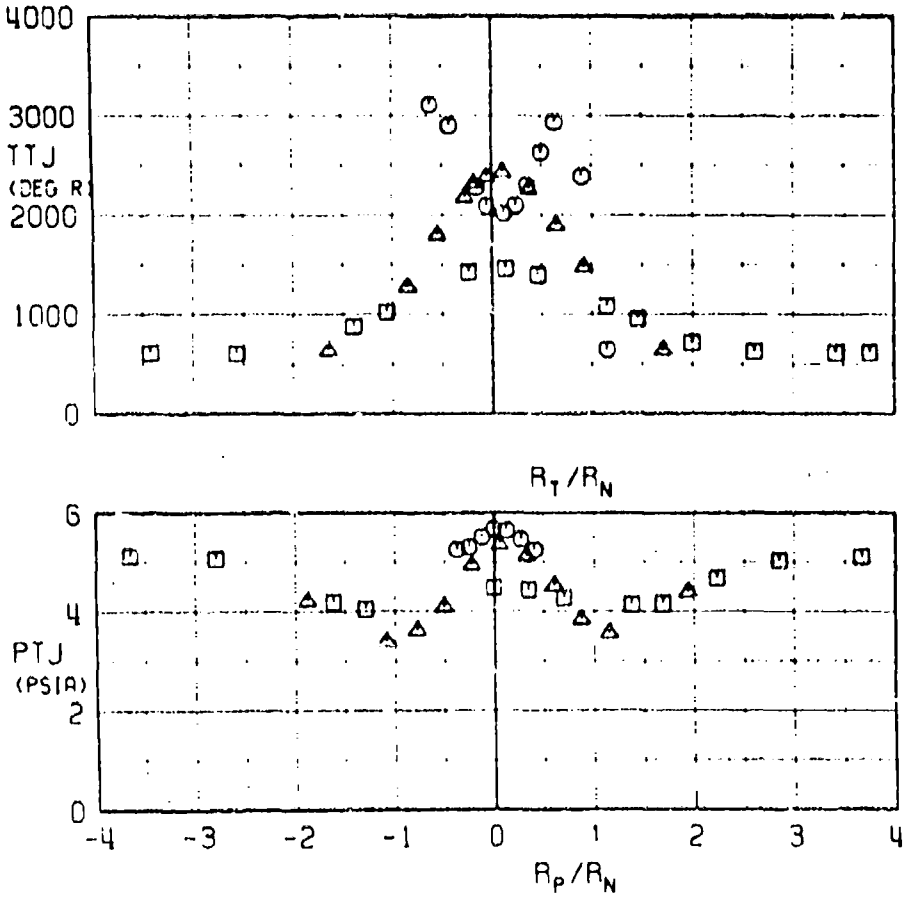

a. TTJ versus R_T/R_N and PTJ versus R_P/R_N

Fig. 16 Variation of Emission Characteristics with Axial Probe Position (Mach 1.6/55,000 ft, A/B)

SYMBOL	M_∞	ALT	PLS	XP/DN	XR
○	1.6	55K	A/B	0.22	HORIZ
△	1.6	55K	A/B	9.30	HORIZ
□	1.6	55K	A/B	19.90	HORIZ

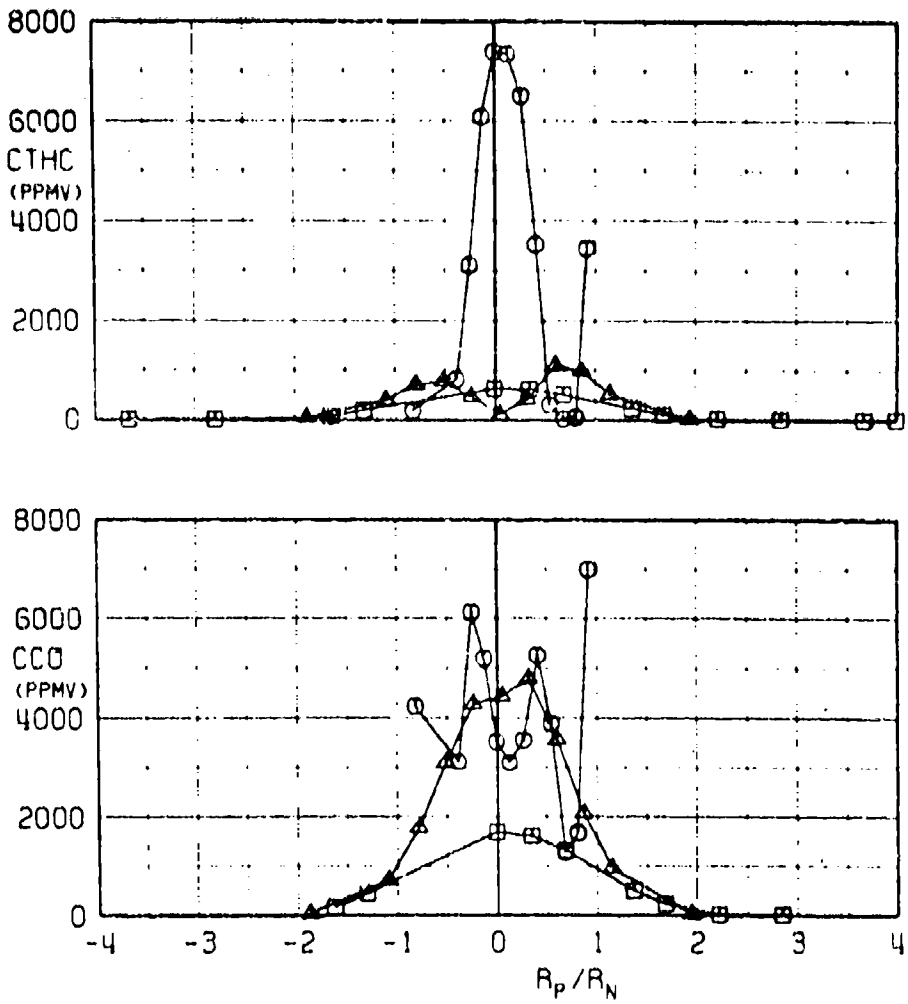

b. CTHC and CCO versus R_P/R_N
Fig. 16 Continued

SYMBOL	M_∞	ALT	PLS	XP/DN	XR
○	1.6	55K	A/B	0.22	HORIZ
△	1.6	55K	A/B	9.30	HORIZ
□	1.6	55K	A/B	19.90	HORIZ

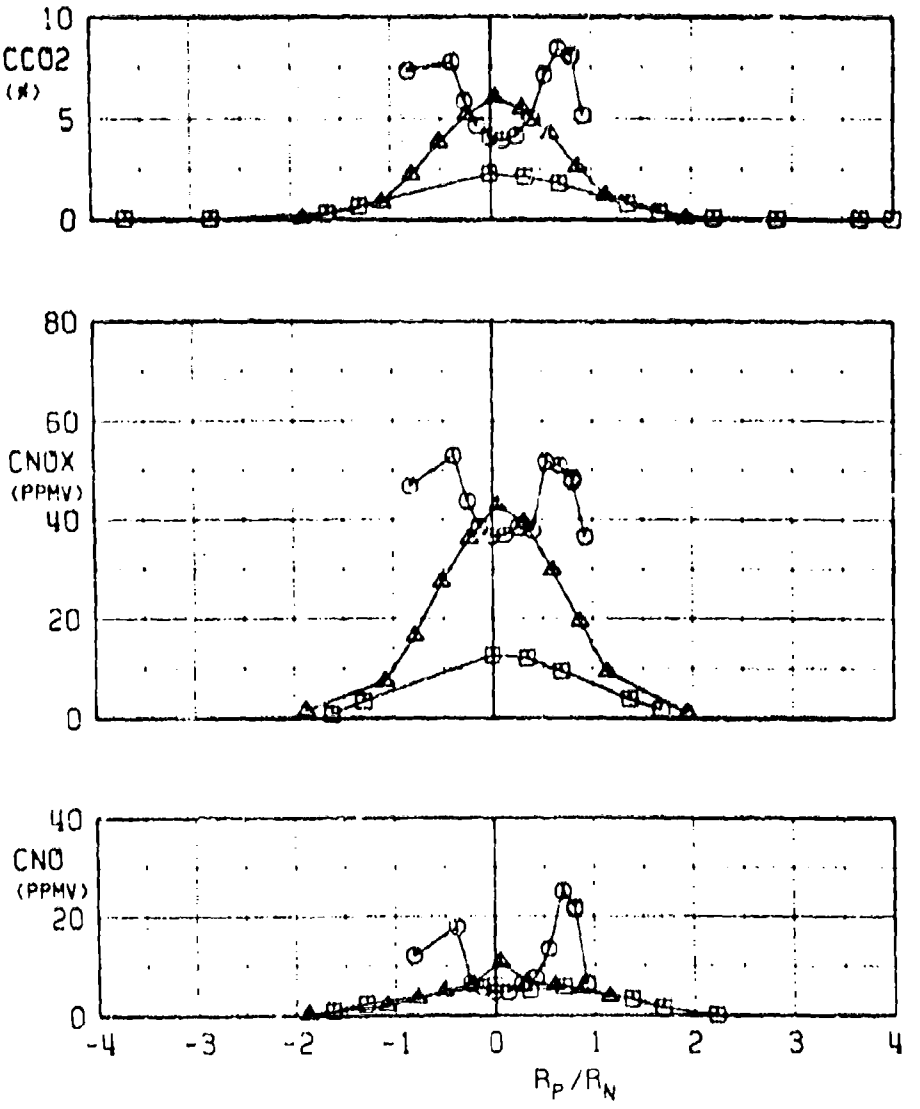

c. CCO_2, CNO_x, and CNO versus R_P/R_N
Fig. 16 Continued

SYMBOL	M_∞	ALT	P/S	XP/DN	XR
○	1.6	55K	A/B	0.22	HORIZ
△	1.6	55K	A/B	9.30	HORIZ
□	1.6	55K	A/B	19.90	HORIZ

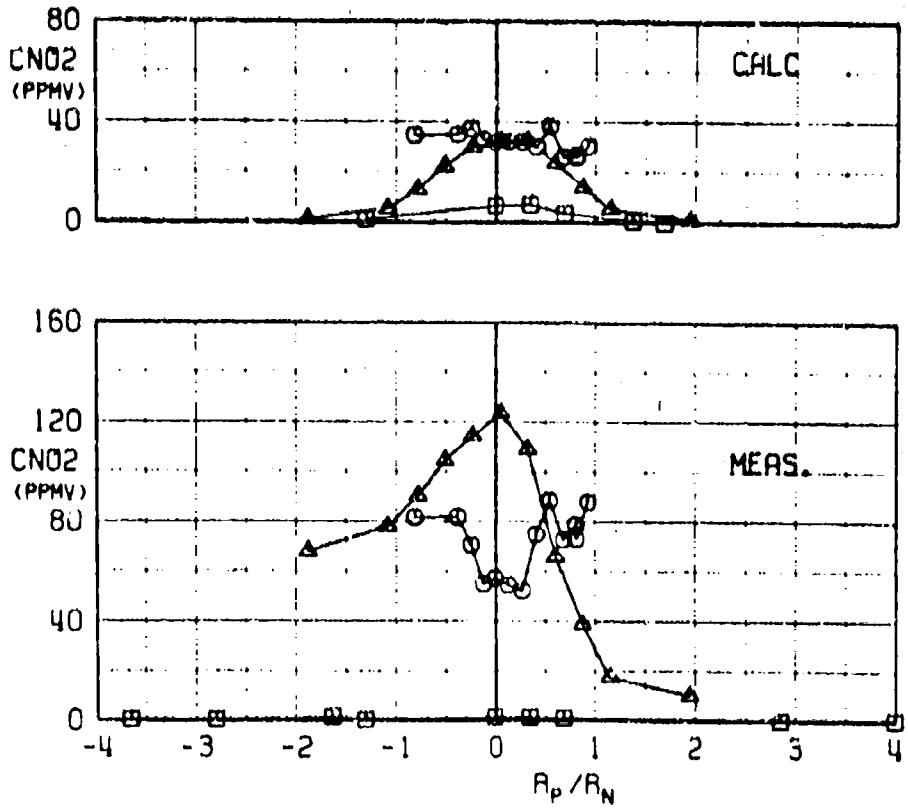

d. Calculated and Measured CNO_2 versus R_P/R_N
Fig. 16 Continued

SYMBOL	M_∞	ALT	PLS	XP/ON	XR
○	1.6	55K	A/B	0.22	HORIZ
△	1.6	55K	A/B	9.30	HORIZ
□	1.6	55K	A/B	19.90	HORIZ

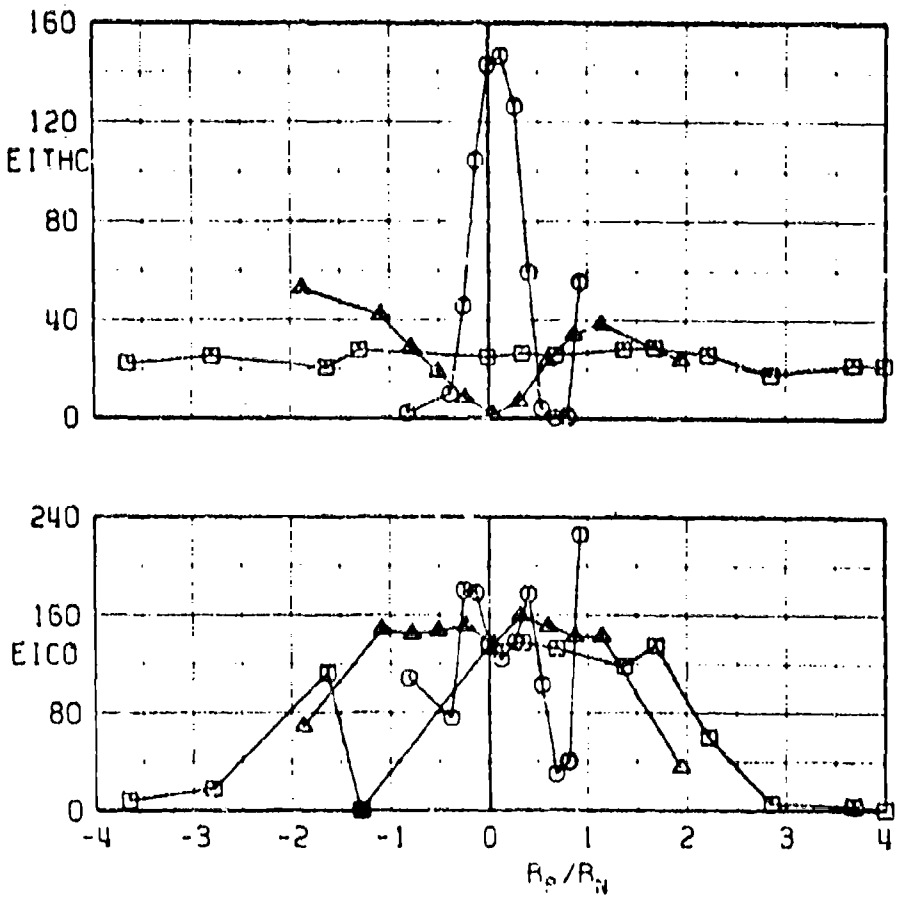

e. EITHC and EICO versus R_p/R_N
Fig. 16 Continued

SYMBOL	M_∞	ALT	PLS	XP/DN	XR
○	1.6	55K	A/B	0.22	HORIZ
△	1.6	55K	A/B	9.30	HORIZ
□	1.6	55K	A/B	19.90	HORIZ

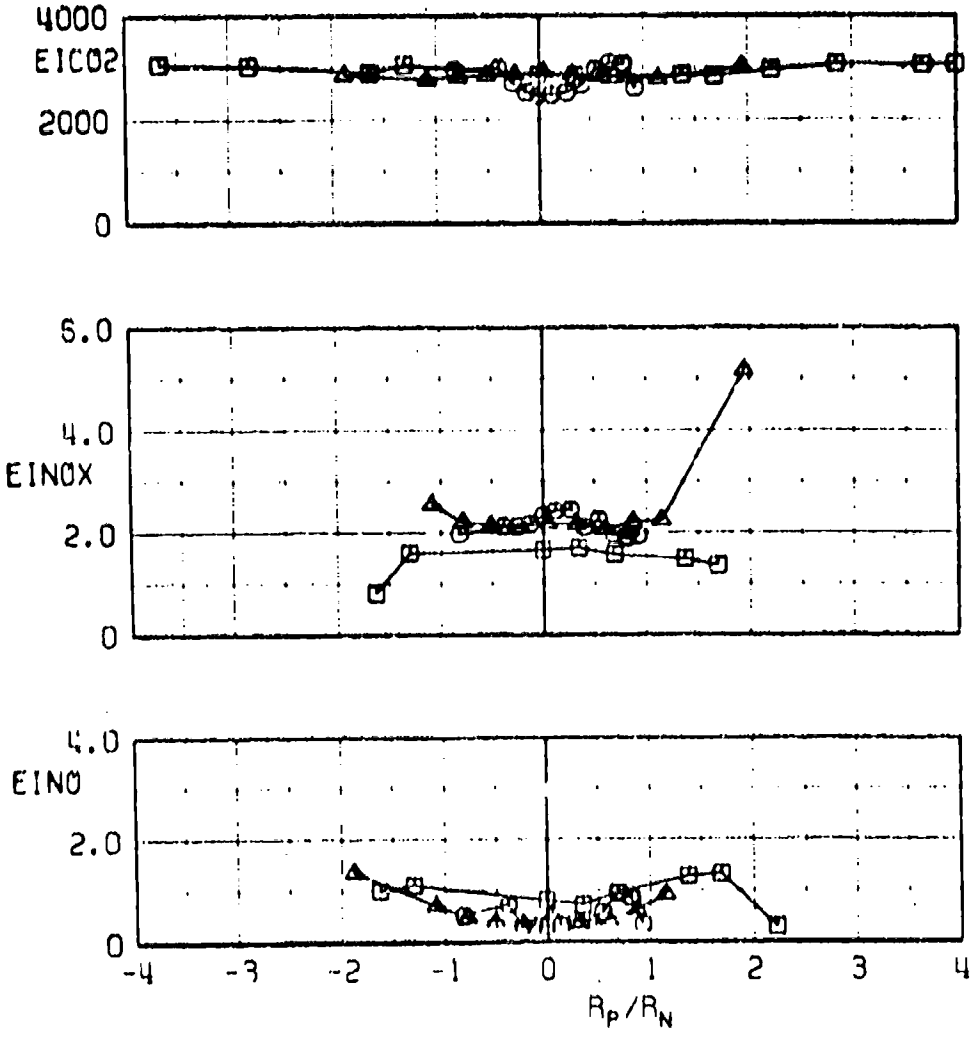

f. $EICO_2$, $EINO_x$, and EINO versus R_P/R_N
Fig. 16 Continued

SYMBOL	M_∞	ALT	PLS	XP/DN	XA
○	1.6	55K	A/B	0.22	HORIZ
△	1.6	55K	A/B	9.30	HORIZ
□	1.6	55K	A/B	19.90	HORIZ

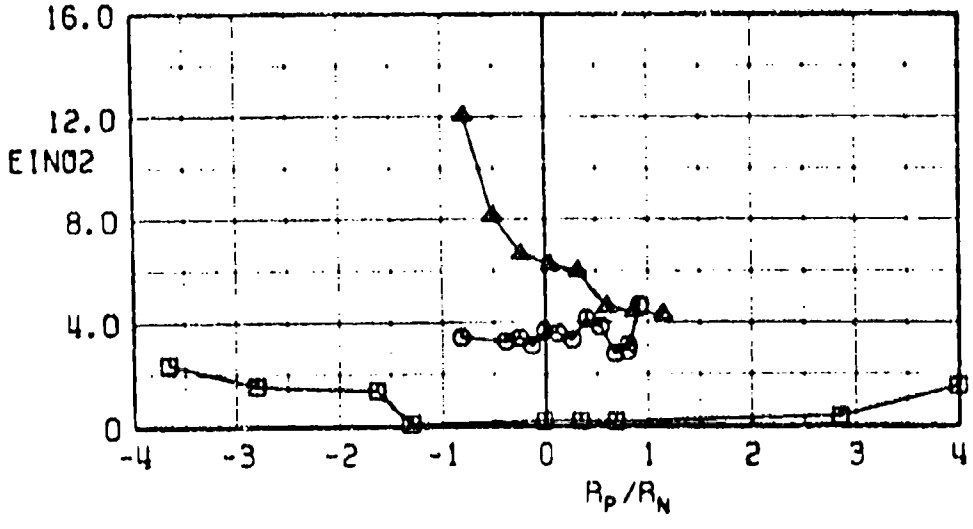

g. $EINO_2$ versus R_P/R_N
Fig. 16 Concluded

SYMBOL	M_∞	ALT	PLS	XP/DN	XR
○	2.0	65K	A/B	0.22	HORIZ
△	2.0	65K	A/B	9.30	HORIZ
□	2.0	65K	A/B	19.90	HORIZ

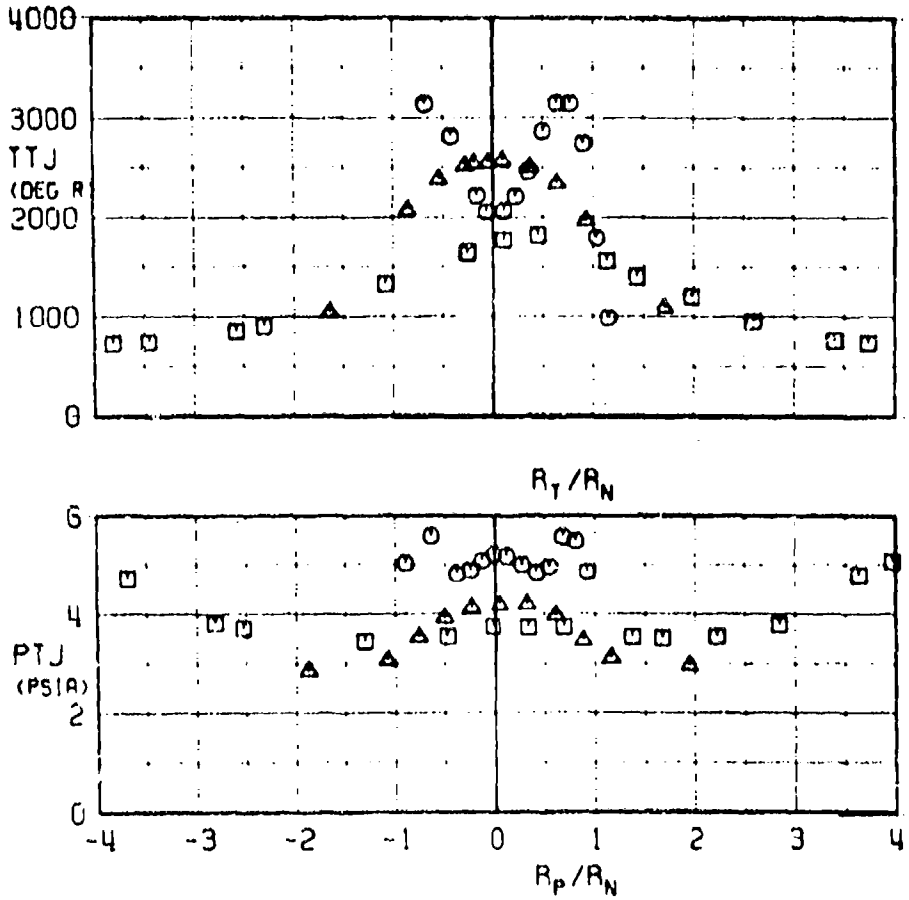

a. TTJ versus R_T/R_N, PTJ versus R_P/R_N

Fig. 17 Variation of Emission Characteristics with Axial Probe Position (Mach 2.0/65,000 ft, A/B)

SYMBOL	M_∞	ALT	PLS	XP/DN	XR
○	2.0	65K	A/B	0.22	HORIZ
△	2.0	65K	A/B	9.30	HORIZ
□	2.0	65K	A/B	19.90	HORIZ

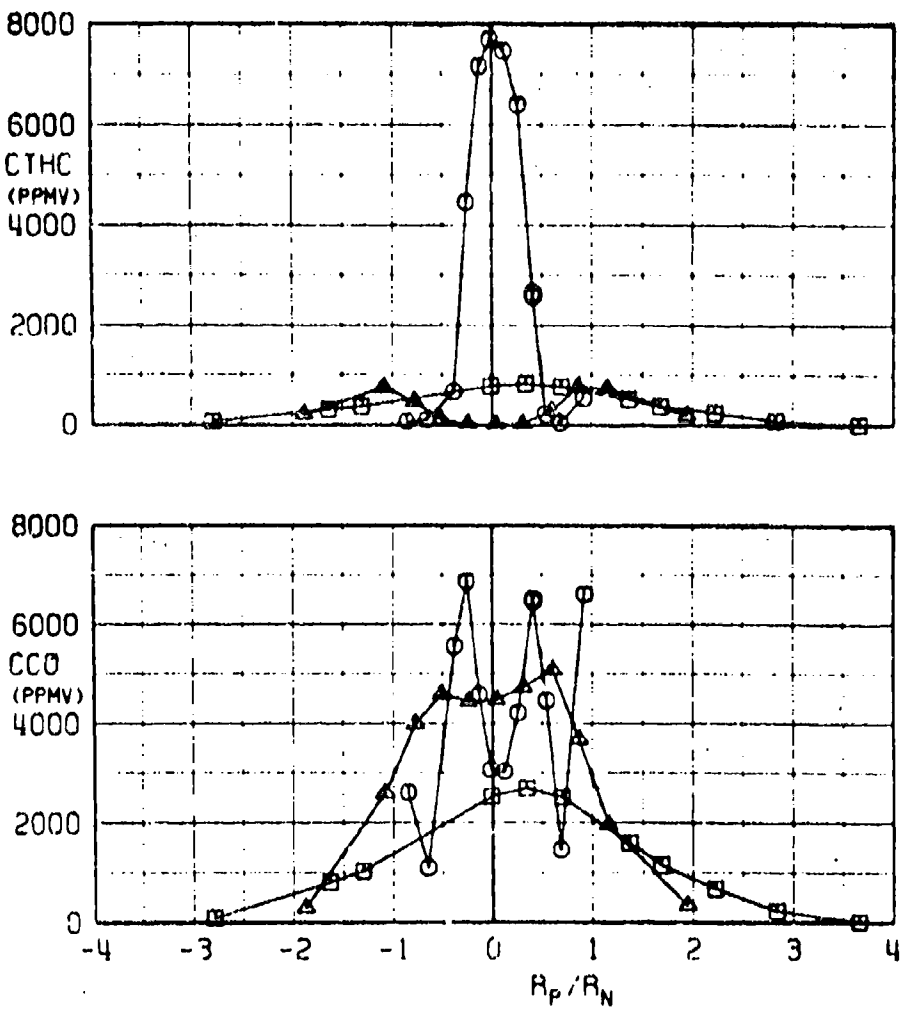

b. CTHC and CCO versus R_P/R_N
Fig. 17 Continued

SYMBOL	M_∞	ALT	PLS	XP/DN	XR
○	2.0	65K	A/B	0.22	HORIZ
△	2.0	65K	A/B	9.30	HORIZ
□	2.0	65K	A/B	19.90	HORIZ

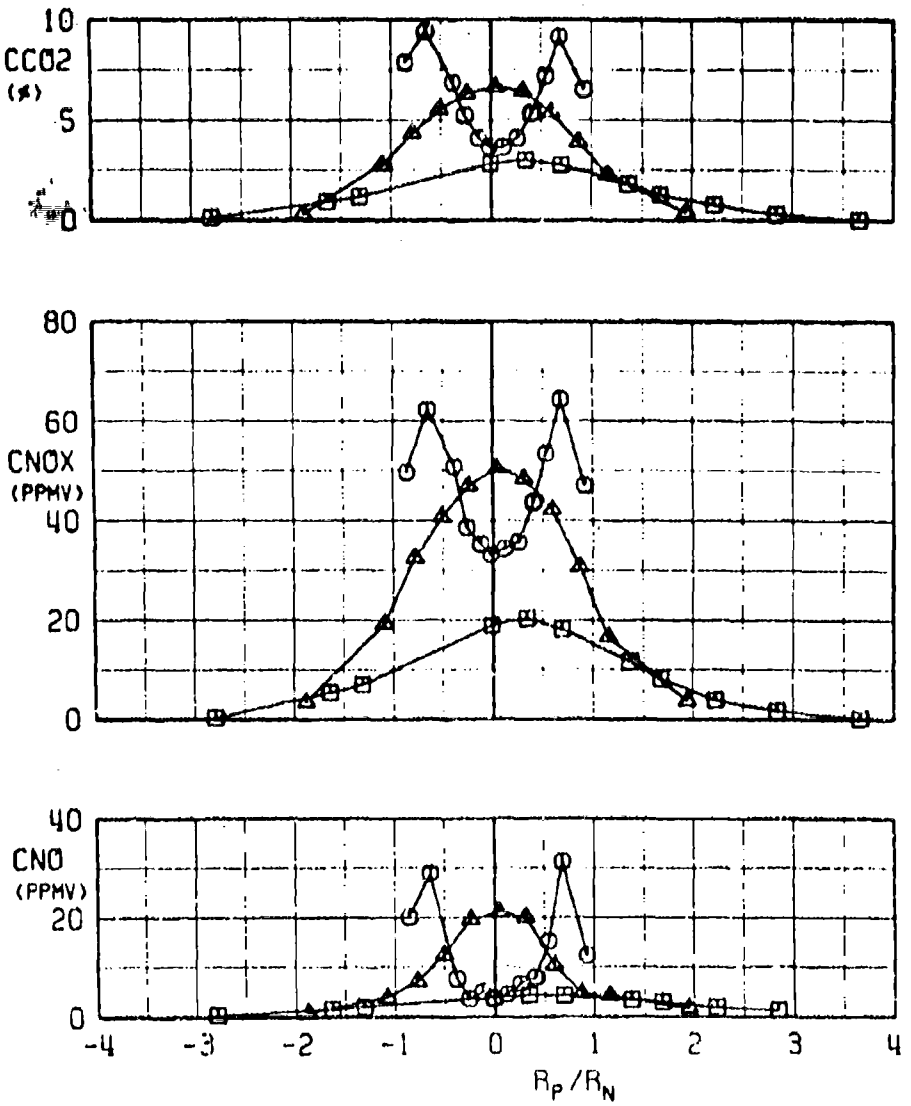

c. CCO_2, CNO_x, and CNO versus R_P/R_N
Fig. 17 Continued

SYMBOL	M_∞	ALT	PLS	XP/DN	XR
○	2.0	65K	A/B	0.22	HORIZ
△	2.0	65K	A/B	9.30	HORIZ
□	2.0	65K	A/B	19.90	HORIZ

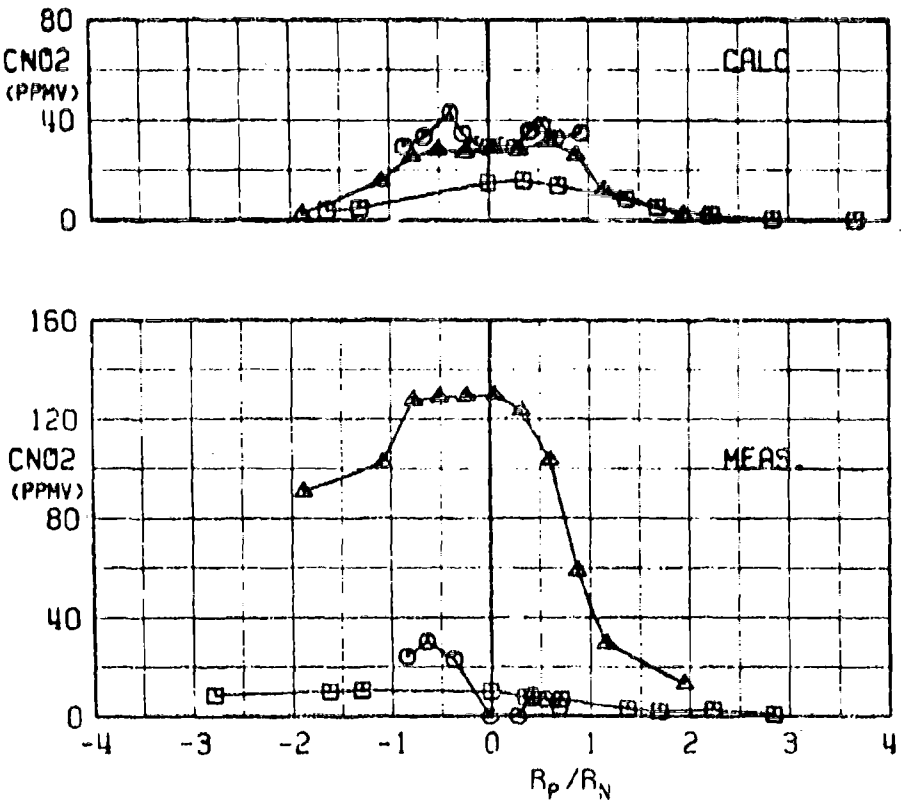

d. Calculated and Measured CNO_2 versus R_P/R_N
Fig. 17 Continued

SYMBOL	M_∞	ALT	PLS	XP/DN	XR
○	2.0	65K	A/B	0.22	HORIZ
△	2.0	65K	A/B	9.30	HORIZ
□	2.0	65K	A/B	19.90	HORIZ

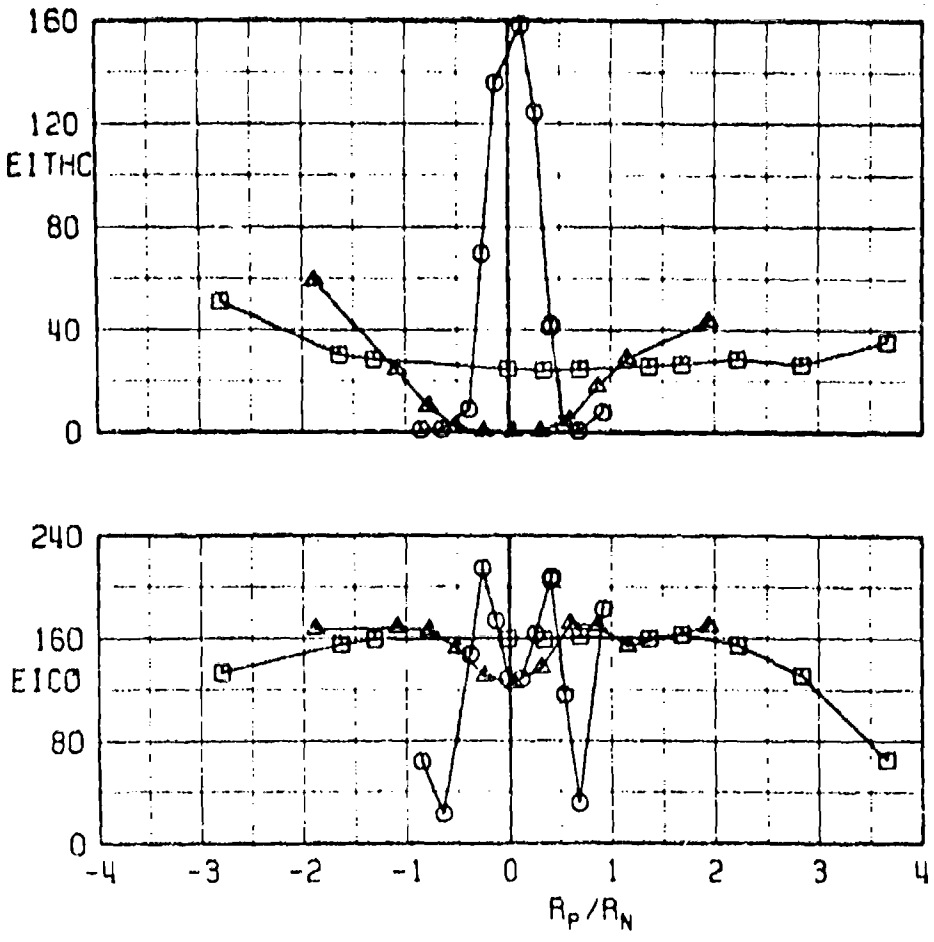

e. EITHC and EICO versus R_P/R_N
Fig. 17 Continued

SYMBOL	M_∞	ALT	PLS	XP/DN	XR
○	2.0	65K	A/B	0.22	HORIZ
△	2.0	65K	A/B	9.30	HORIZ
□	2.0	65K	A/B	19.90	HORIZ

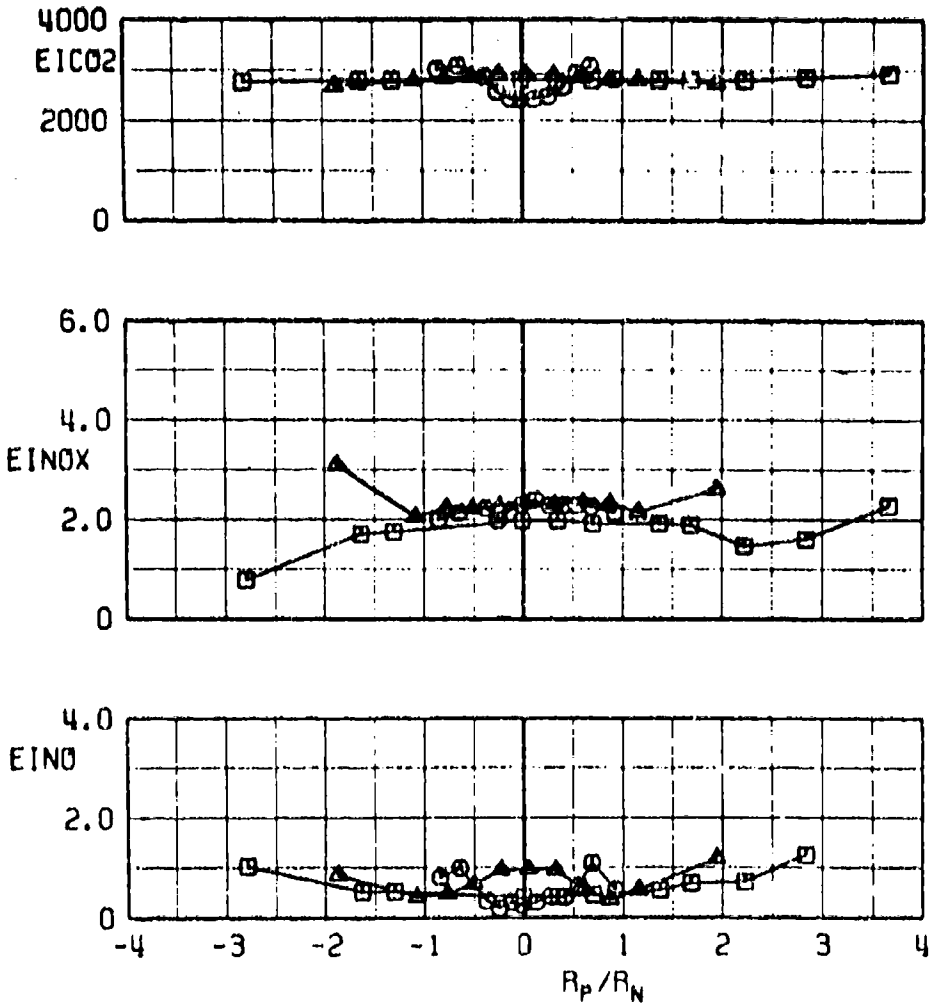

f. $EICO_2$, $EINO_x$, and EINO versus R_P/R_N
Fig. 17 Continued

SYMBOL	M_∞	ALT	PLS	XP/DN	XR
○	2.0	65K	A/B	0.22	HORIZ
△	2.0	65K	A/B	9.30	HORIZ
□	2.0	65K	A/B	19.90	HORIZ

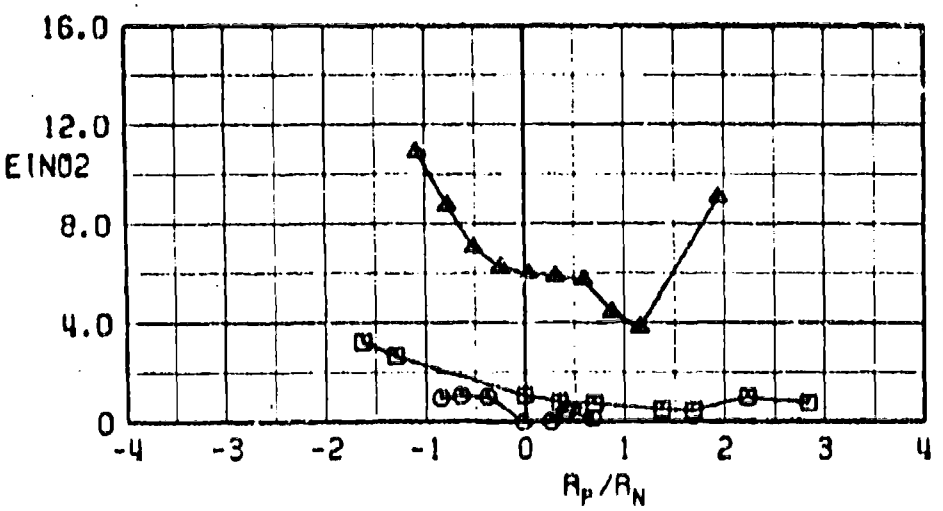

g. $EINO_2$ versus R_p/R_N

Fig. 17 Concluded

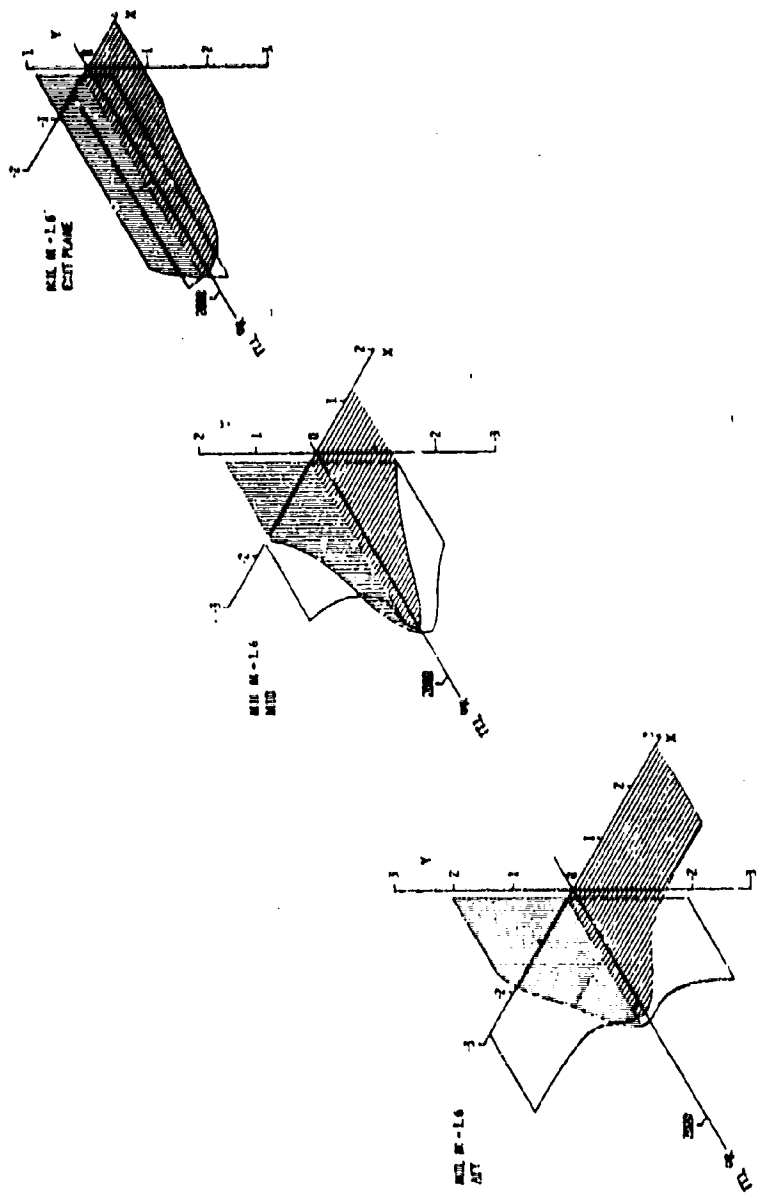

a. TTJ Profiles

Fig. 18 Isometric Plots of Emission Profiles at Exit, Mid, and Aft Stations (Mach 1.6/55,000 ft, MIL)

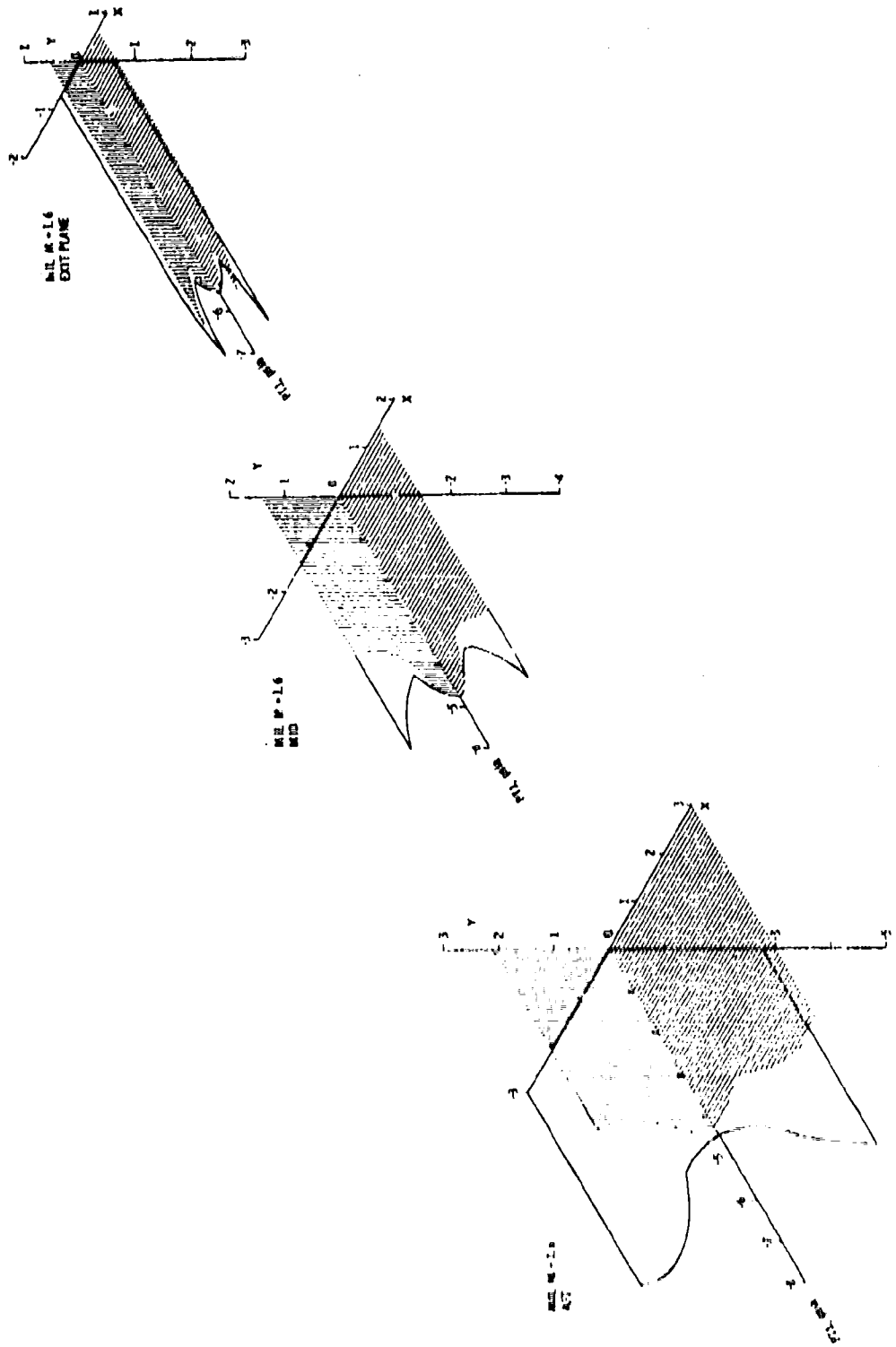

b. PTJ Profiles
Fig. 18 Continued

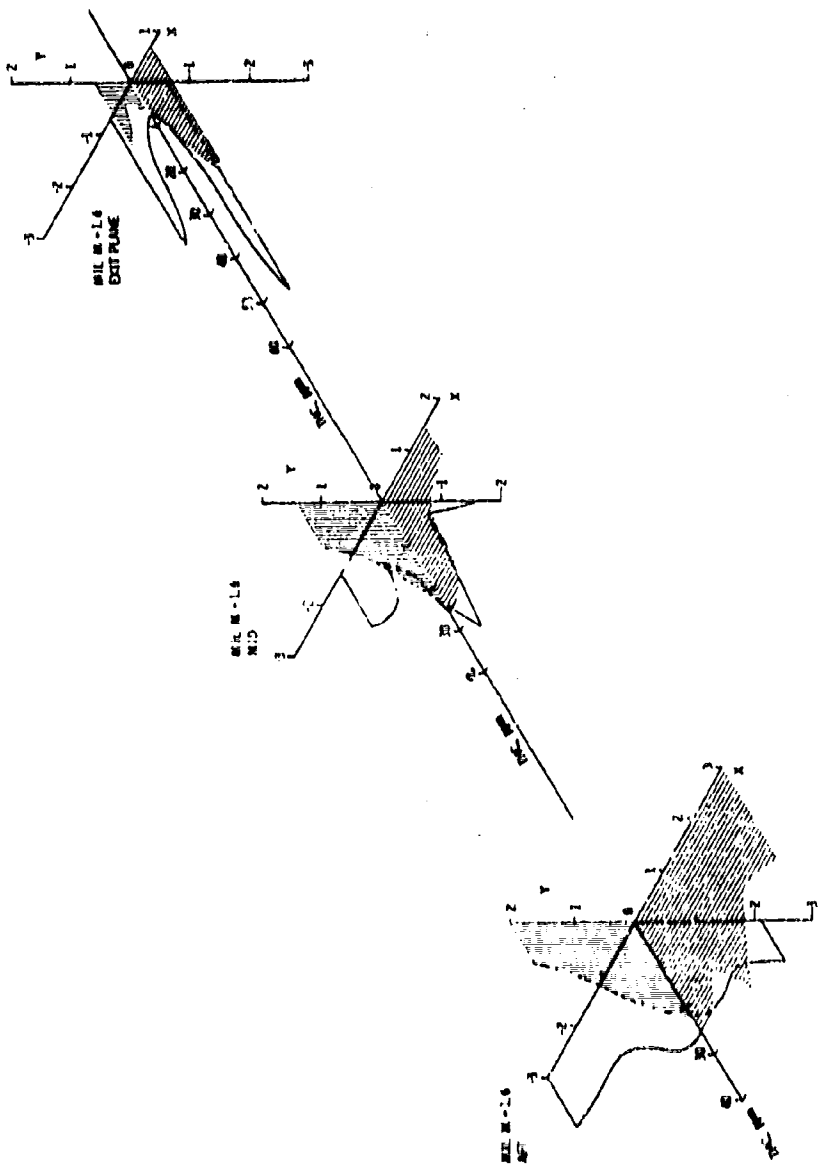

c. THC Profiles
Fig. 18 Continued

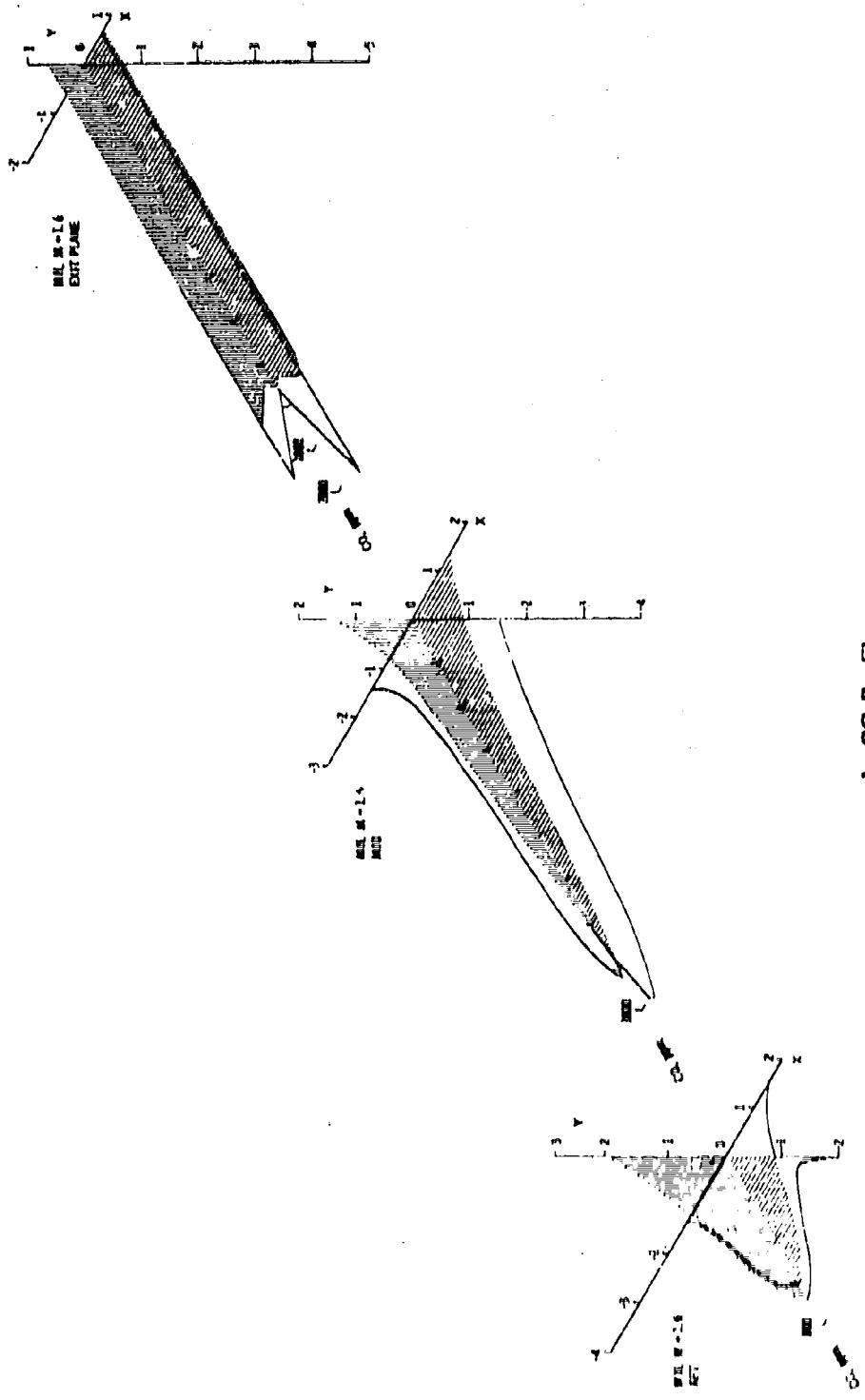

d. CO Profiles
Fig. 18 Continued

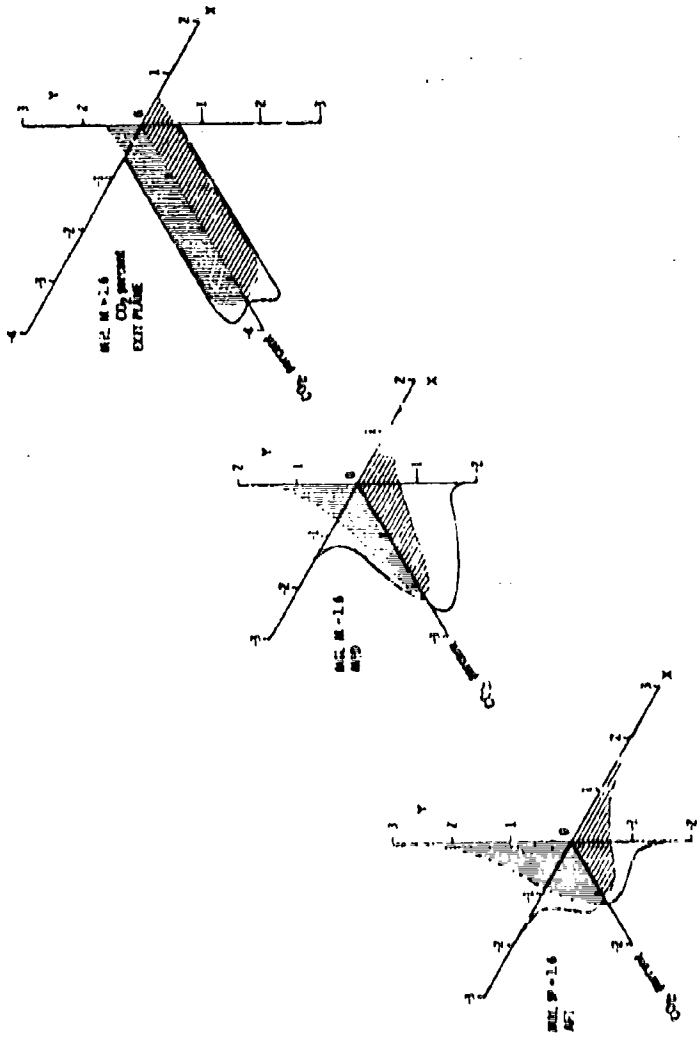

e. CO_2 Profiles
Fig. 18 Continued

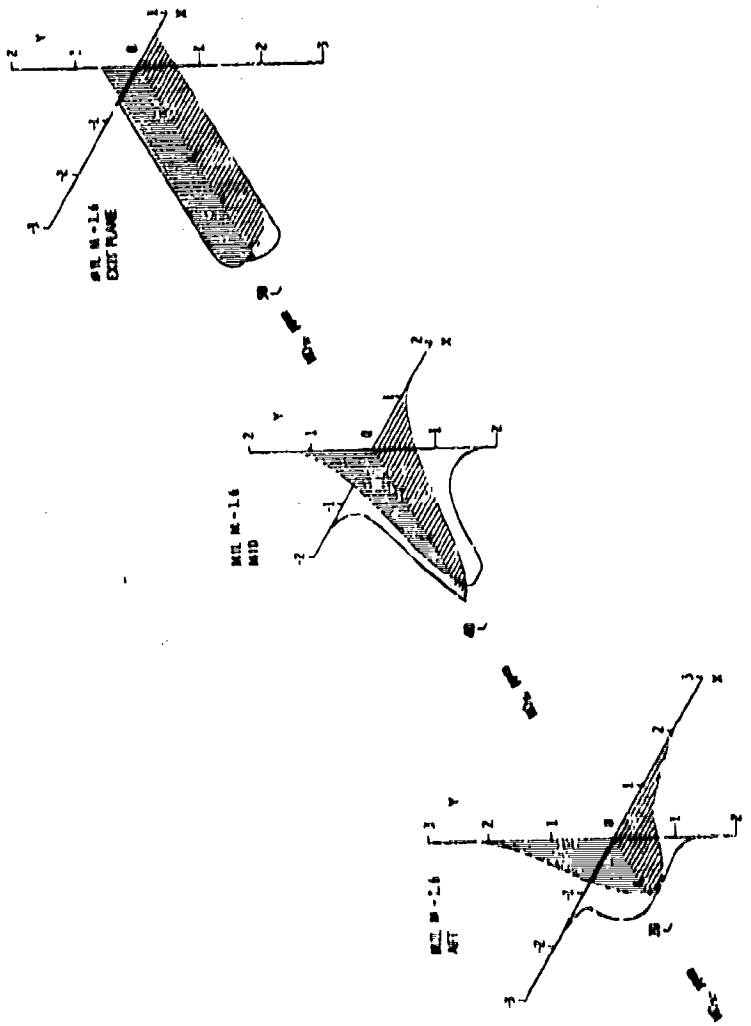

f. NO_x Profiles
Fig. 18 Continued

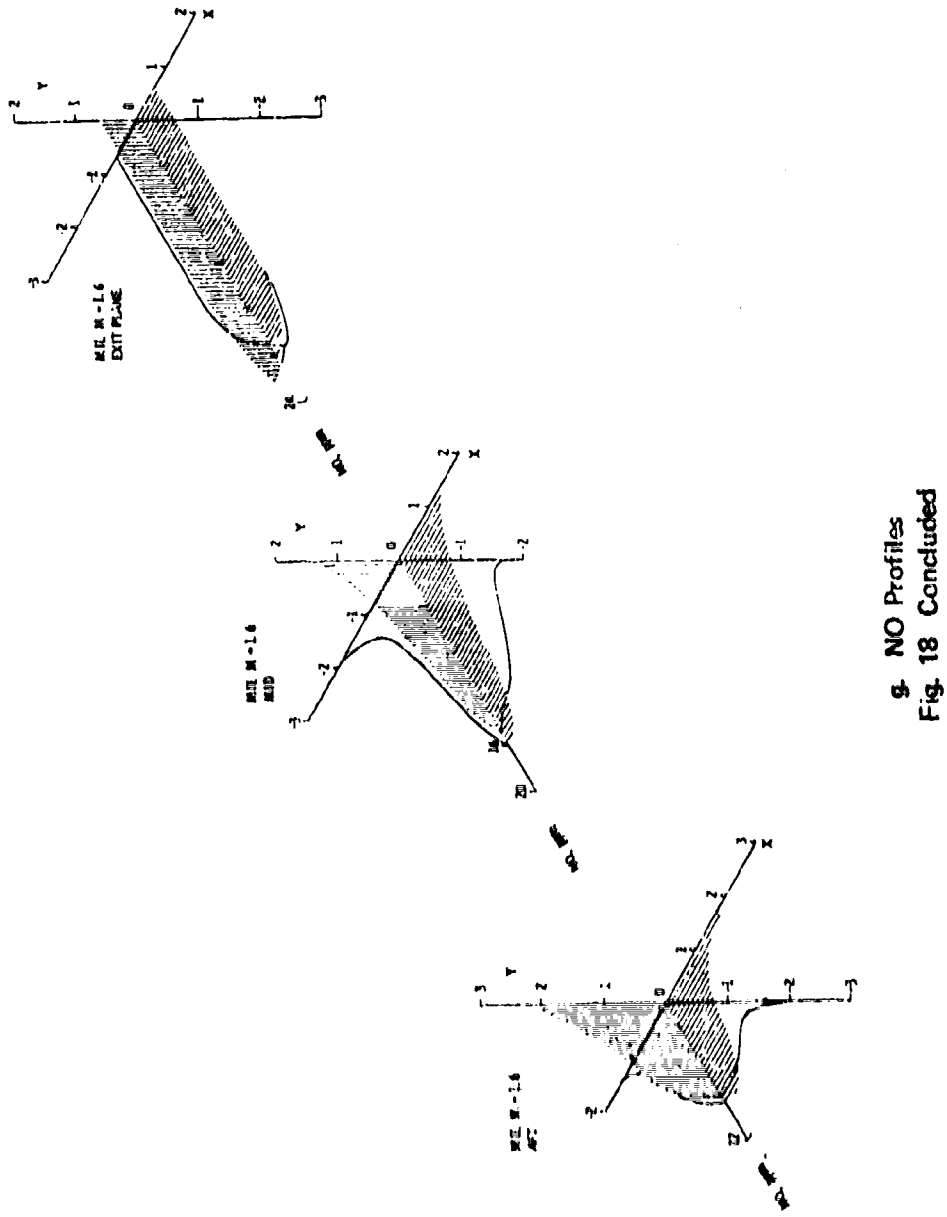

g. NO Profiles
Fig. 18 Concluded

SYMBOL	M_∞	ALT	PLS	XP/DN	XR
⊙	1.6	55K	MIL	0.22	HORIZ
⊡	1.6	55K	MIL	0.22	VERT

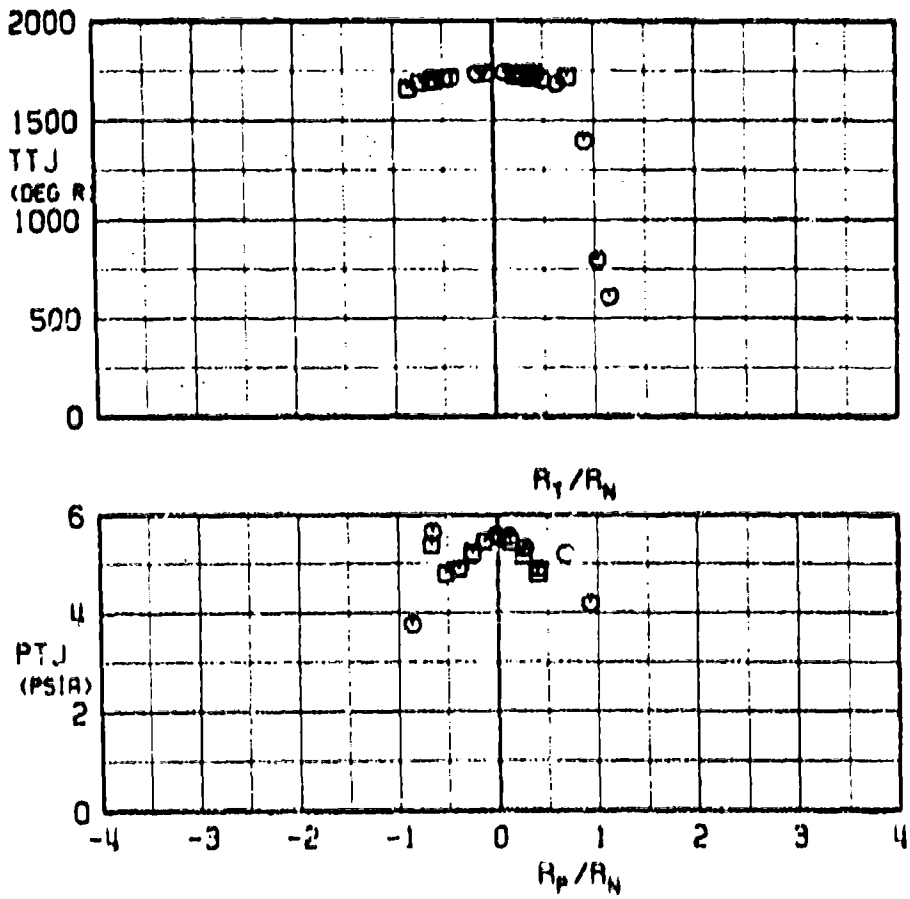

a. TTJ versus R_T/R_N and PTJ versus R_P/R_N

Fig. 19 Comparison of Exhaust Emission Concentrations at Horizontal and Vertical Plume Axis (Mach 1.6/55,000 ft, MIL, Exit Station)

SYMBOL	M_∞	ALT	PLS	XP/DN	XR
○	1.6	55K	MIL	0.22	HORIZ
□	1.6	55K	MIL	0.22	VERT

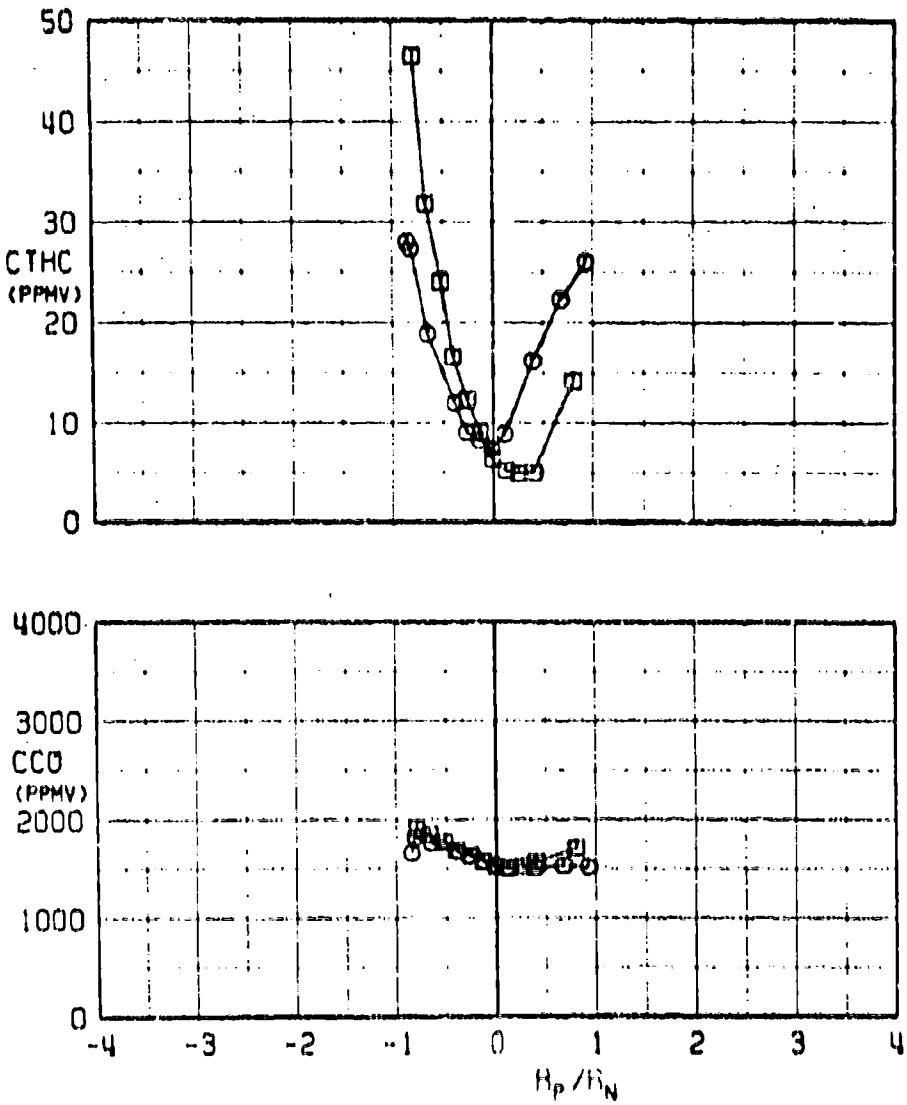

b. CTHC and CCO versus R_P/R_N
Fig. 10 Continued

SYMBOL	M_∞	ALT	PLS	XP/DN	XR
○	1.6	55K	MIL	0.22	HORIZ
□	1.6	55K	MIL	0.22	VERT

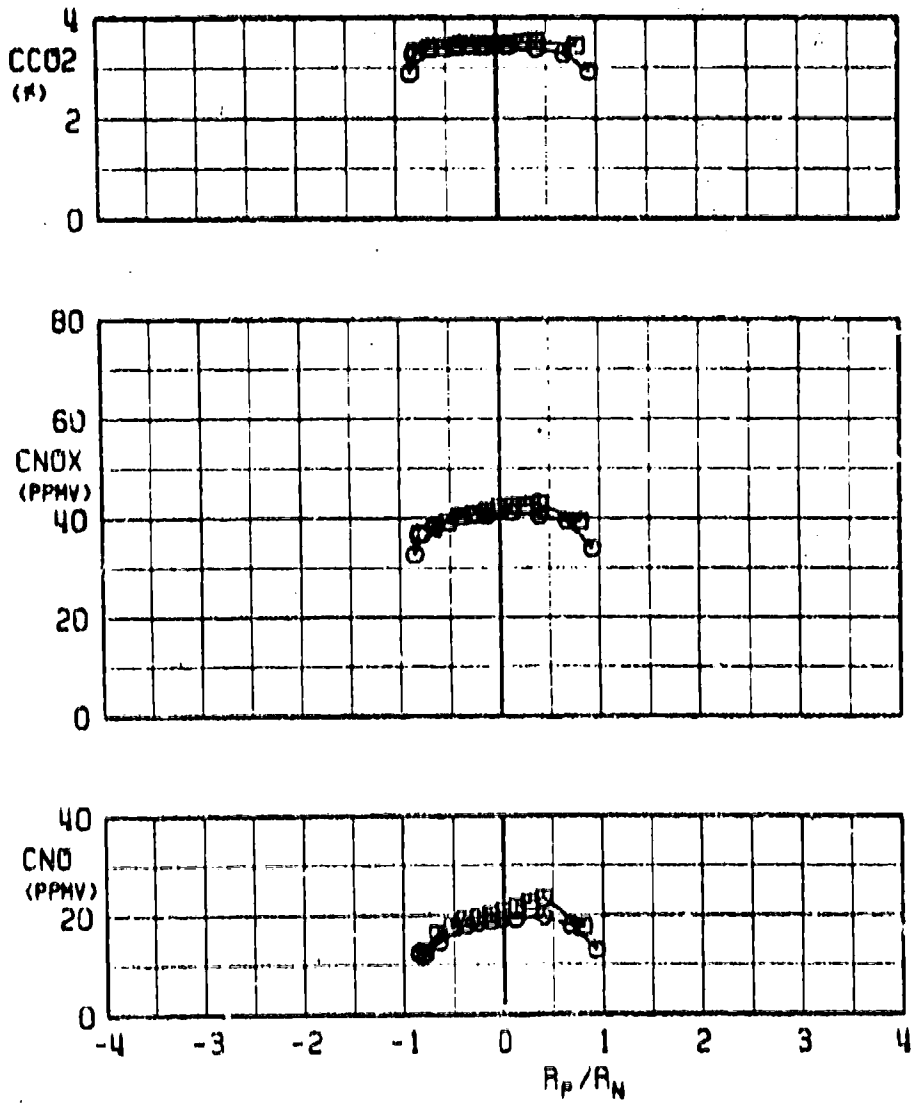

c. CCO_2, CNO_x, and CNO versus R_P/R_N
Fig. 19 Continued

SYMBOL	M_∞	ALT	PLS	XP/ON	XR
⊙	1.6	55K	MIL	0.22	HORIZ
⊡	1.6	55K	MIL	0.22	VERT

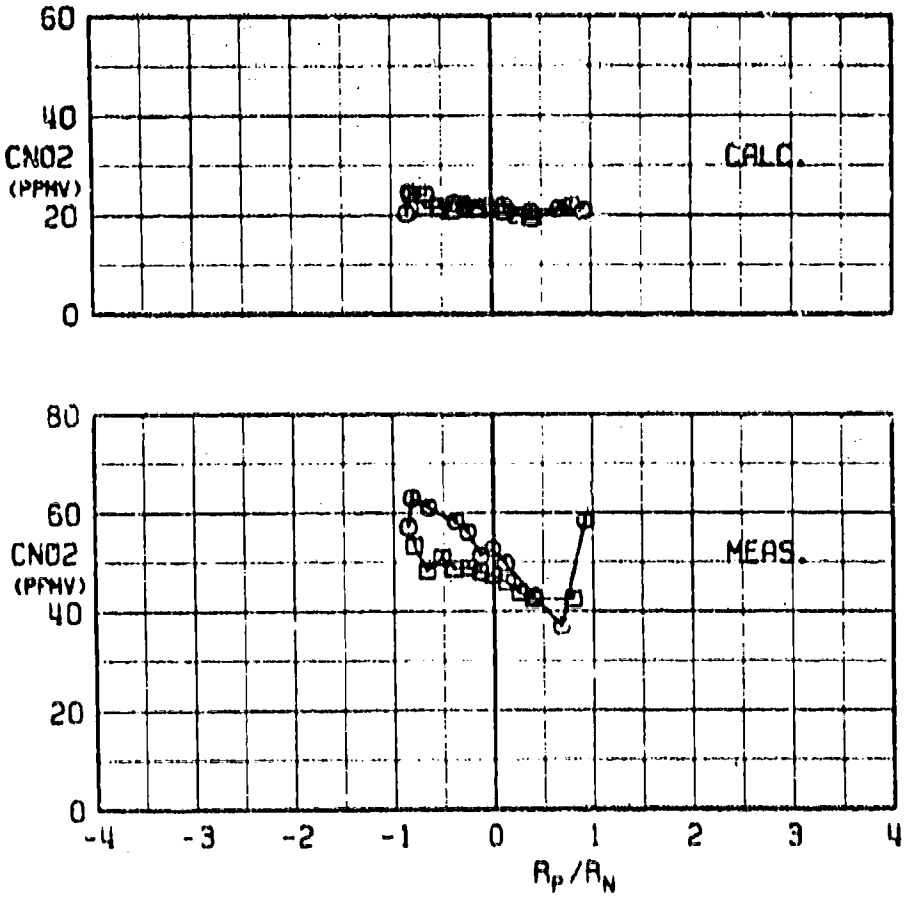

d. Calculated and Measured CNO_2 versus R_P/R_N
Fig. 19 Concluded

SYMBOL	M_∞	ALT	PLS	XP/DN	XR
○	1.6	55K	A/B	0.22	HORIZ
□	1.6	55K	A/B	0.22	VERT
△	2.0	65K	A/B	0.22	RDIAG

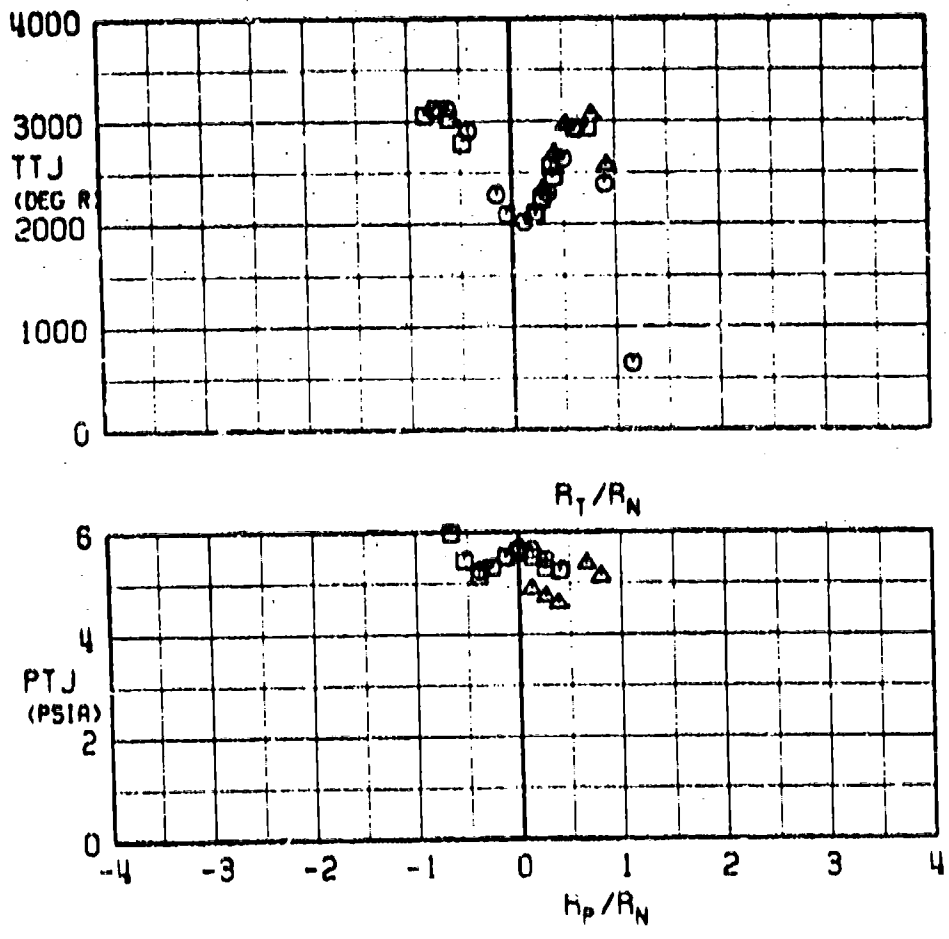

a. TTJ versus R_T/R_N and PTJ versus R_P/R_N

Fig. 20 Comparison of Exhaust Emission Concentrations at Horizontal and Vertical Plume Axis (Mach 1.6/55,000 ft, A/B, Exit Station) and Right Diagonal Axis (Mach 2.0/65,000 ft, A/B, Exit Station)

SYMBOL	M_∞	ALT	PLS	XP/DN	XR
○	1.6	55K	A/B	0.22	HORIZ
□	1.6	55K	A/B	0.22	VERT
△	2.0	65K	A/B	0.22	RDIAG

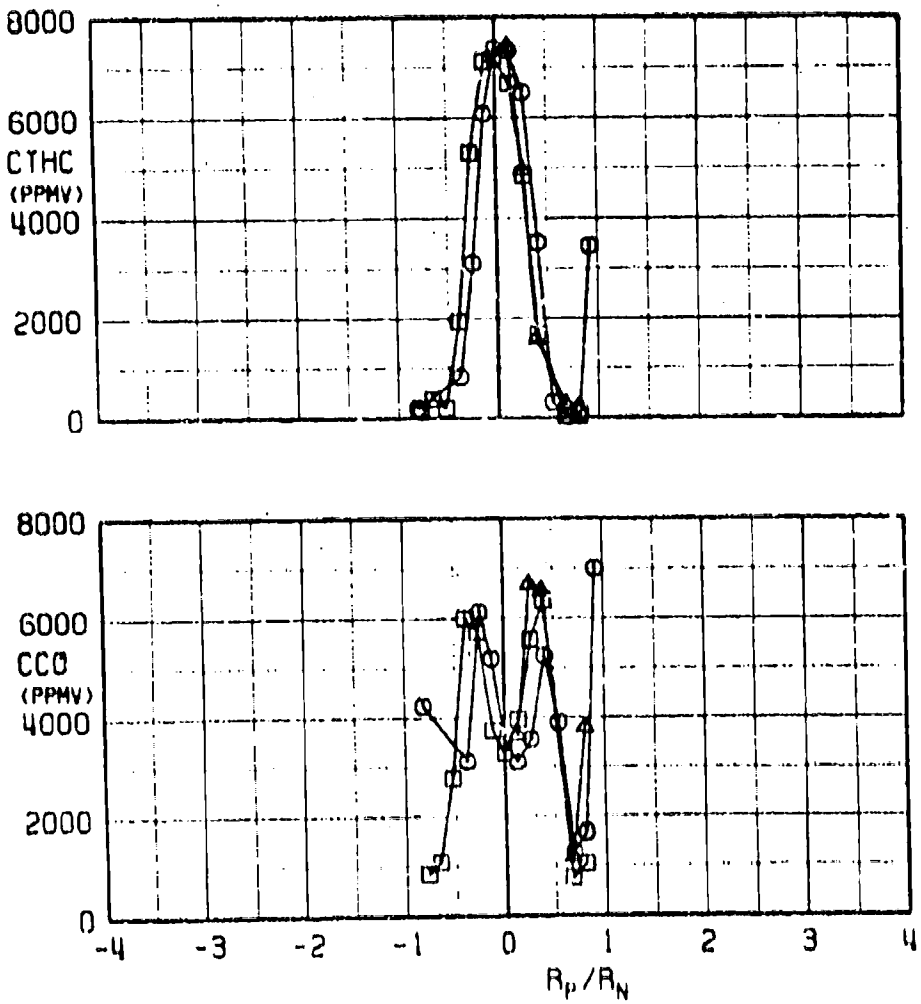

b. CTHC and CCO versus R_p/R_N
Fig. 20 Continued

SYMBOL	M_∞	ALT	PLS	XP/DN	XR
○	1.6	55K	A/B	0.22	HORIZ
□	1.6	55K	A/B	0.22	VERT
△	2.0	65K	A/B	0.22	RDIAG

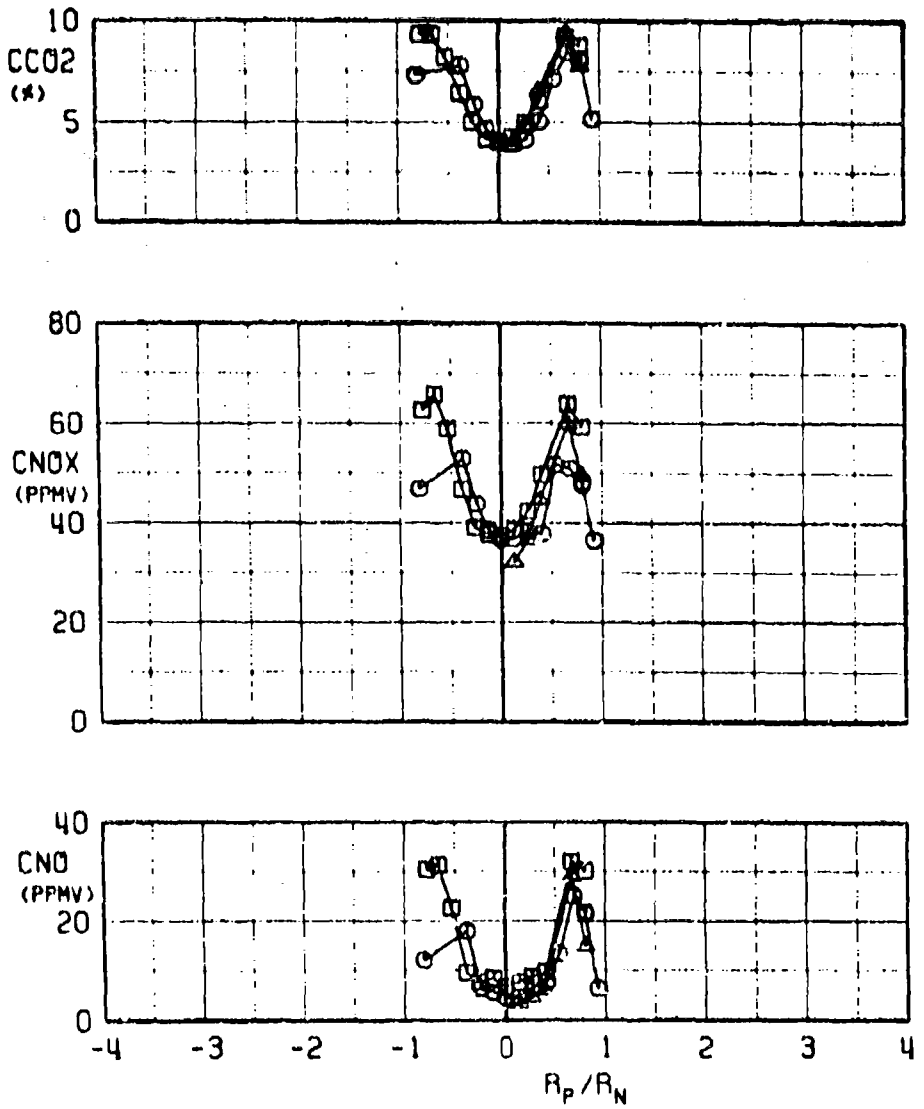

c. CCO_2, CNO_x, and CNO versus R_P/R_N
Fig. 20 Continued

SYMBOL	M_∞	ALT	PLS	XP/DN	XA
○	1.6	55K	A/B	0.22	HORIZ
□	1.6	55K	A/B	0.22	VERT
△	2.0	65K	A/B	0.22	RDIAL

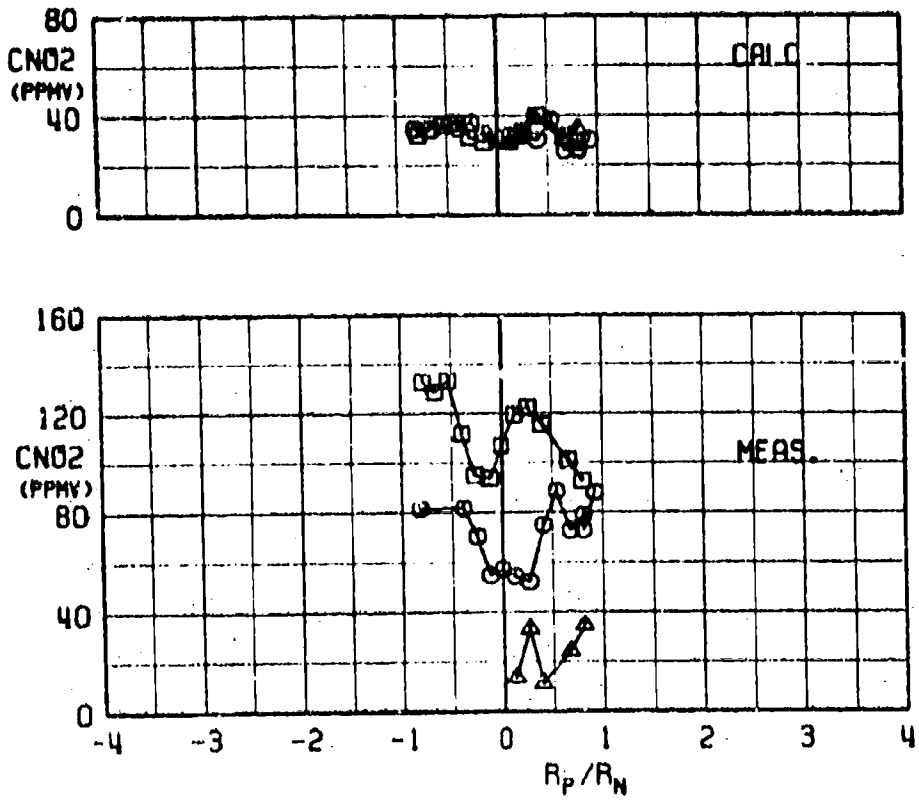

d. Calculated and Measured CNO_2 versus R_P/R_N
Fig. 20 Concluded

SYMBOL	M_∞	ALT	PLS	XP/DN	XR
○	2.0	65K	MIL	9.3	HORIZ
□	2.0	65K	MIL	9.3	VERT

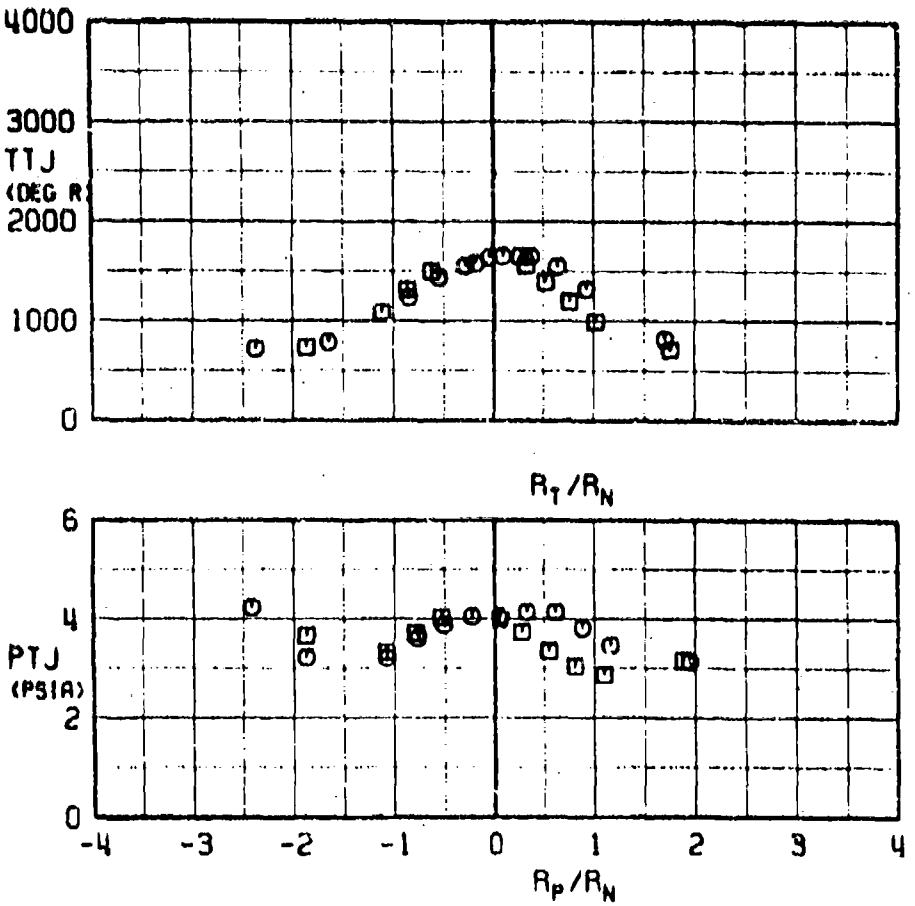

a. TTJ versus R_T/R_N and PTJ versus R_P/R_N

Fig. 21 Comparison of Exhaust Emission Concentrations at Horizontal and Vertical Plume Axis (Mach 2.0/65,000 ft, MIL, Mid Station)

SYMBOL	M_∞	ALT	PLS	XP/DN	XR
○	2.0	65K	MIL	9.30	HORIZ
□	2.0	65K	MIL	9.30	VERT

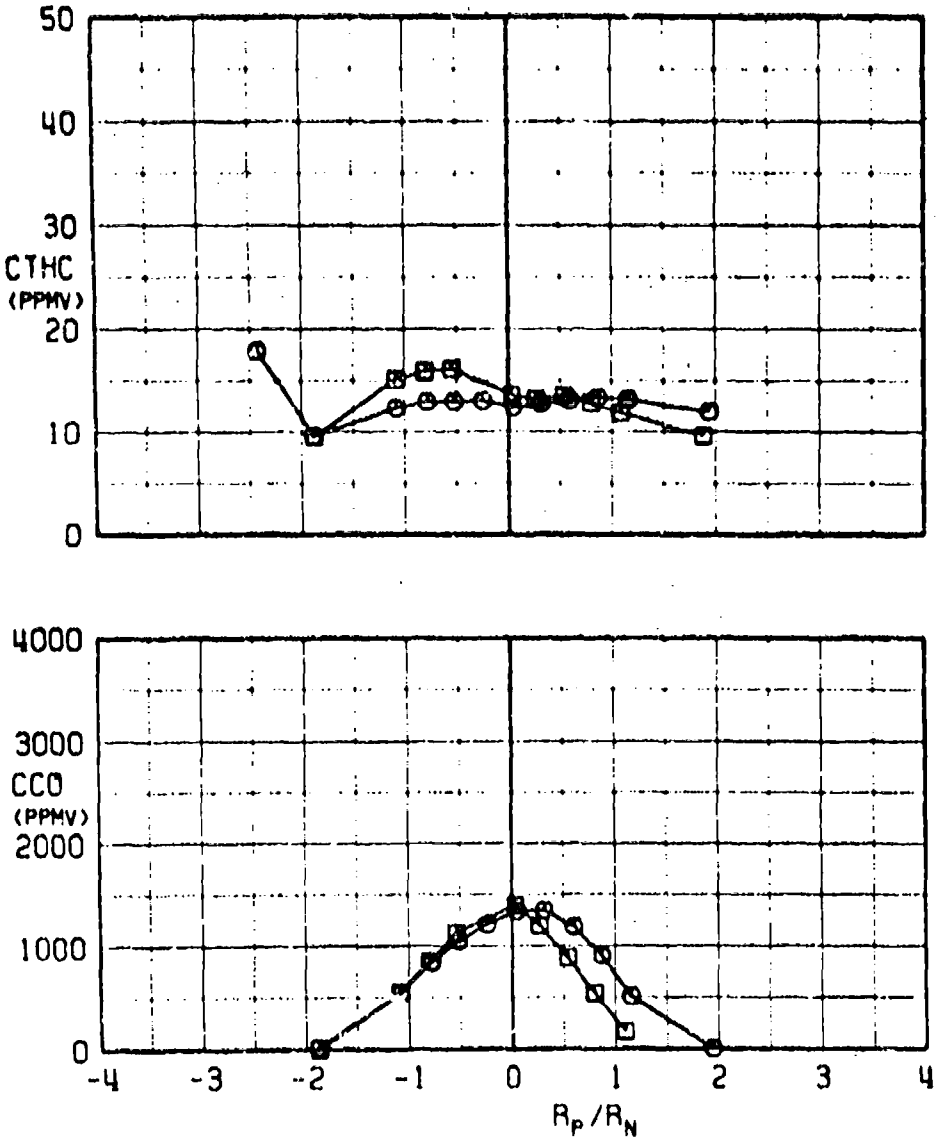

b. CTHC and CCO versus R_P/R_N
Fig. 21 Continued

SYMBOL	M_∞	ALT	PLS	XP/DN	XR
○	2.0	65K	MIL	9.30	HORIZ
□	2.0	65K	MIL	9.30	VERT

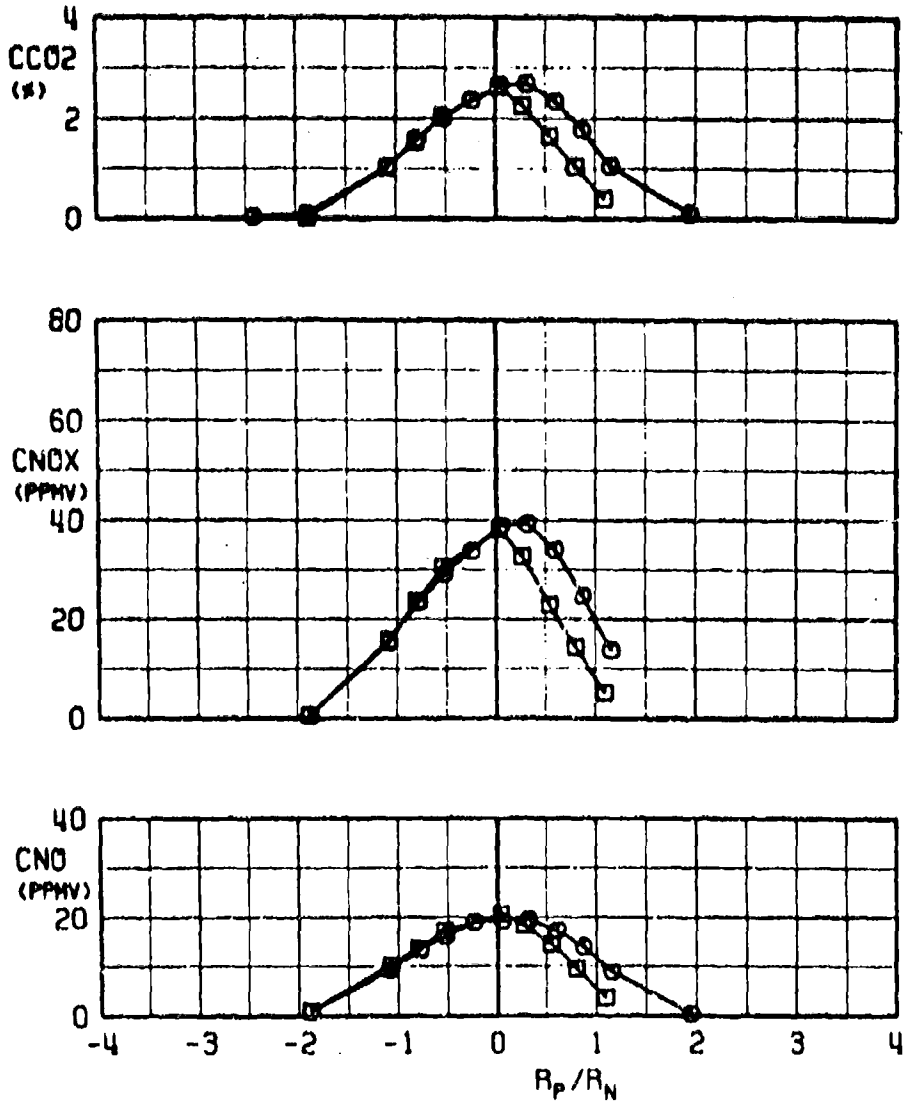

c. CCO_2, CNO_x, and CNO versus R_p/R_N
Fig. 21 Continued

SYMBOL	M_∞	ALT	PLS	XP/ON	XR
○	2.0	65K	MIL	9.30	HORIZ
□	2.0	65K	MIL	9.30	VERT

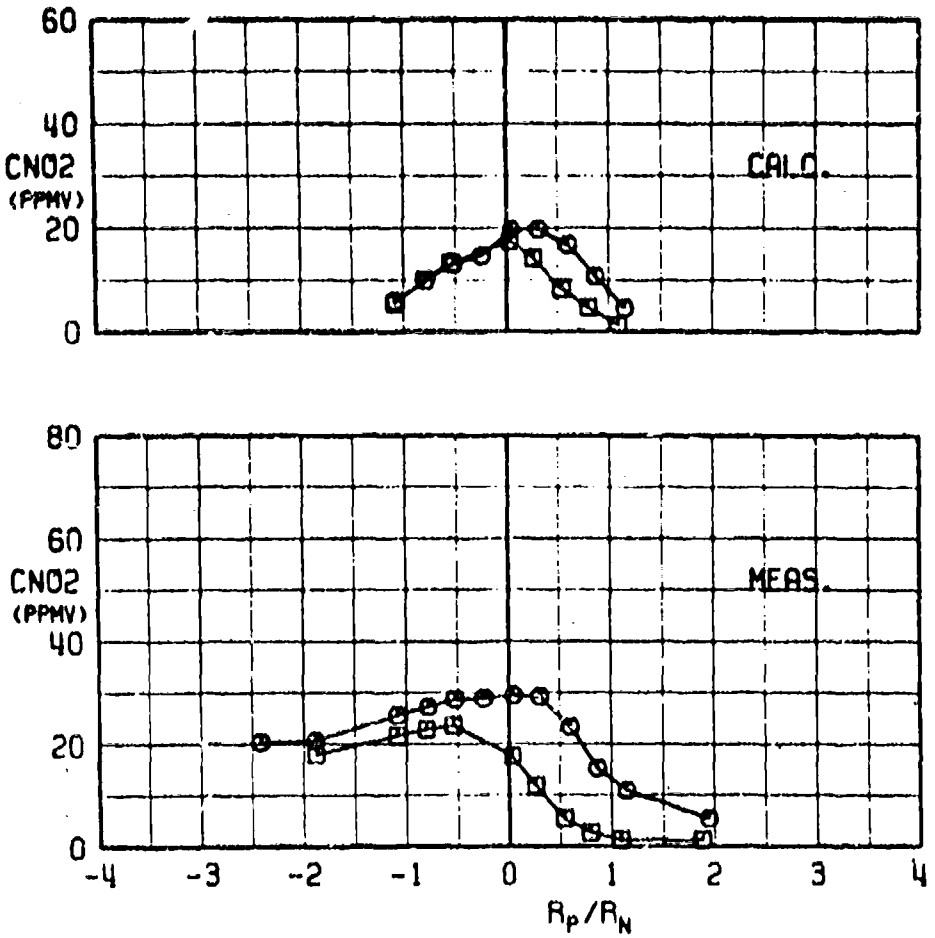

d. Calculated and Measured CNO_2 versus R_P/R_N
Fig. 21 Concluded

SYMBOL	M_∞	ALT	PLS	XP/DN	XR
○	2.0	65K	MIL	19.90	HORIZ
△	2.0	65K	MIL	19.90	LDIAG
◇	2.0	65K	MIL	19.90	RDIAG

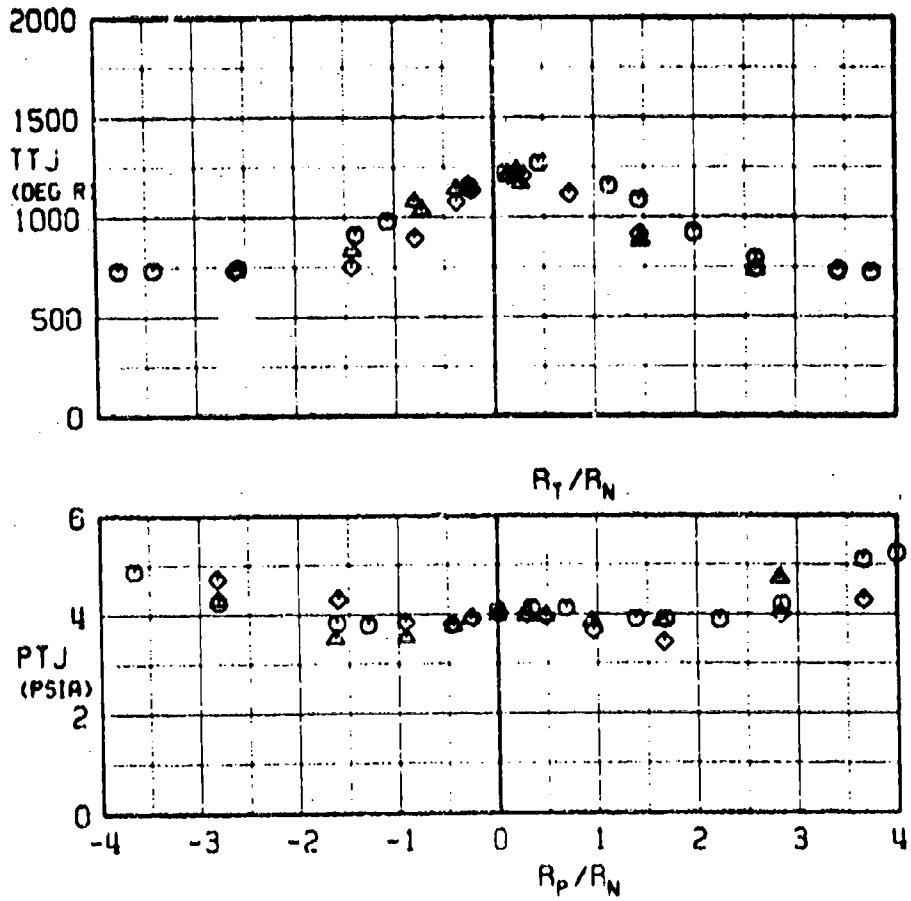

a. TTJ versus R_T/R_N and PTJ versus R_P/R_N

Fig. 22 Comparison of Exhaust Emission Concentrations at Horizontal, Vertical, Left Diagonal, and Right Diagonal Plume Axis (Mach 2.0/65,000 ft, MIL, Aft Station)

SYMBOL	M_∞	ALT	PLS	XP/DN	XR
○	2.0	65K	MIL	19.90	HORIZ
□	2.0	65K	MIL	19.90	VERT
△	2.0	65K	MIL	19.90	LDIAG
◇	2.0	65K	MIL	19.90	RDIAG

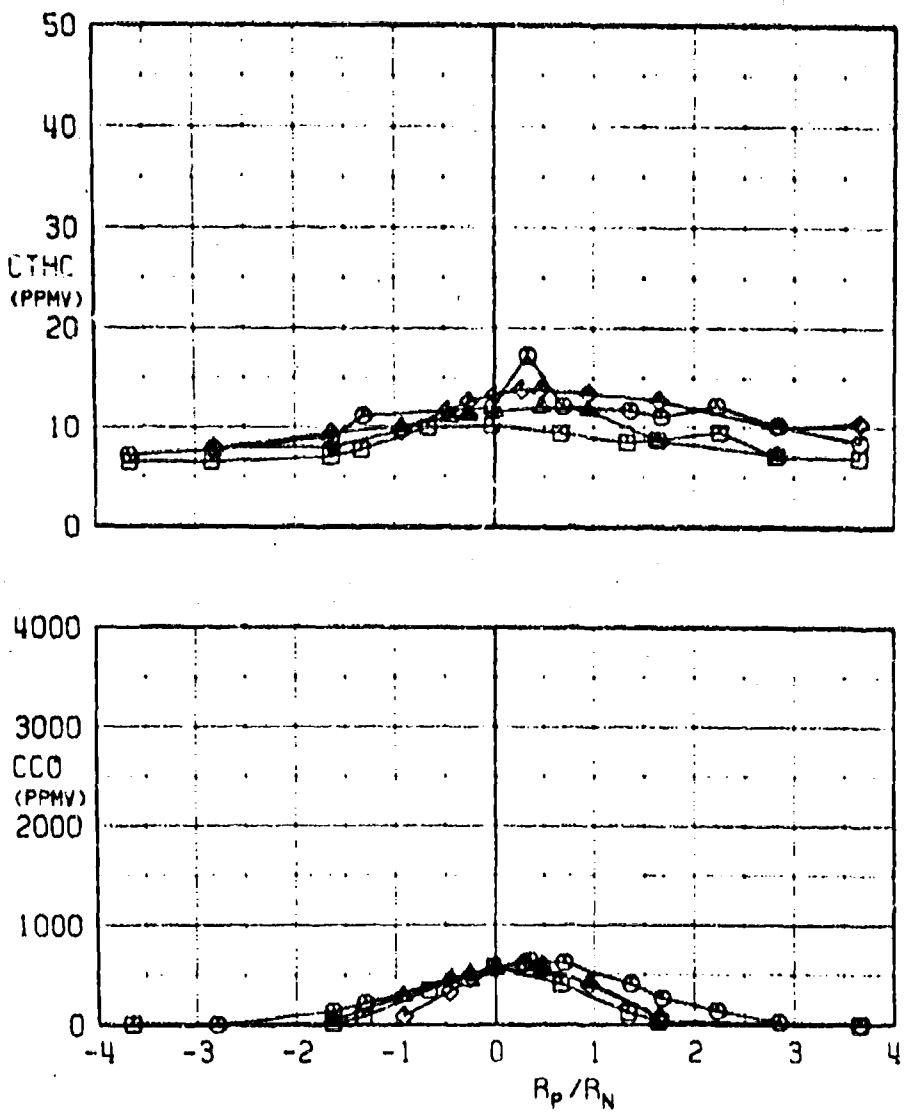

b. CTHC and CCO versus R_P/R_N
Fig. 22 Continued

SYMBOL	M_∞	ALT	PLS	XP/ON	XR
○	2.0	65K	MIL	19.90	HORIZ
□	2.0	65K	MIL	19.90	VERT
△	2.0	65K	MIL	19.90	LDIAG
◇	2.0	65K	MIL	19.90	RDIAG

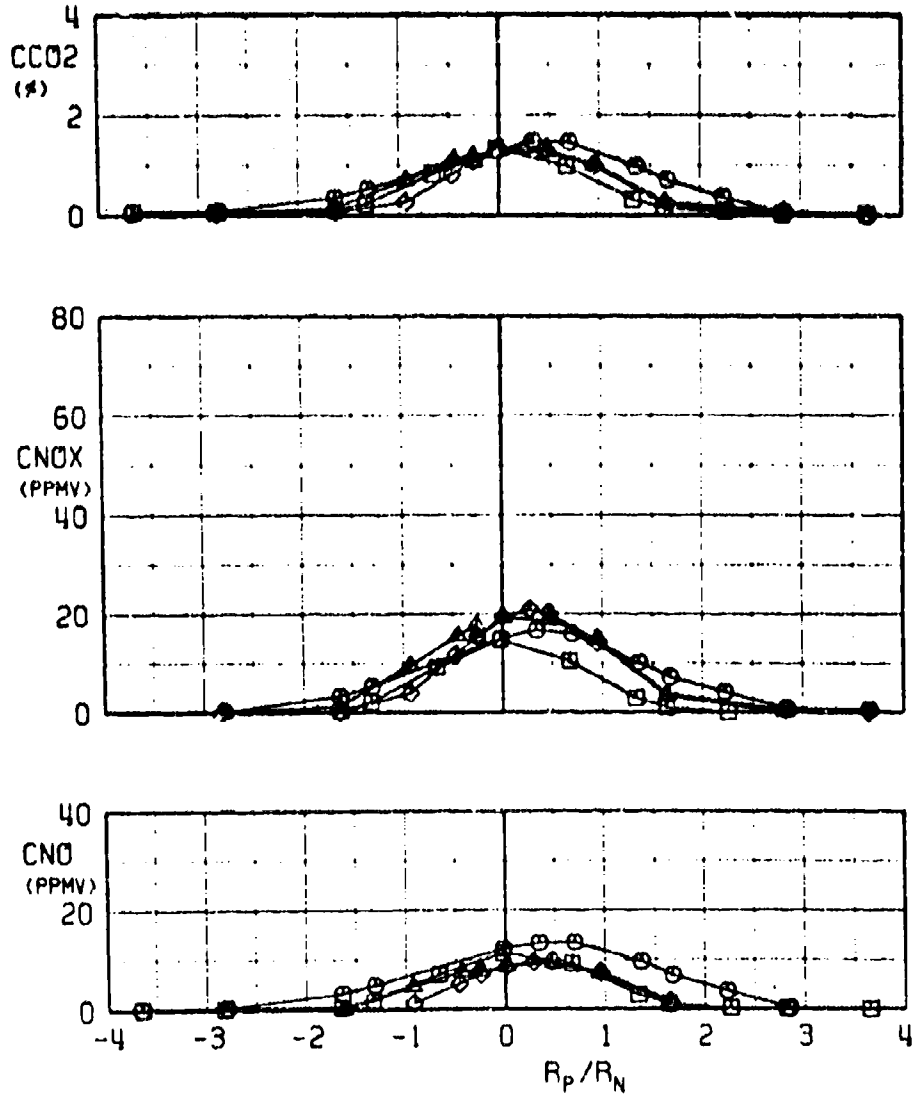

c. CCO_2, CNO_x, and CNO versus R_P/R_N
Fig. 22 Continued

SYMBOL	M_∞	ALT	PLS	XP/ON	XR
○	2.0	65K	MIL	19.90	HORIZ
□	2.0	65K	MIL	19.90	VERT
△	2.0	65K	MIL	19.90	LDIAG
◇	2.0	65K	MIL	19.90	RDIAG

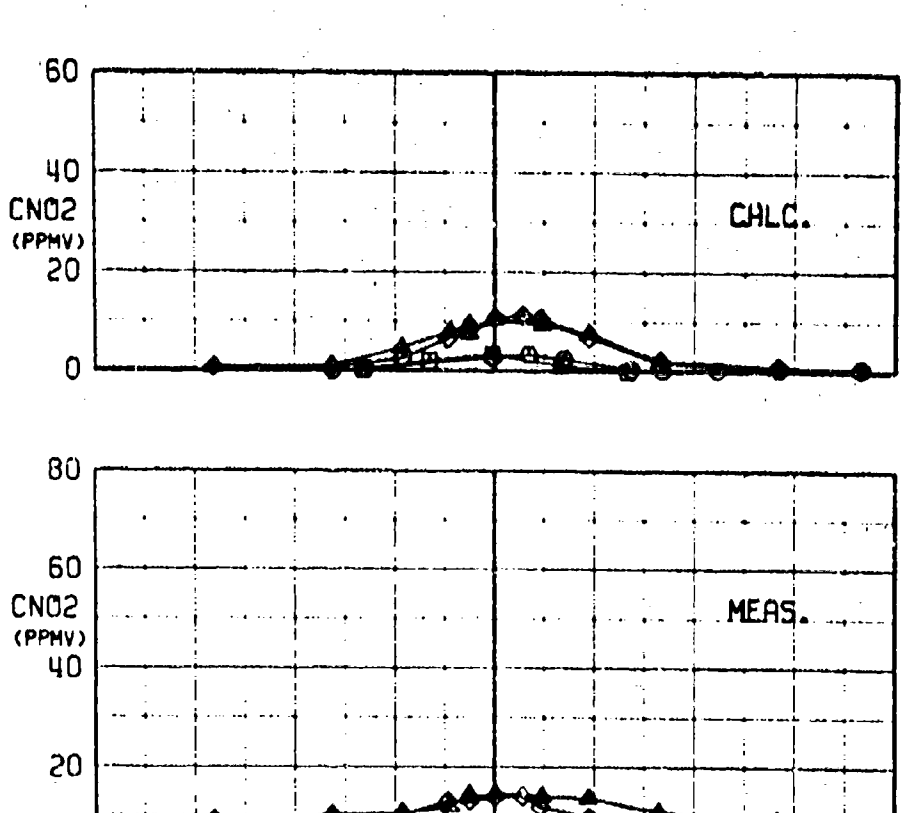

d. Calculated and Measured CNO_2 versus R_P/R_N
Fig. 22 Concluded

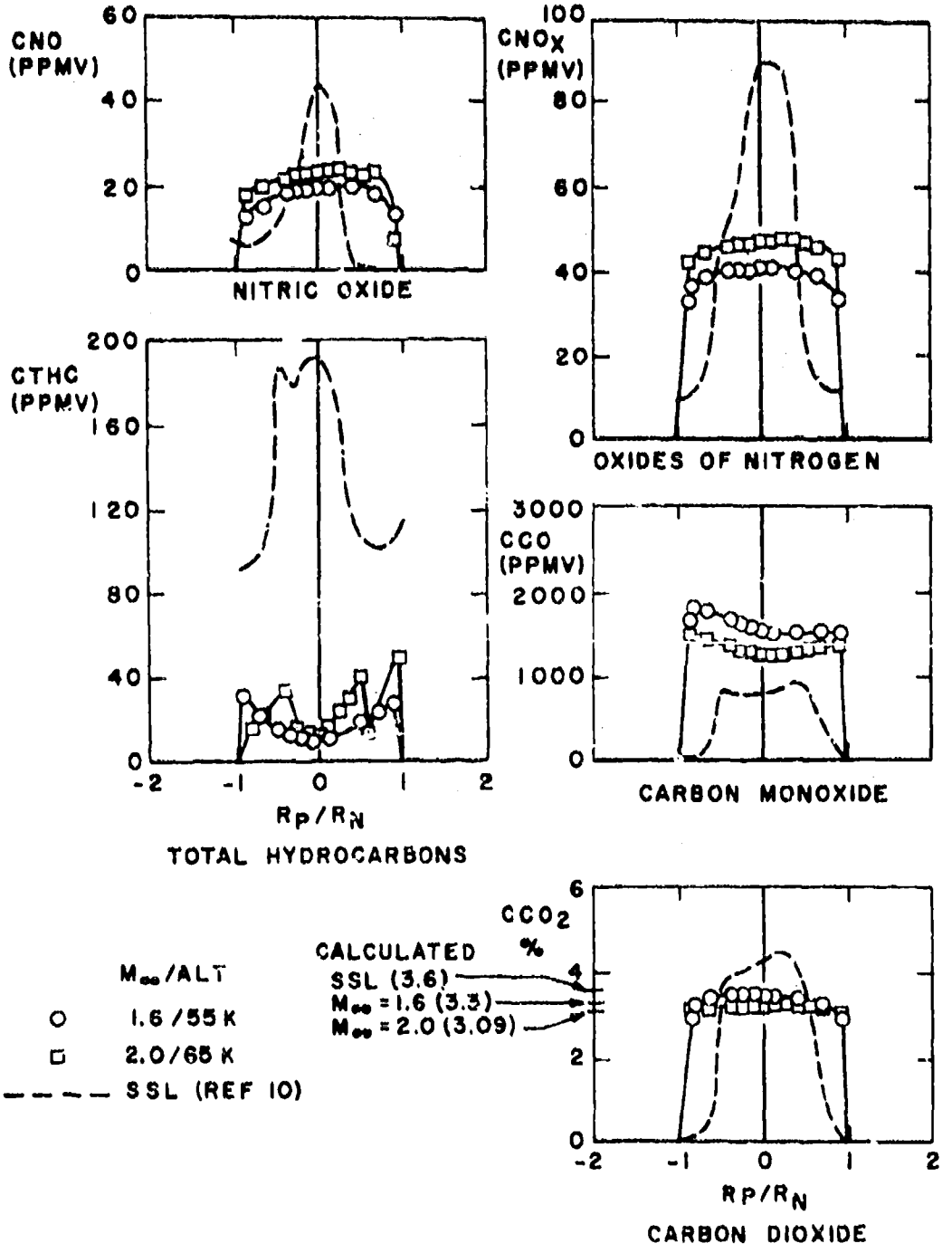

Fig. 23 Comparison of Exit Plane Profile for the Gaseous Emissions of the J85 Turbojet Engine

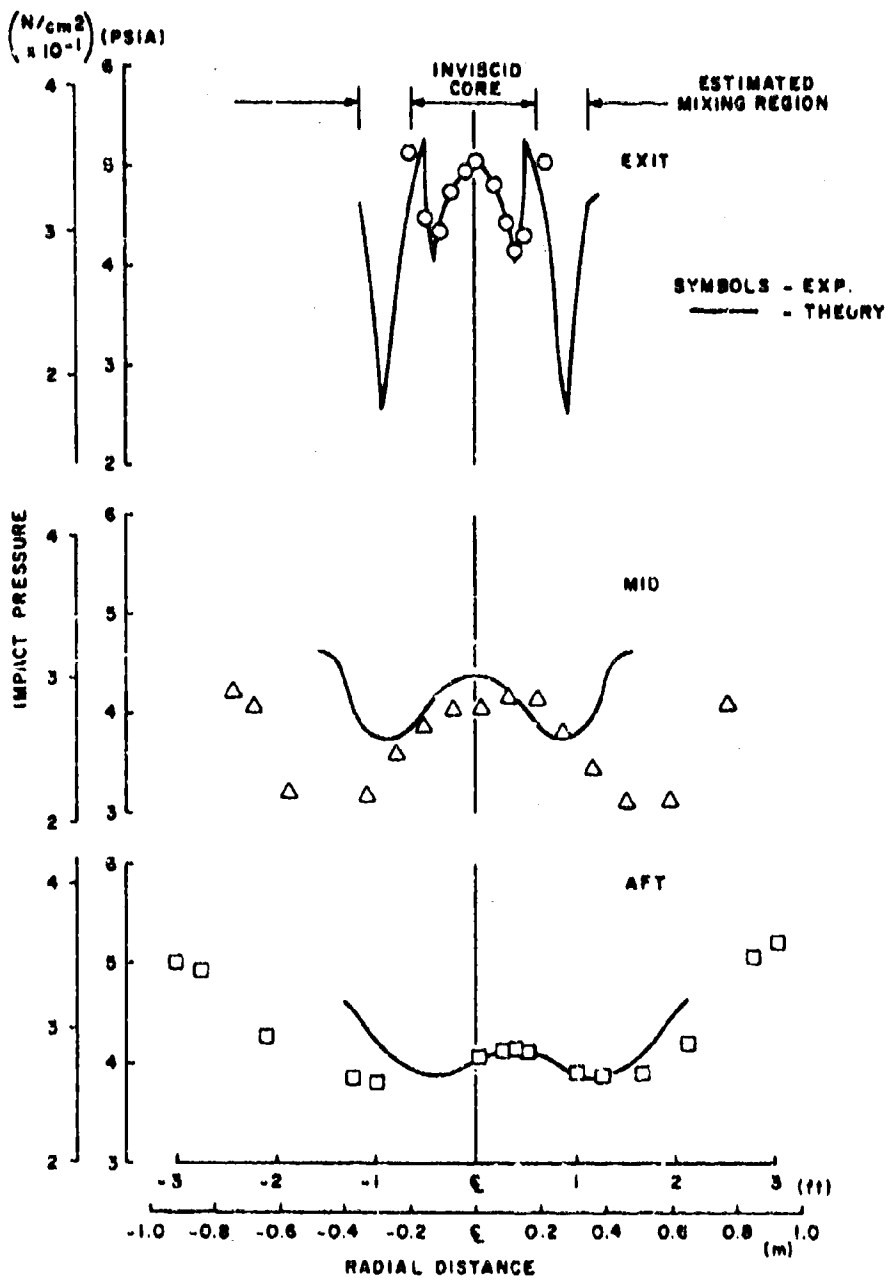

a. Plume Impact Pressure

Fig. 24 Comparison of Theoretical and Experimental Results at Mach 2.0/65,000 ft, Military Power

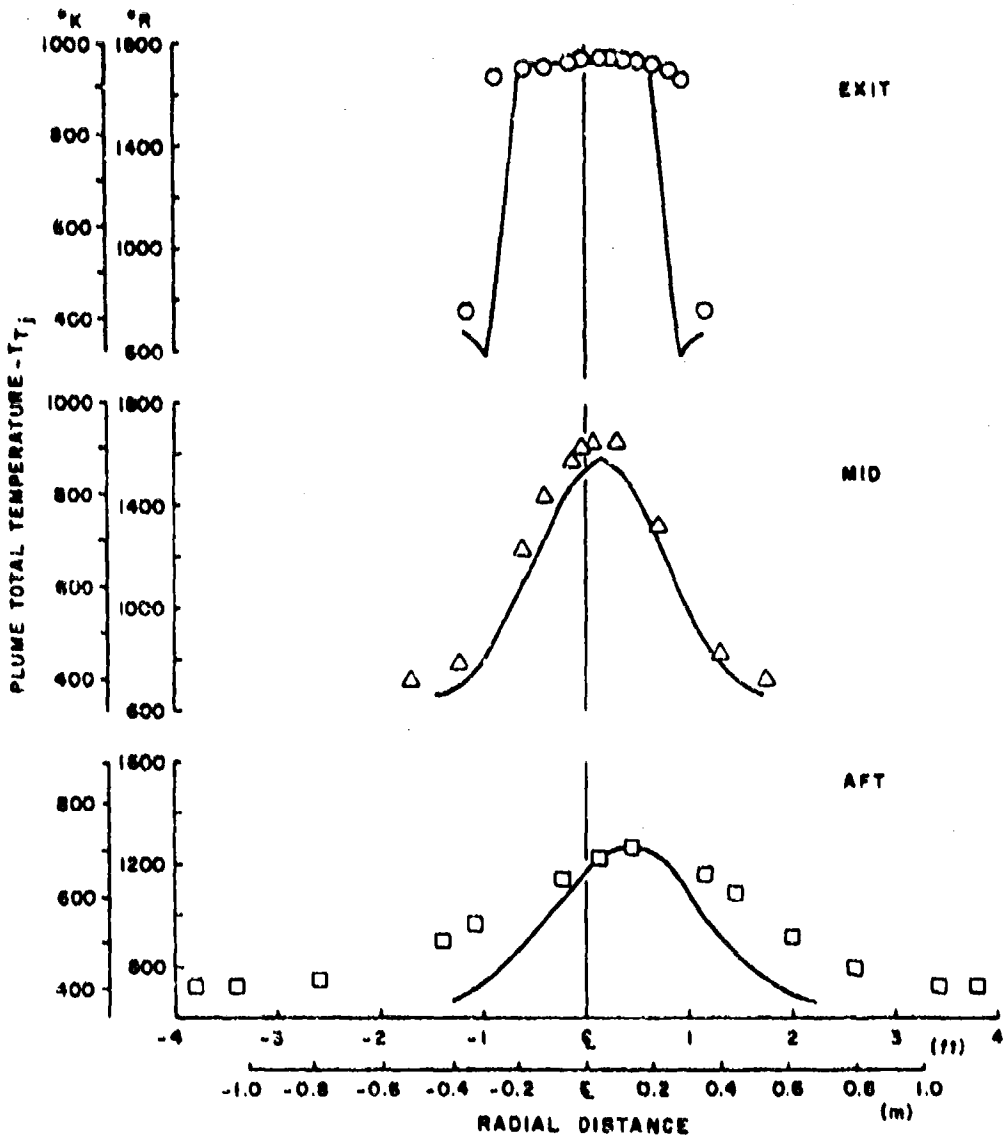

b. Plume Total Temperature
Fig. 24 Continued

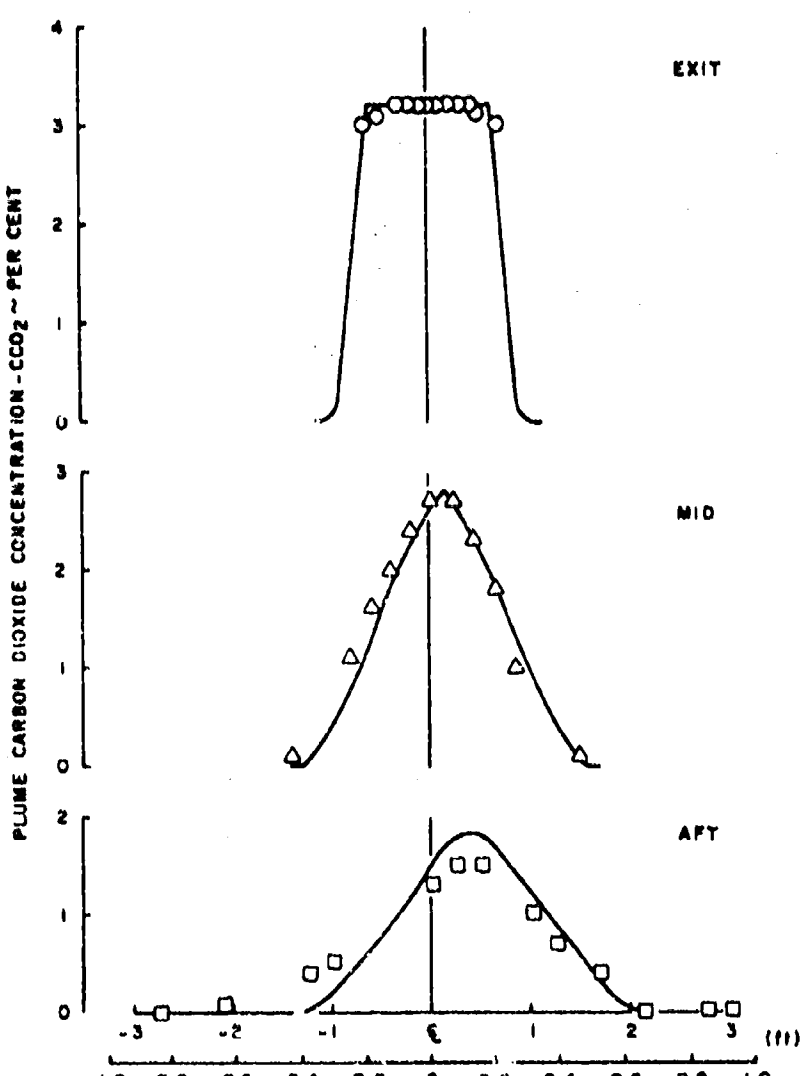

c. Plume Carbon Dioxide Concentration
Fig. 24 Continued

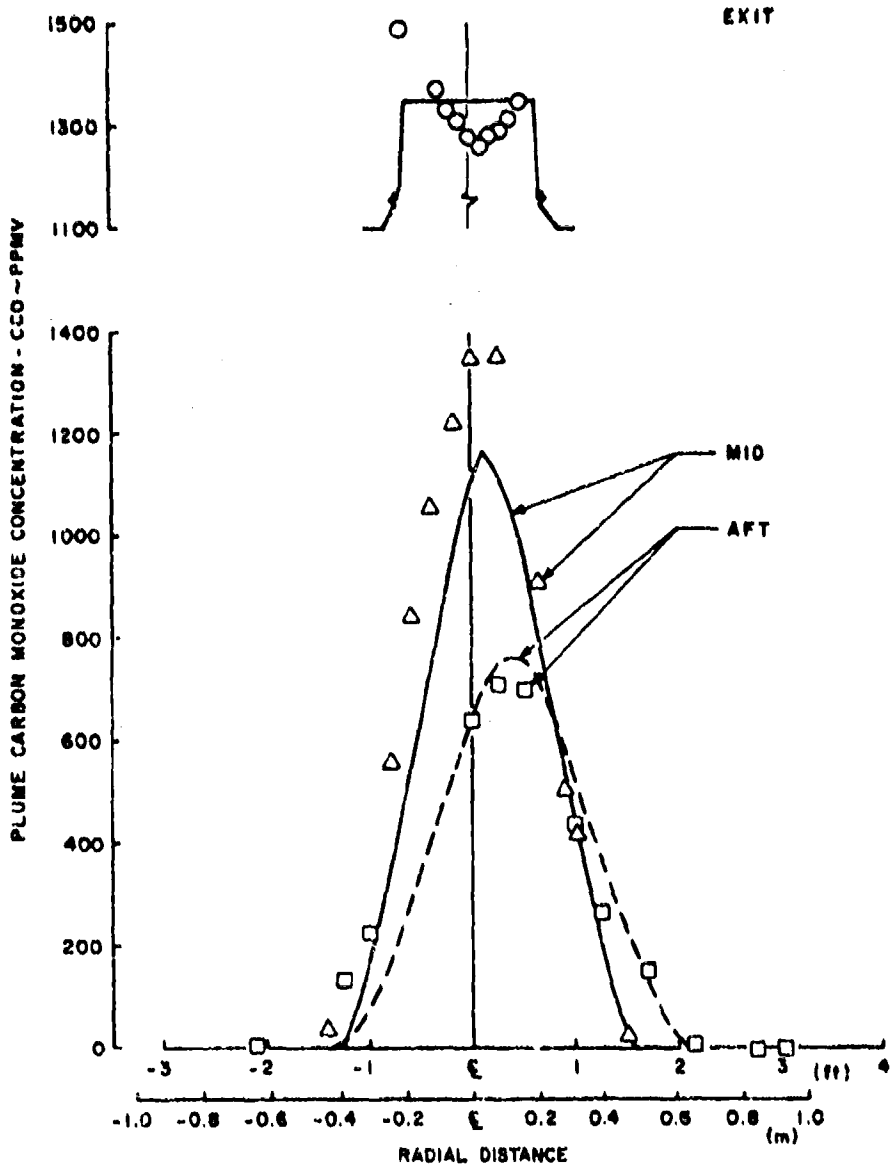

d. Plume Carbon Monoxide Concentration
Fig. 24 Continued

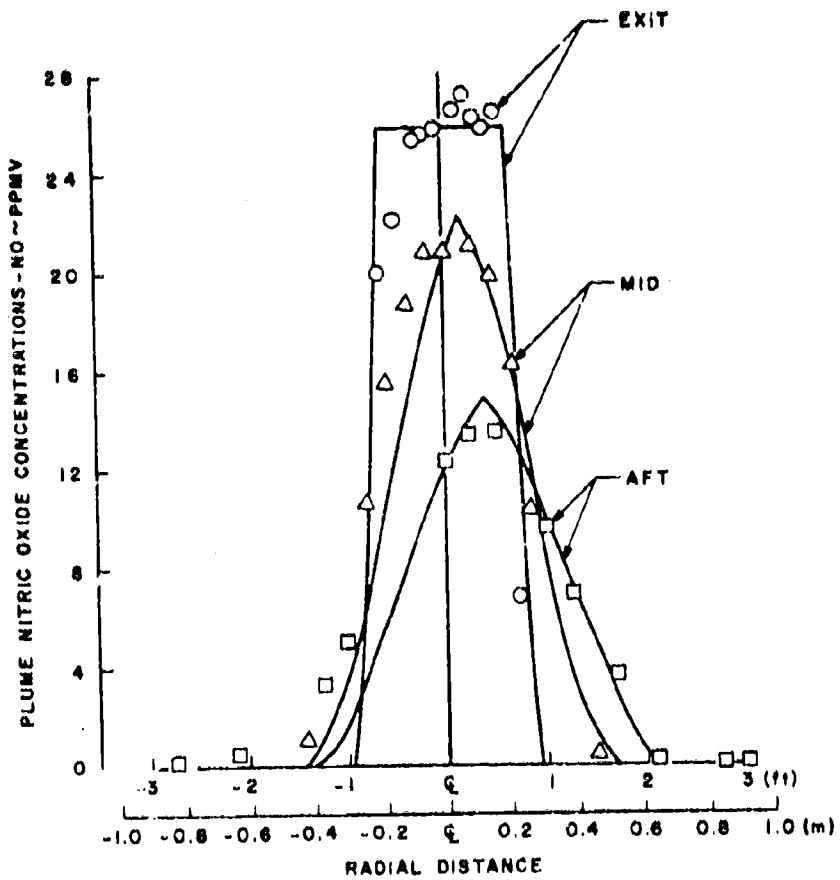

e. Plume Nitric Oxide Concentrations
Fig. 24 Continued

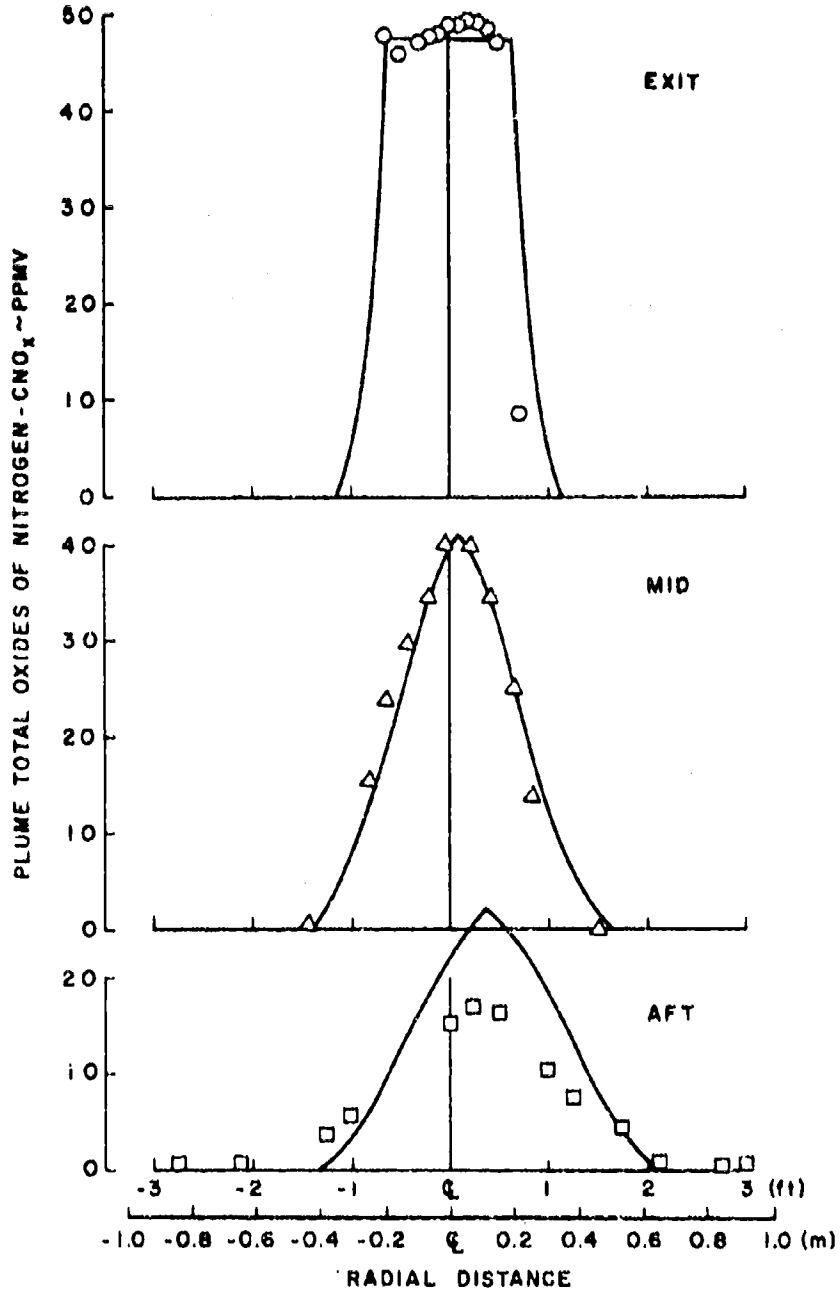

f. Plume Total Oxides of Nitrogen Concentration
Fig. 24 Continued

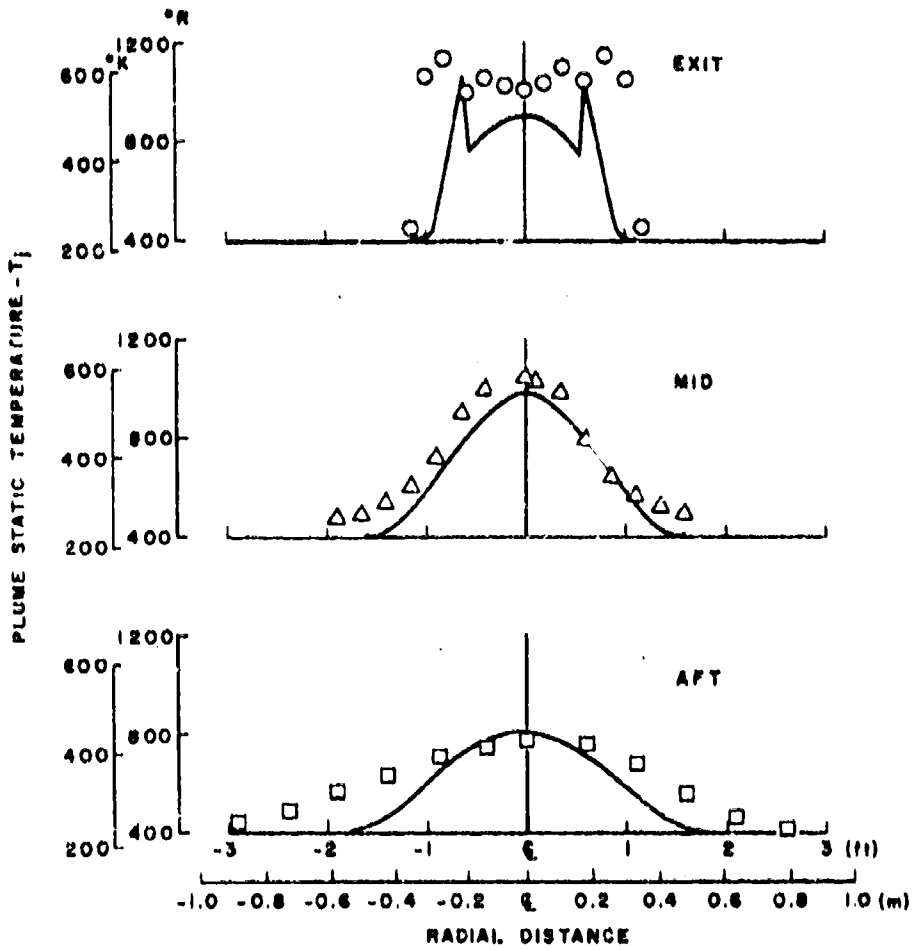

g. Plume Static Temperature
Fig. 24 Continued

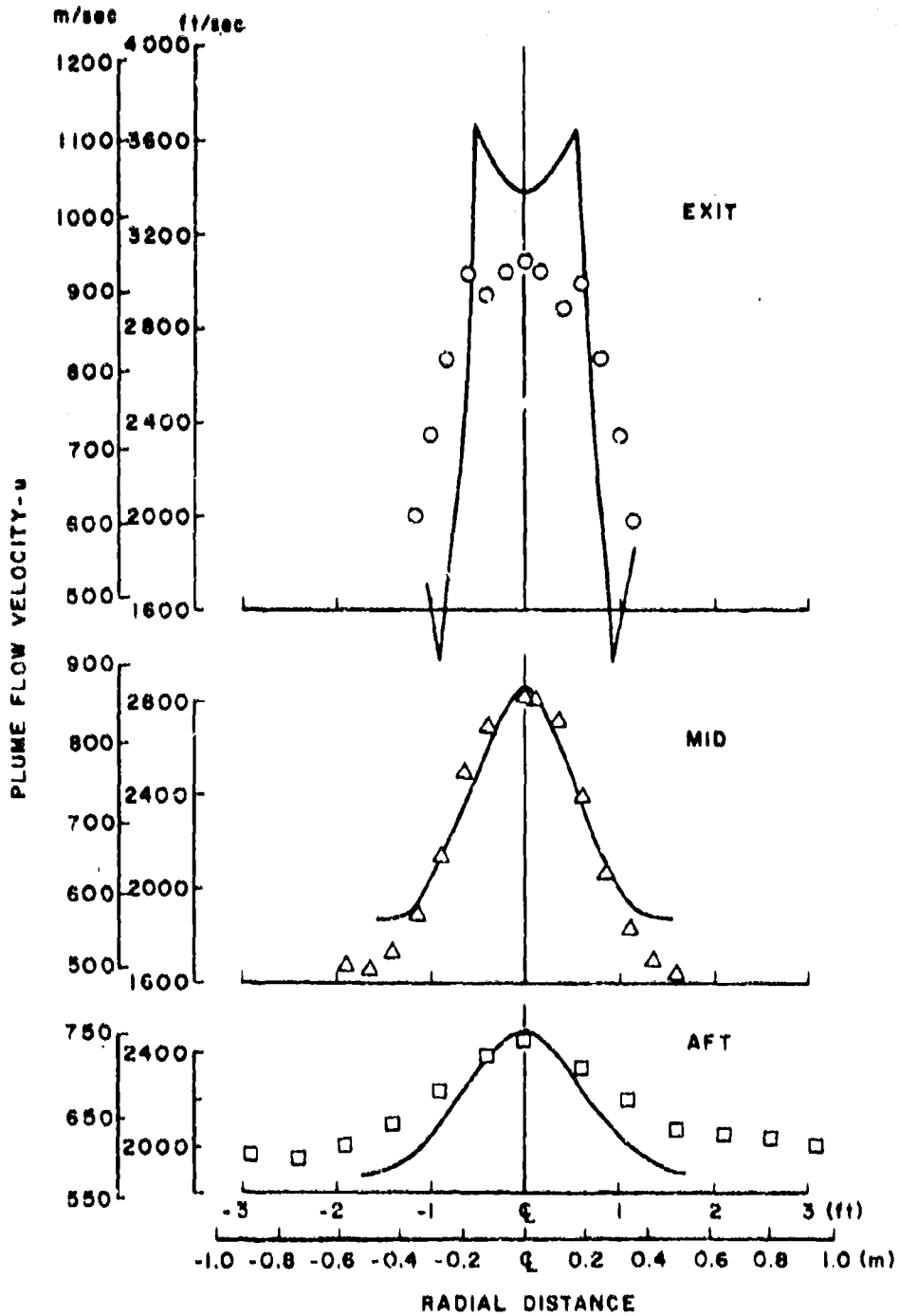

h. Plume Flow Velocity
Fig. 24 Concluded

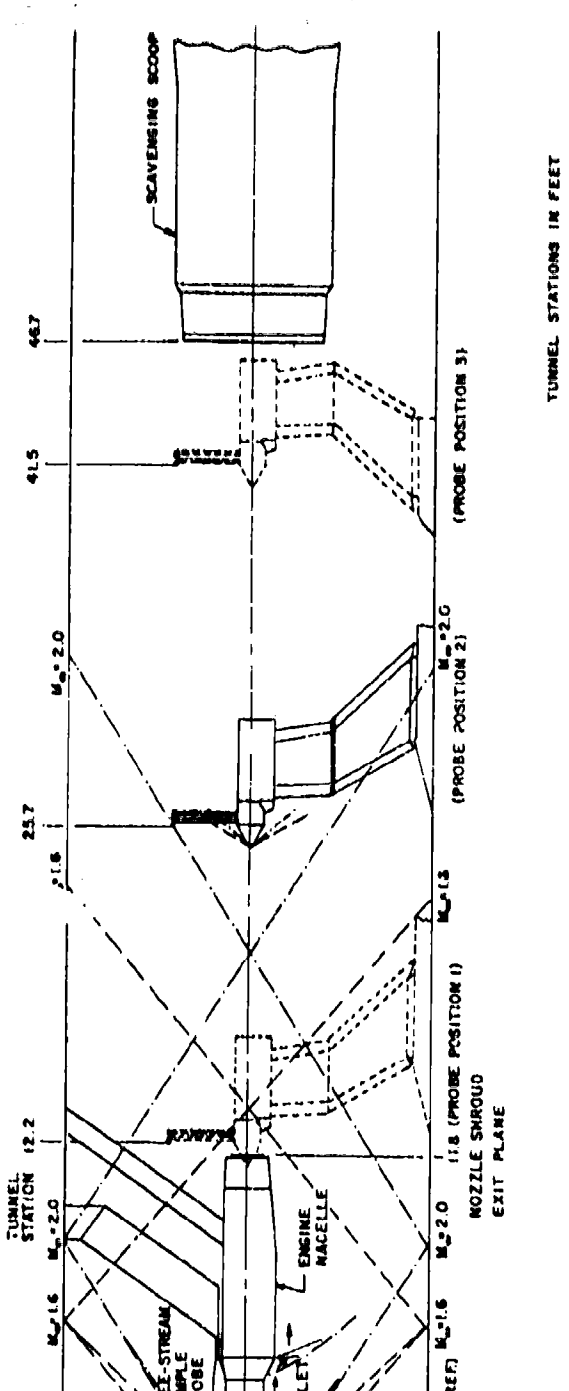

Fig. 25 Estimate of Shock Waves Generated by Model

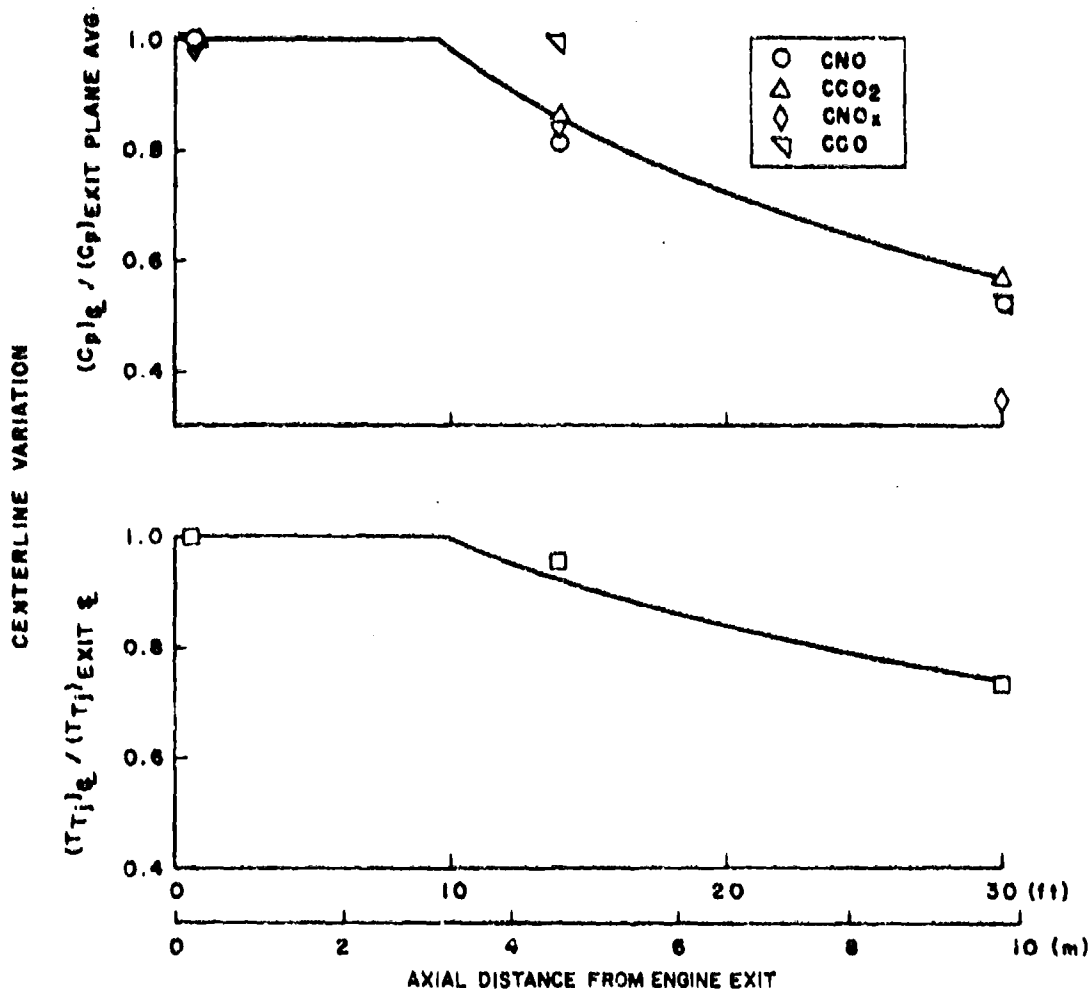

Fig. 26 Centerline Decay Characteristics of the Emission Concentrations and Total Temperature in the Exhaust Plume at Mach 2.0/65,000 ft, Military Power

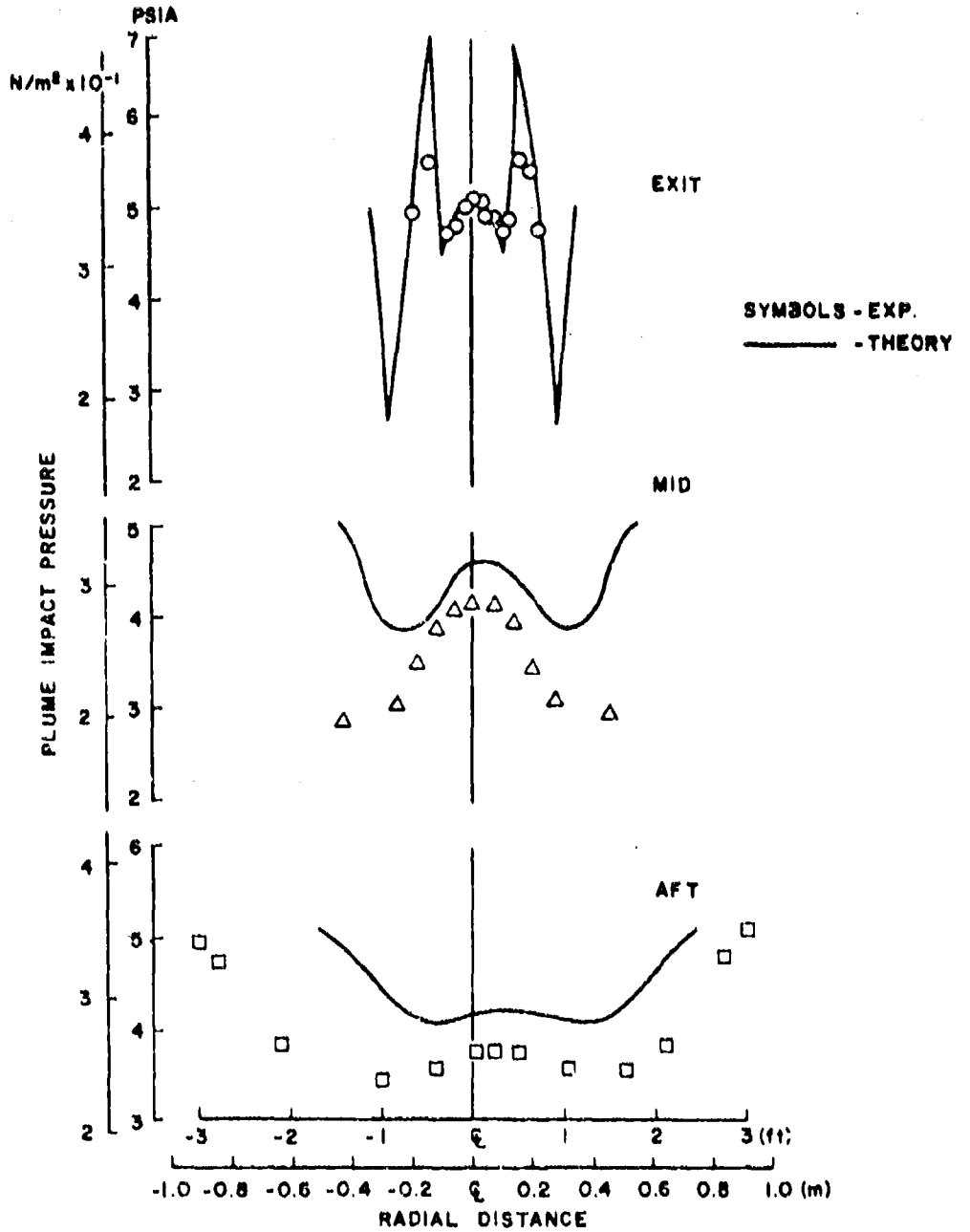

a. Plume Impact Pressure

Fig. 27 Comparison of Theoretical and Experimental Results at Mach 2.0/65,000 ft, Afterburning Power

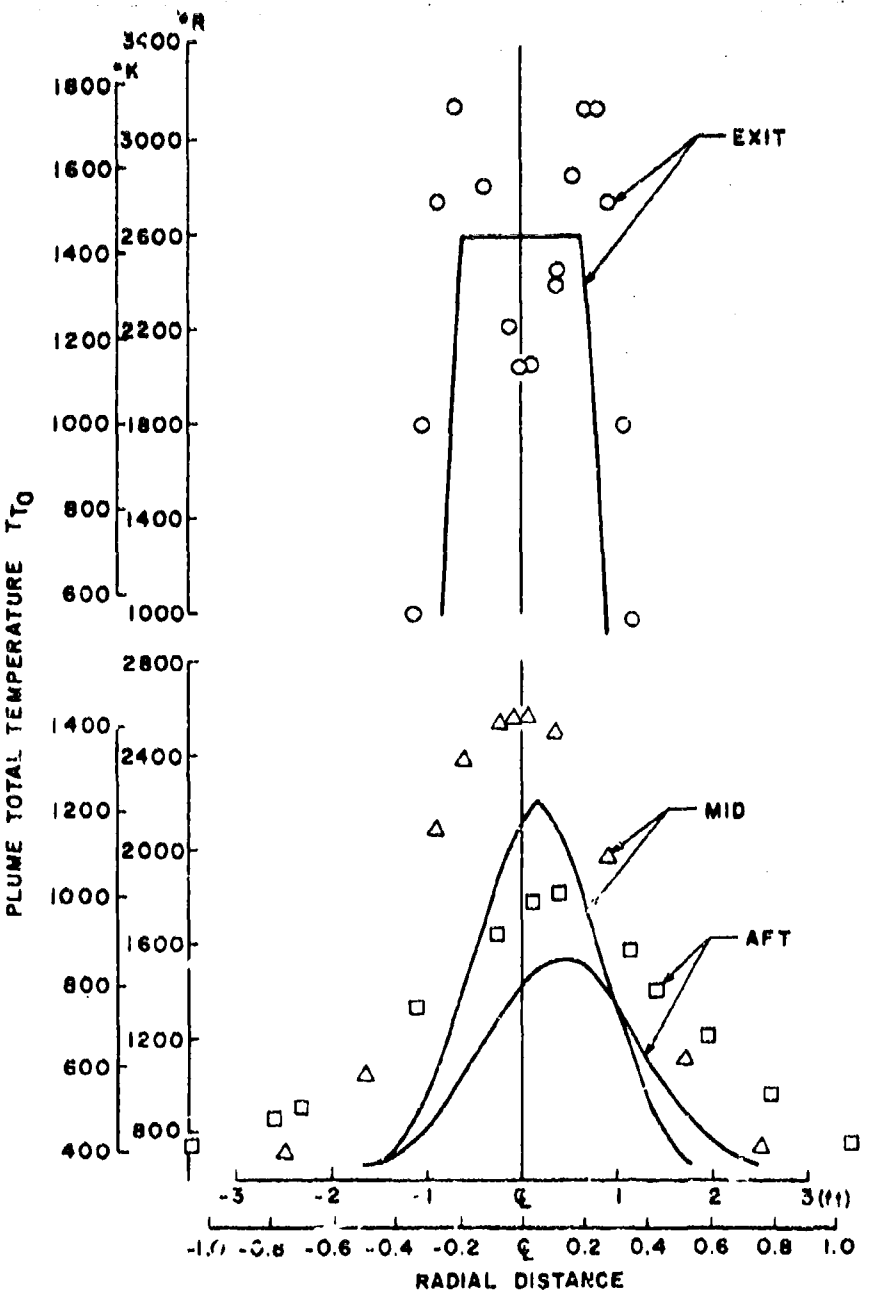

b. Plume Total Temperature
Fig. 27 Continued

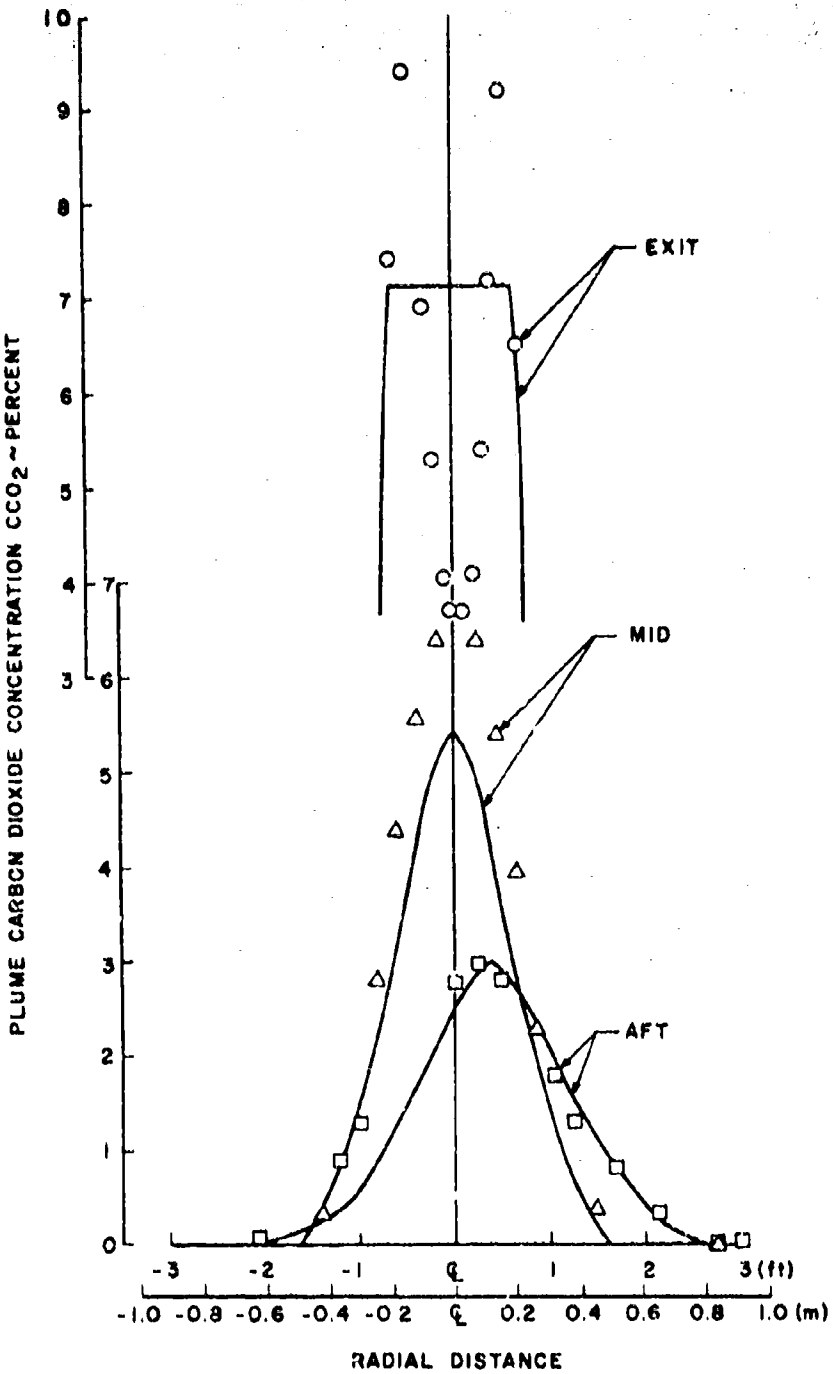

c. Plume Carbon Dioxide Concentration
Fig. 27 Concluded

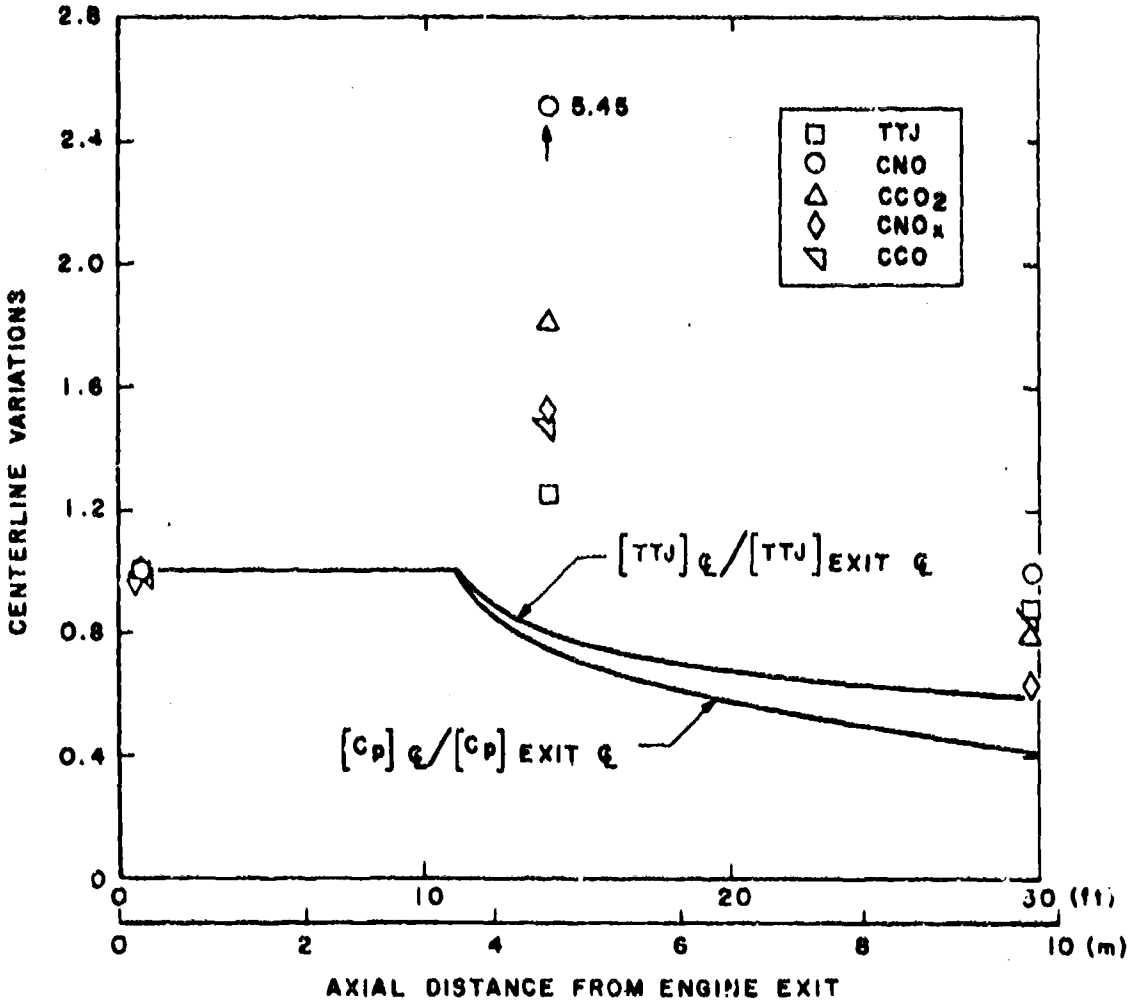

Fig. 28 Centerline Decay Characteristics of the Emission Concentrations and Total Temperature in the Exhaust Plume at Mach 2.0/65,000 ft, Afterburning Power

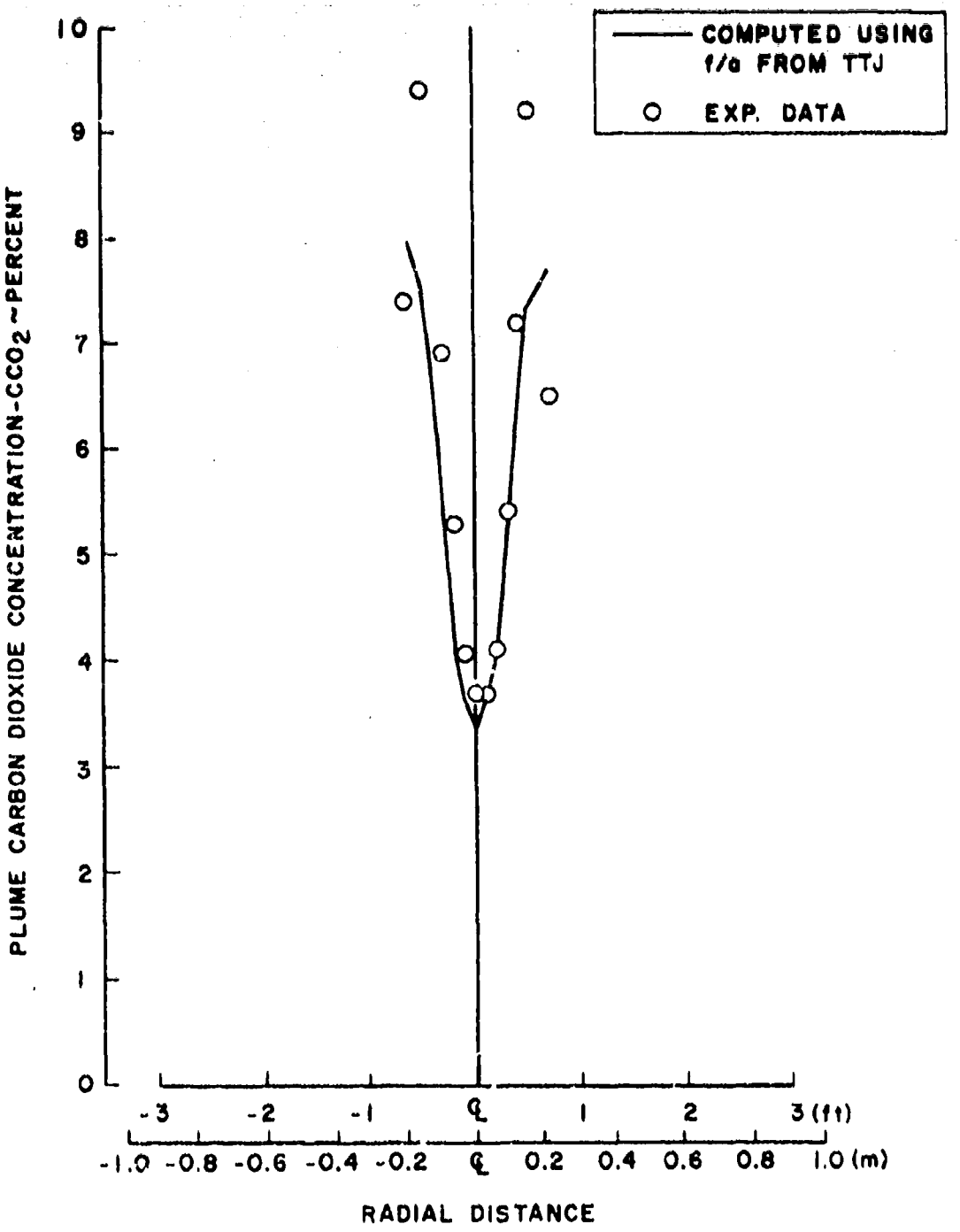

Fig. 29 Comparison of Theoretical and Experimental Carbon Dioxide Concentrations at the Exit Plane for Mach 2.0/65,000 ft, Afterburning Power

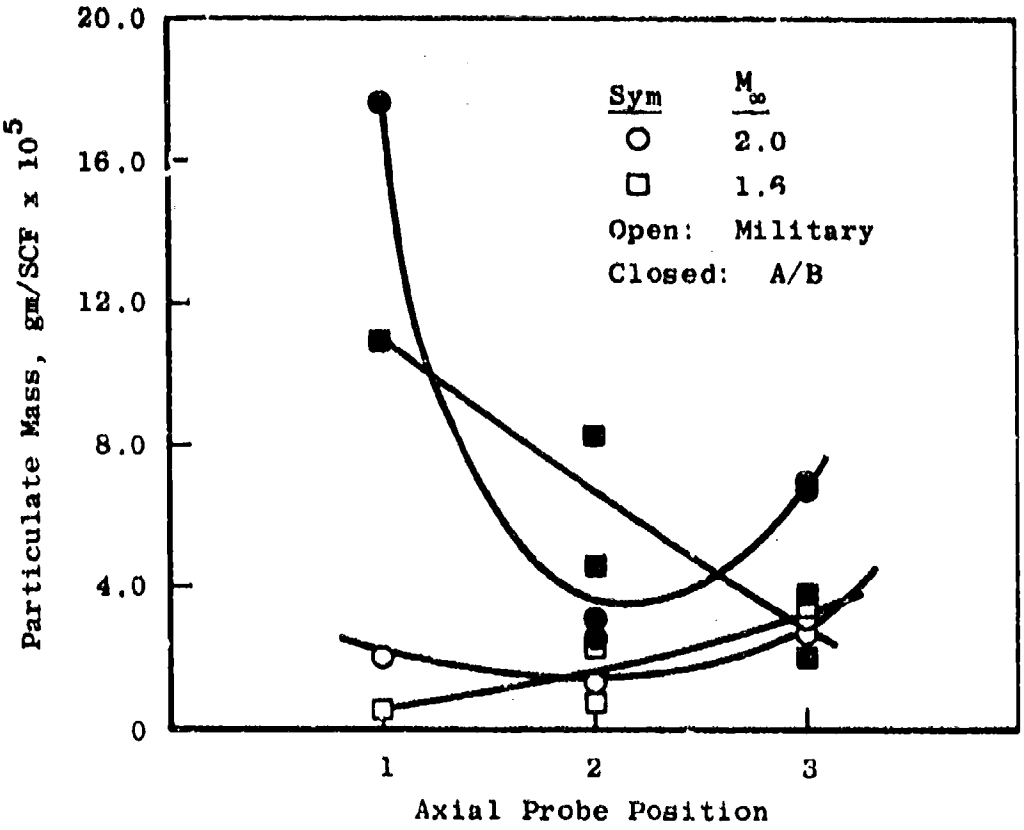

Fig. 30 Results of Gravimetric Filter Measurement of Particulate Emissions for Conditions Tested

TABLE I
EMISSION INSTRUMENTATION

Constituent	Measurement Designation	Analyzer Manufacture and Model	Analysis Technique
CO	CCOA	Beckman 315B	Nondispersive Infrared
	CCOB	Beckman 315BL	Nondispersive Infrared
CO_2	CCO2	Beckman 315B	Nondispersive Infrared
Hydrocarbons	CTHC	Beckman 402	Flame Ionization
NO	CNOA	TECO 10A	Chemiluminescence
NO_2	CNO2A	Beckman 255BL	Nondispersive Ultraviolet
NO_x	CNOXA	TECO 10A	Chemiluminescence with Converter
Particulates	None	Millipore	Gravity Filters
	None	DOT/TSD	Electrostatic Capture Grid

TABLE II
EXHAUST EMISSION INSTRUMENTATION ACCURACIES AND CALIBRATION GASES

Instrumentation Designation	Range No.	Range ppmv or Percent	Accuracy** Percent Full Scale	Span Gas* No.	Span Gas* Concentration, ppmv or Percent
CCOA	1	7500	±1.0	2	3040
	2	3000	±1.0	1	400
	3	1500	±1.0	1	400
CCOB	1	500	±1.0	2	490
	2	100	±1.0	1	43.3
	3	50	±3.0	1	49.3
CCO_2	1	20%	±1.0	2	20%
	2	10%	±1.0	1	2.04%
	3	5%	±1.0	1	2.04%
CTHC	1	20	±1.0	3	9.46
	2	100	±1.0	1	51.3
	3	200	±1.0	1	51.3
	4	1000	±1.0	2	518
	5	2000	±1.0	2	518
	6	10,000	±1.0	2	518
	7	20,000	Ranges Not Used		
	8	100,000			

Instrumentation Designation	Range No.	Range ppmv or Percent	Accuracy** Percent Full Scale	Span Gas* No.	Span Gas* Concentration, ppmv or Percent
CNO	1	2.5	Range Not Used		
	2	10	±5.0	3	8.37
	3	25	±2.5	3	8.37
	4	100	±2.0	1	38.5
	5	250	±2.0	1	38.5
	6	1000	Ranges Not Used		
	7	2500			
	8	10,000			
CNO_2	1	500	±1.0	2	195
	2	150	±2.0	1	36.7
	3	50	±3.0	3	5.67
CNO_x	1	2.5	Range Not Used		
	2	10	±5.0	3	5.67
	3	25	±2.5	3	5.67
	4	100	±2.0	1	36.7
	5	250	±2.0	2	195
	6	1000	Ranges Not Used		
	7	2500			
	8	10,000			

*Scott Laboratory Certified Value
**Accuracies Specified in Manufacturer's Instrumentation Manual with Exception of CNO, CNO_x, and CNO_2 which Were Taken from Ref. 16

TABLE III
GAS SAMPLE CONVERSION CHARACTERISTICS
IN SAMPLE LINE AND GAS ANALYZER

a. Nitrogen Dioxide Conversion
(NO_2 Introduced at Sample Probe)

NO_2 Gas Introduced, ppmv	Sample Temperature, °K (°R)	Measurement Constituents	
		CNO_2, ppmv	CNO, ppmv
36.7	422 (760)	36.7	12.0
195.0	422 (760)	195.0	30.3
36.7	339 (610)	36.7	0.7
195.0	339 (610)	195.0	3.1

b. Carbon Dioxide Conversion
(CO_2 Introduced at Sample Probe)

CO_2 Gas Introduced, Percent by Volume	Sample Temperature, °K (°R)	Measurement Constituents		
		CCO_2, Percent by Volume	CCOA, Percent by Volume	CCOB, * Percent by Volume
2.04	422 (760)	2.04	13.3	20.9
20.0	422 (760)	20.0	32.0	133.2
2.04	339 (610)	2.04	6.7	23.6
20.0	339 (610)	20.0	26.6	139.0

*CCOB measurements are most accurate in this concentration range.

TABLE IV
CROSS REFERENCE VERIFICATION CHECK OF EMISSION MEASUREMENT SYSTEM

Cross Reference Gas	No.* Users	Range of* User Values Measured	Estimated* Standard Deviation	Estimated* Standard Error, Percent	Users Average* Value	AEDC Value
CCO, ppm	22	75.0 - 112	± 8.14	±1.74	91.89	94.5
CCO_2, Percent	20	1.95 - 2.27	± 0.08	±0.02	2.05	2.04
CTHC, ppm	17	51.0 - 71.0	± 5.57	±1.35	63.16	57.5
CNO, ppm	27	373 - 428	±12.34	±2.37	405	396

*Refs. 11 and 12

TABLE V
JP-5 FUEL SPECIFICATIONS AND ANALYSIS

Item	Specified*	Actual
Net Heat of Combustion, Btu/lbm	18, 300 Min	18, 444
Hydrogen, weight percent	---	13.79
ASTM Distillation:		
IBP, °F	---	330
10-percent Min, °F	400	371
20-percent Min, °F	---	384
50-percent Min, °F	---	407
90-percent Min, °F	---	450
FBP Max, °F	550	480
Residue Max, percent	1.5	1.4
Loss Max, percent	1.5	0.1
Specific Gravity, T/°C		
at 40°F	---	0.819
at 100°F	---	0.795

*MIL-T-5624H

TABLE VI
NOMINAL FREE-STREAM AND ENGINE/INLET OPERATING CONDITIONS

Free-Stream Conditions			Inlet Conditions					
M_∞	Altitude, ft	T_{t_∞}, °K (°R)	XS, m (ft)	A_{EJ}, m^2 (ft^2)	A_{BY}, m^2 (ft^2)	$\bar{P}_{t_2}/P_{t_\infty}$	D_2	$\frac{W\sqrt{\theta_2}}{\delta_2}$, kg/sec (lb/sec)
1.6	55,000	328 (590)	0.725 (2.38)	0.0046 (0.05)	0 (0)	0.935	0.09	17.4 (38.3)
2.0	65,000	390 (702)	0.631 (2.07)	0.0093 (0.10)	0.0033 (0.035)	0.910	0.08	15.7 (34.7)

Engine Conditions									
M_∞	Altitude, ft	PLS	RPM	T_{t_5}, °K (°R)	WFP, kg/hr (lb/hr)	WFT, kg/hr (lb/hr)	(f/a)P	(f/a)T	A_8, m^2 (ft^2)
1.6	55,000	MIL	16,590	933 (1680)	340 (750)	340 (750)	0.017	0.017	0.0687 (0.74)
		A/B	16,590	933 (1680)	340 (750)	576 (1670)	0.017	0.035	0.0938 (1.01)
2.0	65,000	MIL	16,940	928 (1670)	281 (620)	281 (620)	0.016	0.016	0.0697 (0.75)
		A/B	16,940	928 (1670)	281 (620)	658 (1450)	0.016	0.036	0.0957 (1.03)

TABLE VII
COMPARISON OF SEA-LEVEL STATIC AND WIND TUNNEL MEASUREMENTS

Free-Stream Conditions		Burner Inlet Conditions			Correlation Parameters			Exit Plane Emission Indices					
M_∞	Altitude, ft	P_3, N/cm^2 (atm)	T_3, °K (°R)	v_3, m/sec (ft/sec)	$\frac{P_3 T_3}{v^3}$, $\frac{\text{N-sec-°K}}{\text{m}^3}$ $\left(\frac{\text{atm-sec-°R}}{\text{ft}}\right)$	$\frac{\sqrt{P_3}\, T_3^3}{\left(\frac{\text{N}}{\text{m}^2}\right)^{1/2}\text{-°K}^3}$ $\left(\frac{}{(\text{atm})^{1/2}\text{-°R}^3}\right)$	$\frac{\sqrt{P_3}\, T_3^3}{\left(\sqrt{P_3}\, T_3^3\right)_{SSL}}$	$EICO_2$	EITHC	EICO	EINO	$EINO_x$	$EINO_2$
								gm/kg (lbm/lbf x 1000)					
0	1,100 Warm Day	66.5 (6.55)	556 (1000)	113.4 (372.0)	3.27×10^6 (9.81)	1.41×10^9 (2.56×10^3)	1.00	3540	5.89	46.8	1.50	5.45	3.90
1.6	55,000 Standard Day	19.6 (1.93)	602 (1082)	126.5 (415.0)	0.93×10^6 (5.04)	0.97×10^9 (1.77×10^3)	0.69	3004	0.49	85.3	1.47	3.25	1.77
2.0	65,000 Standard Day	17.3 (1.71)	709 (1285)	158.0 (518.0)	0.78×10^6 (4.23)	1.48×10^9 (2.77×10^3)	1.08	3303	0.89	85.3	2.30	4.25	1.94

1. $\frac{(\sqrt{P_3}\, T_3^3)\ M = 2.0}{(\sqrt{P_3}\, T_3^3)\ M = 1.6} = 1.565$

2. $\frac{(EINO)\ M = 2.0}{(EINO)\ M = 1.6} = 1.565$

3. $\frac{(EINO_x)\ M = 2.0}{(EINO_x)\ M = 1.6} = 1.310$

4. $\frac{(EITHC)\ M = 2.0}{(EITHC))\ M = 1.6} = 1.815$

5. $\frac{(EINO_2)\ M = 2.0}{(EINO_2)\ M = 1.6} = 1.097$

TABLE VIII
SUMMARY OF EMISSION INDICES

M_∞	Engine Setting	Probe Position Exit	$EICO_2$	EITHC	EICO	EINO (as NO)	$EINO_x$ (as NO)	EINO (as NO_2)	$EINO_x$ (as NO_2)	$EINO_2$
			gm/kg							
0.0 (Ref. 9)	Military	Exit	3540	5.300	46.0	---	---	1.50[2]	5.45[1]	3.90[1]
1.6	Military	Exit	3004	0.486	85.4	0.96	1.98	1.47	3.25	1.77[3]
		Mid	2963	2.270	108.3	1.20	1.21	1.84	1.99	1.53[3]
		Aft	3013	5.550	70.0	1.15	1.41	1.75	2.32	0.74[3]
2.0	Military	Exit	3003	0.889 (1.90)	85.3	1.50	2.59	2.30	4.25	1.94[3]
		Mid	2985	1.676 (2.50)	88.8	1.88	2.42	2.88	3.97	1.20[3]
		Aft	3002	5.370	77.5	1.93	1.95	2.96	3.20	0.41[3]
1.6	Partial A/B	Exit	2906	21.6	105.8	0.51	1.21	0.78	1.99	1.21[3]
		Mid	2838	29.8	132.5	0.48	1.45	0.73	2.38	1.63[3]
		Aft	2905	21.1	107.7	0.54	0.67	0.83	1.10	0.36[3]
2.0	Partial A/B	Exit	2945	13.3	97.3	0.56	1.31	0.86	2.15	1.29
		Mid	2779	36.7	156.9	0.45	1.34	0.69	2.20	1.52
		Aft	2795	29.0	161.7	0.42	1.08	0.63	1.78	1.17

1. Measured
2. Calculated as $NO_x - NO_2$
3. Calculated as $NO_x - NO$

TABLE IX
RESULTS OF GRAVIMETRIC FILTER ANALYSIS

M_∞	Altitude, ft	PLS	XP/DN	Weight, g	Filter Flow, scf	$\frac{\text{Weight}}{\text{Fuel Flow}}$, g/scf
1.6	55,000	MIL	0.22	8×10^{-5}	15.2	0.53
		A/B	0.22	218×10^{-5}	20.0	10.9
2.0	65,000	MIL	0.22	30×10^{-5}	15.0	2.0
		A/B	0.22	249×10^{-5}	14.2	17.6
1.6	55,000	MIL	9.30 9.30	5×10^{-5} 31×10^{-5}	7.5 13.0	0.67 2.38
		A/B	9.30 9.30	55×10^{-5} 44×10^{-5}	12.0 5.3	4.58 8.30
2.0	65,000	MIL	9.30	16×10^{-5}	12.4	1.29
		A/B	9.30	31×10^{-5} 35×10^{-5}	10.0 13.8	3.1 2.54
1.6	55,000	MIL	19.90	44×10^{-5}	13.25	3.32
		A/B	19.90	38×10^{-5} 10×10^{-5}	10.0 5.0	3.80 2.00
2.0	65,000	MIL	19.90	33×10^{-5} 40×10^{-5}	10.75 14.75	3.06 2.71
		A/B	19.90	60×10^{-5} 89×10^{-5}	9.0 13.0	6.67 6.85

APPENDIX III
NITROGEN DIOXIDE INSTRUMENTATION DEFICIENCIES

The Beckman Nondispersive Ultraviolet long path analyzer, which was used to measure concentrations of nitrogen dioxide (CNO_2), was the only instrument that gave questionable results. Since there was no consistent method of correcting these results, they are presented as measured without any corrections.

The results indicate that the instrument exhibited both zero shifts and an increase in the measured value with time because of some contamination of the sample cell. A typical plot of these characteristics is shown in the following figure:

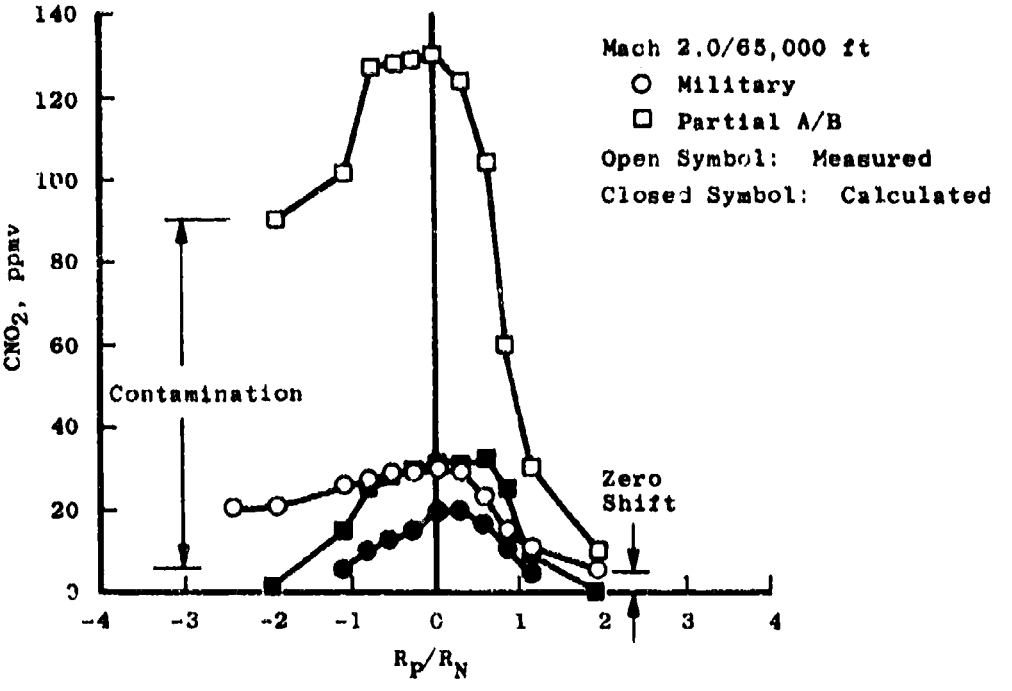

A comparison of the measured and calculated CNO_2 shows a greater shift in the results at afterburning power. Checks of the instrument sensitivity to water vapor prior to the test did not show an appreciable influence on the performance of the instrument. Table III shows considerable conversion (16.2 to 34.3 percent) of the CNO_2 into CNO in the sampling line and analyzer. This does not explain the increase in CNO_2 with time.

Modifications were made during the test to increase the rigidity of the light source and of the phototube which greatly decreased the zero shift sensitivity. However, the contamination effect was not improved. Calibration of the instrument every two hours

was not sufficient to eliminate the shift and in many cases the contamination effect was noted immediately after calibration. A further check of the sensitivity of the instrument to methane introduced in the sampling probe did not affect the instrument. During the test, an accumulation of a yellow deposit in the sample line approaching the NO_2 instrument was observed. The instrument's performance showed a noticeable improvement when the lines were cleaned.

It should be noted that the manufacturer replaced the gold anodized sample cell with a Monel steel sample cell at the beginning of the test to correct irregularities in the operation which were attributed to pitting of the anodized gold on the sample cell. This change resulted in increased sensitivity to the unbalance in light reflected through the gold reference cell and the Monel steel sample cell. It is, therefore, understandable that any accumulation of deposit on the sample cell would cause a further shift in the calibration. It is recommended that a systematic investigation of the instrument's sensitivity to contaminants (such as heavy hydrocarbons that can condense in the sample cell at 338°K (610°R) be made before the instrument is used to measure CNO_2 in the exhaust of a turbojet engine.

APPENDIX IV
THEORETICAL CALCULATIONS OF EXHAUST PLUME PROPERTIES

Theoretical predictions of the exhaust plume properties (i.e. total temperature, impact pressure, concentrations) as a function of both the axial distance from the engine exit plane and the plume radius were made using the turbulent mixing layer version of the turbulent boundary-layer calculation procedure given in Ref. 16. The calculation procedure utilizes a numerical, implicit, finite difference method to solve the equations of continuity, energy, and conservation of species. Boundary-layer assumptions are used in deriving the conservation equations, and a Prandtl mixing length-eddy viscosity model is used to relate the mean flow properties to the fluctuating flow properties. Since the solution is an implicit difference scheme, it is necessary to supply a set of initial conditions in terms of mixing region profiles (total temperature, velocity, and concentration), initial thickness of the mixing region, and the conditions at the edges of the mixing region. The initial conditions for the tests reported herein were computed using a flow model shown in the following sketch.

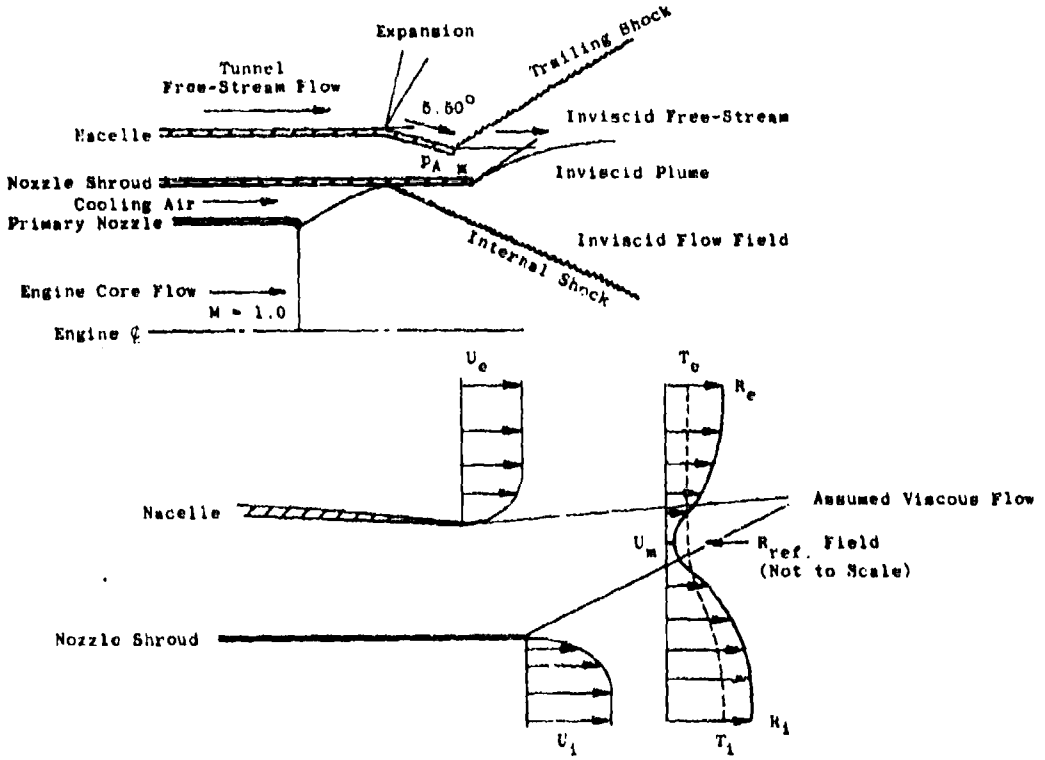

The inviscid flow field was generated under the following assumptions:

1. Tunnel free-stream conditions existed on the engine nacelle ahead of the nacelle boattail.

2. Because of the short length of the boattail, a simple Prandtl-Meyer expansion gave the boattail conditions.

3. The internal nozzle cooling air was neglected in the nozzle flow.

4. The flow between the nacelle and nozzle shroud was neglected (measurements of the total and static pressure at point A showed that little or no flow existed in the annulus).

5. The internal nozzle flow was generated from a Method of Characteristics solution (Ref. 14) using the engine manufacturer's specifications for the engine core flow.

6. The pressure at point A (p_A) was matched between the external and internal flows.

The viscous flow was computed by calculating the turbulent boundary layer along the engine nacelle and the internal nozzle wall. The initial profiles for the velocity, temperature, and concentrations were generated by matching error functions at the reference radius (R_{ref}). The point at which these initial profiles were calculated was somewhat arbitrary and in the cases considered was 2.54 cm (1.0 in.) downstream of the nozzle shroud exit. This position becomes more critical when trying to compare mixing region properties at the first axial location probed, which was 10.13 cm (4.0 in.) downstream of the nozzle shroud exit. Unfortunately the probe was not traversed through the mixing region at that plane, and a direct comparison is not possible. The following table gives the values of the flow properties used as initial conditions for the plume mixing calculations:

Free-Stream Conditions		Initial Conditions for Plume Mixing												
M_∞	Altitude, ft	T_{TJ}, °K (°R)	u_e, m/sec (ft/sec)	T_{0_j}, °K (°R)	p_e, N/cm^2 (psfa)	u_j, m/sec (ft/sec)	T_j, °K (°R)	p_j, N/cm^2 (ft/sec^2)	R_{ref}, m (ft)	R_j, m (ft)	y_o, m (ft)	a_j, m (ft)	b_j, m (ft)	$\delta_{M,I.}$, cm (in.)
2.0	65,000 MIL	958 (1725)	572 (1875)	227 (408)	0.625 (130)	925 (3036)	580 (1000)	0.625 (130)	0.258 (0.846)	0.222 (0.720)	0.342 (1.12)	0.0464 (0.152)	0.0190 (0.0052)	11.91 (4.70)
2.0	65,000 A/B	1444 (2600)	505 (1852)	230 (415)	0.715 (149)	1143 (3753)	917 (1652)	0.715 (149)	0.258 (0.846)	0.224 (0.733)	0.342 (1.12)	0.0464 (0.152)	0.0192 (0.0630)	11.80 (4.66)
1.6	55,000 MIL	958 (1725)	476 (1560)	215 (388)	0.890 (193)	900 (2951)	609 (1096)	0.880 (183)	0.258 (0.846)	0.222 (0.728)	0.323 (1.06)	0.0369 (0.121)	0.0190 (0.0052)	10.22 (4.03)
1.6	55,000 A/B	1444 (2600)	455 (1490)	224 (404)	1.005 (210)	1080 (3540)	574 (1755)	1.005 (210)	0.258 (0.846)	0.224 (0.733)	0.323 (1.06)	0.0369 (0.121)	0.0192 (0.0630)	10.11 (3.98)

where the initial profiles are given by:

$$R_{ref} \leq R \leq R_e \qquad u = u_m + (u_e - u_m)\ \mathrm{erf}\left(\frac{R - R_{ref}}{a}\right)$$

$$R_i \leq R \leq R_{ref} \qquad u = u_m + (u_i - u_m)\ \mathrm{erf}\left(\frac{R_{ref} - R}{b}\right)$$

$$R \leq R_{ref} \qquad T = T_e + (T_i - T_e)\ \mathrm{erf}\left(\frac{R_{ref} - R}{b}\right)$$

$$R < R_{ref} \qquad T = T_e$$

The concentration profile was assumed to be similar to the temperature profile with $X_e = 0.0$ and $X_i = 1.0$, and U_m was arbitrarily set at 30.5 m/sec (100 ft/sec). This was the approximate minimum value needed to eliminate numerical instabilities in the computations. It should be emphasized that, although the numerical procedure allows for the inclusion of finite-rate chemistry, only frozen chemistry is programmed and all the calculations were carried out assuming frozen chemical composition. By assuming that the turbulent transport coefficients (i.e., the turbulent Schmidt numbers) are the same for all the species in the exhaust plume and frozen chemistry, only one conservation of species equation needs to be solved since the initial exit plane values may be normalized to unity. An obvious assumption made in the viscous mixing calculations is that of uniform properties in the inviscid flows (both internal and external). As shown in Fig. 27a and b this assumption is grossly in error for the afterburning power setting.

The thermodynamic properties of the mixing region are computed as if the entrained air and exhaust gases are a mixture of thermally and calorically perfect gases. Real gas curve fits are utilized for the air since they were existing in the numerical program, and curve fits are used for the specific heat variation with temperature for the exhaust gases. The real gas curve fits for air, being developed for high temperatures, are in error at low temperatures, for example, at 700°R, they are 25°R too low. Comparisons of the theoretical predictions made with the above method and the experimental data are discussed in Section 4.2.5.

APPENDIX V
INTEGRATED EMISSION INDEX CALCULATION PROCEDURES

Since, in most aircraft turbine engines, the values of the flow properties across the exhaust exit plane are not uniform, an integrated mass flow of each species will give a more accurate evaluation of the pollutants being emitted. The usual definition of the emission index can then be applied to the integrated mass flows of each species. This can be done in the following manner: Let C_p = the concentration of the p^{th} species (given in ppmv - mole fraction) then,

$$C_p = \frac{n_p}{n_g}$$

where n_p is the number denstiy of the p^{th} species and n_g is the number density of the mixture. The flux of the p^{th} species across any exhaust plume plane in terms of particles per unit time is

$$\dot{n}_p = 2\pi \int_0^{R_p} n_p u_g r \, dr \qquad \text{(V-1)}$$

and if m_p represents the mass of a p^{th} particle, then the mass flow is

$$\dot{m}_p = 2\pi \int_0^{R_p} n_p m_p u_g r \, dr \qquad \text{(V-2)}$$

Let m_g be the average particle mass of the gas mixture; then since

$$\frac{n_p m_p}{n_g m_g} = \frac{m_p}{m_g} C_p = \frac{\rho_p}{\rho_g}$$

Eq. (V-2) becomes

$$\dot{m}_p = 2\pi \frac{m_p}{m_g} \int_0^{R_p} C_p \rho_g u_g r \, dr \text{ (mass/unit time)} \qquad \text{(V-3)}$$

The fuel burned on a molar basis is the sum of the moles of the species containing all of the carbon atoms (the carbon emitted in the form of particulates will be neglected) so that the fuel flow is

$$WFT = 2\pi \frac{m_f}{m_g} \int_0^{R_p} [CCO + CCO_2 + CTHC] \rho_g u_g r \, dr \text{ (mass/unit time)} \qquad \text{(V-4)}$$

The mass of species "p" emitted per mass of fuel burned is the ratio of Eqs. (V-3) and (V-4). If the product of $\rho_g u_g r dr$ is given in g/sec (lbm/sec), then the emission index is given as

$$EI(C_p) = 1000 \frac{\dot{m}_p}{\dot{m}_f} = 1000 \frac{M_p}{M_f} \frac{\int_0^{R_p} C_p \rho_g u_g r\, dr}{\int_0^{R_p} [CCO + CCO_2 + CTHC] \rho_g u_g r\, dr} \qquad \text{(V-5)}$$

(g/kg fuel), (lbm/10^3 lbm fuel)

where the molecular weights have been substituted for the particle masses.

The integrals in Eq. (V-5) are evaluated using a simple trapezoidal integration of the experimental data. The bulk exhaust gas properties are computed from the measured total temperature, impact pressure, and static pressure at the plane where the measurements were made. An iteration across the normal shock wave in front of the sample probe is used to compute the free-stream conditions ahead of the shock wave (ρ_g and u_g). The values of the CCO_2 is input in percent by volume, and the remaining species are input as parts per million by volume. If no reactions take place in the exhaust, the $EI(C_p)$ will remain constant at any axial location downstream of the engine exit plane. In addition, if all the flow properties are uniform, Eq. (V-5) reduces to the usual definition of the emission index.

$$EI(C_p) = 0.1 \frac{M_p}{M_f} \frac{C_p}{\frac{CCO}{10^4} + CCO_2 + \frac{CTHC}{10^4}} \qquad \text{(V-6)}$$

where C_p, CCO, and CTHC are given in ppmv and the CCO_2 is given in percent by volume. Equation (V-5) has been used in this report to calculate the emission indices with the following values of M_p/M_f:

p^{th} Species	M_p	M_p/M_f
JP5 Fuel	14	1.00
CCO	28	2.00
CCO_2	44	3.14
CNO (as CNO_2)	46	3.29
CNO_x (as CNO_2)	46	3.29
CNO_2	46	3.29
CNO	30	2.14
CTHC	14	1.00

where the fuel has been assumed to have nearly a C/H ratio of 2.0 so that $M_f \simeq 12 + 2 = 14$. These values are in agreement with those recommended by the SAE Committee E-31 to be issued in SAE ARP 1256 (Ref. 6).

Equation (V-4) may also be used as a means of checking the experimental data for consistency. As noted, if the profiles are uniform across the exit plane of the engine exhaust, Eq. (V-4) becomes:

$$WFT = 2\pi \frac{M_f}{M_g}[CCO + CCO_2 + CTHC]\int_0^R \rho_g u_j r\, dr$$

which reduces to

$$WFT = \frac{M_f}{M_g}[CCO + CCO_2 + CTHC](WFT + W_a)$$

By taking the usual definition of the fuel-air ratio ($f/a = WFT/W_a$), the above equation can be solved for the CCO_2.

$$CCO_2 = \frac{M_g}{M_f}\frac{f/a}{1 + f/a} - [CCO + CTHC] \qquad (V\text{-}7)$$

Since the fuel-air ratio is usually known to a greater degree of confidence than the measured concentrations, Eq. (V-7) can be used to estimate the CCO_2 levels expected from the measured f/a, CCO, and CTHC. The usual procedure of calculating a fuel-air ratio and comparing that with the measured value can also be used as a check. Equation (V-7) can also be applied locally in the exhaust flow if local value of the fuel-air ratio is deduced from the measured total temperature profile. This approach can be used for afterburning power settings where some combustion takes place externally to the engine. The methods described were applied to the experimental data obtained during the tests reported herein, and the results are discussed in Section IV.